Max-Planck-Institut
für Meteorologie

MAX PLANCK
GESELLSCHAFT

International Max Planck Research School
on Earth System Modelling

The Deep Western Boundary Current in an Eddying Ocean

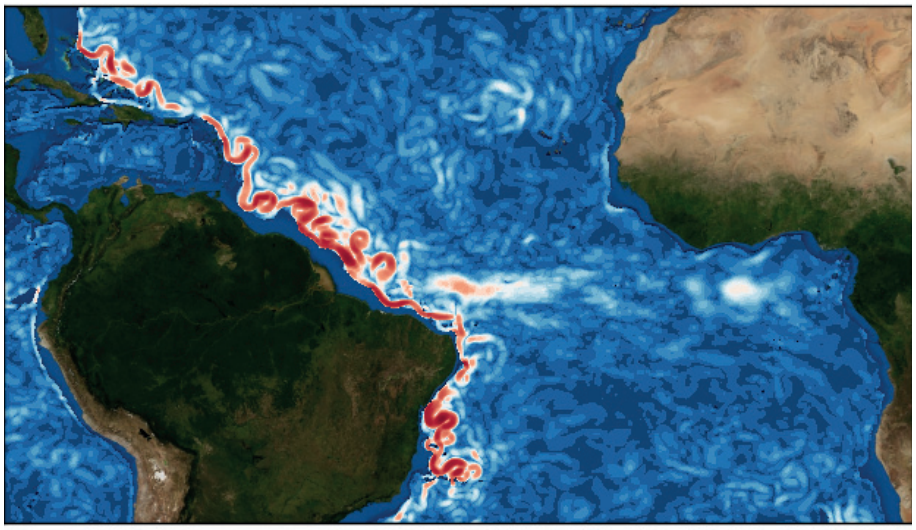

Veit Magnus Lüschow

Hamburg 2020

Berichte zur Erdsystemforschung
Reports on Earth System Science

229
2020

Hinweis

Die Berichte zur Erdsystemforschung werden vom Max-Planck-Institut für Meteorologie in Hamburg in unregelmäßiger Abfolge herausgegeben.

Sie enthalten wissenschaftliche und technische Beiträge, inklusive Dissertationen.

Die Beiträge geben nicht notwendigerweise die Auffassung des Instituts wieder.

Die "Berichte zur Erdsystemforschung" führen die vorherigen Reihen "Reports" und "Examensarbeiten" weiter.

Notice

The Reports on Earth System Science are published by the Max Planck Institute for Meteorology in Hamburg. They appear in irregular intervals.

They contain scientific and technical contributions, including Ph. D. theses.

The Reports do not necessarily reflect the opinion of the Institute.

The "Reports on Earth System Science" continue the former "Reports" and "Examensarbeiten" of the Max Planck Institute.

Anschrift / Address

Max-Planck-Institut für Meteorologie
Bundesstrasse 53
20146 Hamburg
Deutschland

Tel./Phone: +49 (0)40 4 11 73 - 0
Fax: +49 (0)40 4 11 73 - 298

name.surname@mpimet.mpg.de
www.mpimet.mpg.de

Layout

Bettina Diallo and Norbert P. Noreiks
Communication

Copyright

The Deep Western Boundary Current in an Eddying Ocean

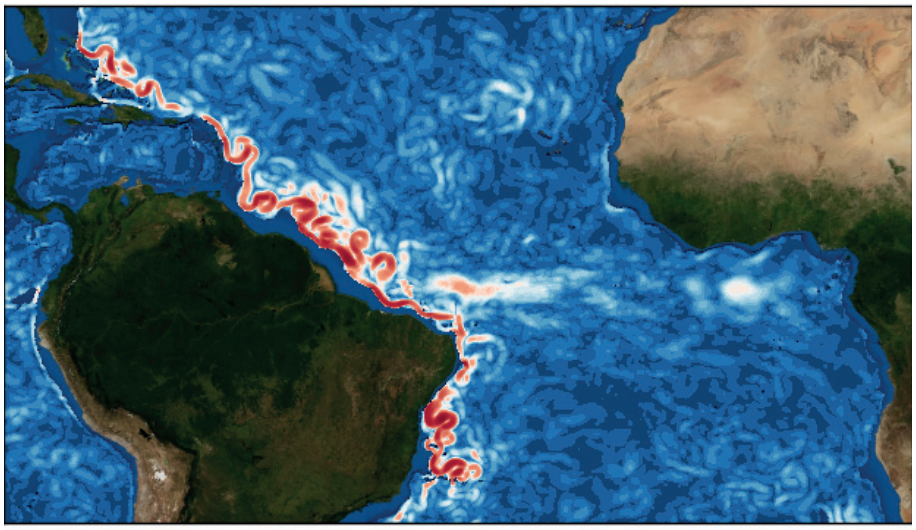

Veit Magnus Lüschow

Hamburg 2020

Veit Magnus Lüschow
aus Meerbusch, Deutschland

Max-Planck-Institut für Meteorologie
The International Max Planck Research School on Earth System Modelling
(IMPRS-ESM)
Bundesstrasse 53
20146 Hamburg

Universität Hamburg
Geowissenschaften
Meteorologisches Institut
Bundesstr. 55
20146 Hamburg

Tag der Disputation: 14. Mai 2020

Folgende Gutachter empfehlen die Annahme der Dissertation:
Prof. Dr. Jin-Song von Storch
Prof. Dr. Johanna Baehr

Vorsitzender des Promotionsausschusses:
Prof. Dr. Dirk Gajewski

Dekan der MIN-Fakultät:
Prof. Dr. Heinrich Graener

– ———————

The figure on the front page shows the low-latitude part of the eddying DWBC. Depicted is a snapshot of the flow field in 1670 m depth, using a non-linear colorbar: Dark red refers to 7 cm/s, white to 1 cm/s and dark blue to 0 cm/s.

This document was typeset using the typographical lookand-feel classicthesis developed by André Miede and Ivo Pletikosi´c.
classicthesis is available for both LaTeX and LyX:
https://bitbucket.org/amiede/classicthesis/

Berichte zur Erdsystemforschung / Max-Planck-Institut für Meteorologie 229
Reports on Earth System Science / Max Planck Institute for Meteorology 2020

ISSN 1614-1199

ABSTRACT

Our understanding of the interaction between the large-scale ocean circulation and ocean mesoscale eddies is mainly based on those parts of the circulation and those eddies that lie in the upper ocean. In this dissertation, I use a 0.1 degree, eddy-resolving ocean model to reveal two so far unknown eddy phenomena that are distinct to eddies in the deep ocean and cannot be observed for the well-known eddies in the upper ocean.

Firstly, eddies that are generated near the deep western boundary current (DWBC) in the Atlantic have a two-fold effect on mean density: Above the DWBC core (the level of maximum flow, ~ 2000 m depth), they decrease the available potential energy of the mean flow by flattening isopycnals; this behavior is in agreement with our expectation from baroclinic instability theory and is furthermore the foundation of common eddy parameterizations. However, below the DWBC core, eddies systematically increase the available potential energy of the mean flow by steepening isopycnals. Two consequences arise from this anomalous eddy behavior: a so far unknown mean circulation normal to the DWBC evolves that balances the eddy effect on mean density; moreover, the steepening of isopycnals below the DWBC core can also be interpreted as a deepening of the DWBC. This eddy-induced deepening might serve as an explanation for a too shallow DWBC in coarse-resolution ocean models that do not resolve eddies and thus do not capture the effect. I think that the two-fold eddy effect might be a general property of eddies near deep mean currents and thus, it might be relevant in other regions of the world ocean that exhibit deep currents.

Secondly, I observe different DWBC response behaviors in eddying and non-eddying ocean models that are subject to the same increase in surface wind stress: In the non-eddying model, the upper meridional overturning cell strengthens due to stronger winds over the southern ocean. For the DWBC, which closes both, the upper and bottom overturning cell in the southward direction, this strengthening implies a speed-up; In the eddying model, the upper cell strengthens by roughly the same amount, however, the DWBC now slows down. This becomes possible if the bottom overturning weakens drastically so that the total DWBC transport can decrease. I show that the DWBC slow down is balanced by eddy fluxes of relative vorticity which are not present in the non-eddying model. Thereby, I can attribute the described response difference to whether eddies are resolved or not. For the real (eddying) ocean, this implies that the suggested link between the upper and the bottom overturning cell ('ocean seesaw') might be weaker than previously thought and that both cells are allowed to respond independently to forcing changes.

ZUSAMMENFASSUNG

Unser Verständnis von der Wechselwirkung zwischen der groß-skaligen Ozeanzirkulation und den meso-skaligen Ozeanwirbeln beruht im Wesentlichen auf den Teilen der Zirkulation und den Wirbeln, die im oberen Teil des Ozeans liegen. In dieser Dissertation verwende ich ein wirbelauflösendes Ozeanmodell mit 0,1 Grad Auflösung, um zwei bisher unbekannte Eigenschaften von Wirbeln im tiefen Ozean aufzudecken. Diese Eigenschaften sind charakteristisch für tiefe Wirbel und können nicht für solche im oberen Ozean beobachtet werden.

Erstens haben die tiefen Wirbel in der Nähe des tiefen westlichen Randstroms (TWR) im Atlantik zwei unterschiedliche Auswirkungen auf die mittlere Dichteverteilung: Oberhalb des TWR-Kerns (die Tiefe mit der maximalen Geschwindigkeit, ~2000 m) verringern Wirbel die verfügbare potentielle Energie der mittleren Strömung durch Abflachung der Isopyknen; dieses Verhalten entspricht unserer Erwartung aus der Theorie der baroklinen Instabilität und ist darüber hinaus die Grundlage für gängige Wirbelparametrisierungen. Jedoch, unterhalb des TWR-Kerns erhöhen die Wirbel systematisch die verfügbare potentielle Energie der mittleren Strömung durch das Aufsteilen der Isopyknen. Zwei Konsequenzen ergeben sich aus diesem ungewöhnlichen Verhalten der Wirbel: Es entsteht eine bisher unbekannte Zirkulation in der Ebene senkrecht zum TWR, die den Wirbel-Effekt auf die mittlere Dichte ausgleicht; darüber hinaus kann das Aufsteilen der Isopyknen unterhalb des TWR-Kerns auch als Vertiefung des TWRs interpretiert werden. Diese wirbelinduzierte Vertiefung könnte als Erklärung für einen zu flachen TWR in grob aufgelösten Ozeanmodellen dienen, die die Wirbel nicht auflösen und somit den genannten Effekt nicht erfassen. Möglicherweise ist die Tatsache, dass Wirbel zwei unterschiedliche Effekte auf die mittlere Dichte, abhängig von der Tiefe, haben, eine allgemeine Eigenschaft von Wirbeln in der Nähe von tiefen Strömungen. Folglich könnte dies auch in anderen Regionen des Ozeans, in denen sich tiefe Strömungen befinden, relevant sein.

Zweitens ist die Reaktion des TWRs auf eine Zunahme des Windes an der Meeresoberfläche unterschiedlich, abhängig davon, ob Wirbel in einem Modell aufgelöst werden oder nicht: Im nicht-wirbelauflösenden Modell verstärkt sich die obere Zelle der meridionalen Umwälzzirkulation aufgrund der Zunahme der Winde über dem südlichen Ozean. Für den TWR, der sowohl die obere als auch die untere Zelle der Umwälzzirkulation in südlicher Richtung vervollständigt, bedeutet diese Verstärkung eine Beschleunigung; im wirbelauflösenden Modell verstärkt sich die obere Zelle um dasselbe Maß, jedoch wird der TWR nun langsamer. Dies ist möglich, wenn die untere Zelle der Umwälzzirkulation deutlich schwächer wird, so dass der gesamte TWR-Transport abnehmen kann. Ich zeige, dass die Verlangsamung des TWR durch wirbelinduzierte Flüsse von relativer Vortizität ausgeglichen wird. Diese Flüsse sind im nicht-wirbelauflösenden Modell nicht vorhanden.

Somit können wir den beschriebenen Unterschied in der Reaktion des TWRs der beiden Modelle darauf zurückführen, ob Wirbel aufgelöst werden oder nicht. Für den realen Ozean (der Wirbel enthält) bedeutet dies, dass die angenommene Kopplung zwischen der oberen und der unteren Zelle der Umwälzzirkulation ('Ozeanwippe') schwächer sein könnte als bisher vermutet und dass beide Zellen unabhängig voneinander eine Reaktion auf Änderungen im Strömungsantrieb zeigen können.

PUBLICATIONS RELATED TO THIS DISSERTATION

Lüschow, Veit, Jin-Song von Storch, and Jochem Marotzke (2019). Diagnosing the Influence of Mesoscale Eddy Fluxes on the Deep Western Boundary Current in the 1/10° STORM/NCEP Simulation. *Journal of Physical Oceanography* 49, pp 751-764. See chapter Chapter 2.

Lüschow, Veit, Jin-Song von Storch, and Jochem Marotzke (2020). Overturning response to a surface wind stress doubling in an eddying and a non-eddying ocean, *in preparation*. See chapter Chapter 3.

CONTENTS

1

DEEP EDDIES AND DEEP CURRENTS

An observer watching the ocean through a modern satellite telescope might be startled by the omnipresence of small meanders and swirls covering the sea surface. These swirls or currents form on scales between 20 and 500 km (e.g., Treguier et al., 2017) in formations called *mesoscale eddies*. They are the largest carriers of oceanic kinetic energy, contributing up to 2/3 to the total kinetic energy budget (von Storch et al., 2012). Accordingly, a large body of oceanographic literature has evolved since the first discoveries of ocean mesoscale activity in the late 1960s (Gill et al., 1974; Phillips, 1966; Swallow, 1971). Eddy research boomed in particular when the NASA launched the TOPEX/POSEIDON (T/P) satellite mission in 1992, allowing precise maps of the ocean surface currents to be produced overnight (Fu et al., 2010; Morrow and Le Traon, 2012). Since then, our understanding of the eddies' role in the ocean has grown considerably (please see Section 1.1 for a review).

Whereas most research into eddies has focused on eddies in the upper ocean, relatively little attention has been granted to eddies in the deep ocean, so-called *deep eddies*. There may be two reasons for the lack of attention on deep eddies: Firstly, observing deep eddies is by far more complicated than observing those near the surface and secondly, available observational (Scott et al., 2010) and numerical (e.g., von Storch et al., 2012) studies indicate that globally, eddy kinetic energy (EKE) monotonically decreases with depth (please see the dashed line in Fig. 1.1 for a globally averaged EKE depth profile). Based on this, it seems likely that eddies play a less important role in the deep ocean.

We will see that the global picture of EKE tells only one part of the story – that of a mainly wind-driven and therefore surface-intensified ocean circulation accompanied by a surface-intensified mesoscale eddy field. Yet, important parts of the circulation lie in the deep ocean with one prominent example being the deep western boundary current (DWBC) in the Atlantic. By closing the Atlantic meridional overturning circulation (AMOC) in the southward direction, the DWBC is an integral element of the global ocean heat and mass transport (Fine, 1995; Lumpkin and Speer, 2007). And instabilities of the DWBC can generate eddies in a way analogous to the strong surface currents. These deep eddies generated by the deep currents in some regions can even generate a secondary EKE maximum at depth, as can be seen in Fig. 1.1 for a location at 13° N in the western Atlantic (solid line). The deep EKE maximum in the DWBC

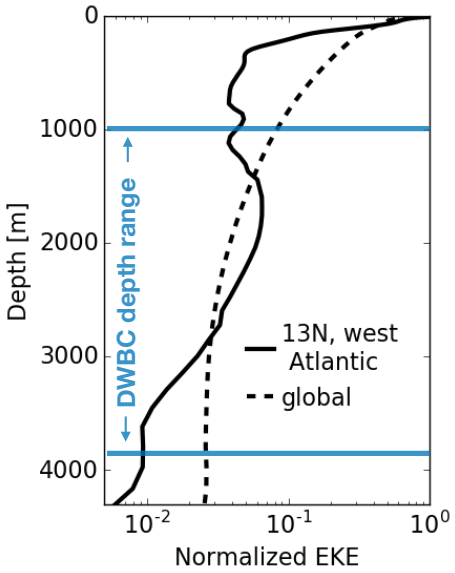

Figure 1.1: Occurrence of mesoscale eddies vs. depth in an eddy-resolving global ocean simulation; shown is the normalized eddy kinetic energy (EKE) at 13° N in the western Atlantic (solid) and globally averaged (dashed). The depth range of the deep western boundary current (DWBC) in the Atlantic is shown in blue. While globally, EKE decreases monotonically with depth, it has secondary maxima at depth in certain regions with strong deep currents like the DWBC.

suggests that locally, mesoscale eddies and their interaction with the deep currents deserve more attention than they previously received.

In this dissertation, I use an eddy-resolving ocean model to shed new light on two specific phenomena where mesoscale eddies interact with the deep circulation. The first phenomenon concerns the way in which eddy density fluxes shape the depth structure of the DWBC and thereby induce an overturning normal to the mean flow; the second phenomenon deals with the role of eddy vorticity fluxes for the decadal response of the DWBC to surface wind forcing changes.

Firstly however, I review the role of mesoscale eddies in the oceanic energy cycle (Section 1.1.1), their role in Earth's climate (Section 1.1.2) and their impact on the ocean mean circulation (Section 1.1.3). Subsequently, I outline previous findings on deep eddies (Section 1.1.4) before summarizing the results from our two papers, Lüschow et al. (2019, Section 1.2) and Lüschow et al. (2020, in prep., Section 1.3).

1.1 WHAT ROLE DO MESOSCALE EDDIES PLAY IN THE OCEAN AND CLIMATE SYSTEM?

Gill et al. (1974) were the first to recognize that seen from a global perspective, the primary role of ocean eddies is to drain the vast amounts of potential energy that the surface wind stress and buoyancy forcing introduce into the ocean. However, this conception was not entirely new: It had already been described in the atmosphere in relation to the strong zonal jets, under the term *baroclinic instability* (Charney, 1947; Eady, 1949). The underlying assumption is that available potential energy can accumulate in the mean flow until the vertical shear of the flow is so large that it becomes baroclinically unstable. Beyond this threshold, excess energy feeds into the mesoscale eddy field. In short, eddies limit the strength of the ocean mean currents (McWilliams, 2008).

1.1.1 *Energy cycle*

A popular framework used to quantify the role of eddies in the ocean and atmosphere is the Lorenz energy cycle (Lorenz, 1955). Besides reservoirs for kinetic and potential energy of the *mean* state it takes into account potential and kinetic *eddy* energy. Similar to the atmosphere, estimates of the ocean energy cycle show that the largest conversion between the different reservoirs is the above mentioned baroclinic conversion from mean potential to eddy potential energy and then to eddy kinetic energy (von Storch et al., 2012). However, once the energy has reached the reservoir for eddy kinetic energy, it is essentially dissipated in Lorenz' model of the energy cycle. In contrast, in the real ocean, eddy kinetic energy is "reused" for a range of purposes.

In the spectral domain, there are two principal directions in which energy can leave the mesoscale: The *upscale* transfer to the large scale flow is an integral feature of homogeneous, two-dimensional turbulence (Charney, 1971) and it can be observed in the ocean (e.g., Scott and Wang, 2005). Yet, many regions of the ocean conflict with the very idealized setting of homogeneous turbulence, and so most of the mesoscale energy is transferred *downscale*. At small scales, a huge amount of energy is required for the mixing that sustains the global overturning circulation (Ferrari, 2014; Munk and Wunsch, 1998), and it is clear that a fraction of this energy originates from the mesoscale (Wunsch and Ferrari, 2004). However, quantifying this fraction is difficult and estimates range between almost one half (Nikurashin et al., 2013) to considerably less than this (Wunsch and Ferrari, 2004). Not only a robust quantification of the total eddy contribution to mixing is missing, it is furthermore unclear which mechanism of downscale energy transfer is dominant. Among the most important mechanisms are spontaneous emission of internal gravity waves through eddies (Chouksey et al., 2018; Molemaker et al., 2010;

von Storch et al., 2019), eddy-induced mixing near western boundaries (Aiki et al., 2016; Zhai et al., 2010) and the generation of Lee waves via the interaction of eddies with the bottom topography (e.g., Nikurashin and Ferrari, 2013; Nikurashin et al., 2013). Those trying to understand the fate of eddy kinetic energy might place considerable hope in the next generation of ocean models. The reason is that some of the models begin to use *sub-mesoscale* horizontal resolution and therefore resolve more of the relevant processes (McWilliams, 2016, 2019).

1.1.2 *Climate*

The oceanic impact on the planetary heat budget and therefore on how the surface warms in response to increased greenhouse gas concentrations is unquestionable (e.g., Church et al., 2013; Griffies et al., 2015; Otto et al., 2013). But what role do ocean eddies play? And when using climate models to estimate the climate sensitivity, how well do common eddy parameterizations perform when being compared to resolved and hence more realistic eddies? The most straightforward approach to this question lies in comparing the climate sensitivity of eddy-resolving models and models that apply a parameterization. To date, only very few of these computationally costly experiments are available and the existing ones agree that if eddies are resolved or not is only one out of many factors determining climate sensitivity (Bryan et al., 2014; Winton et al., 2014, Putrasahan et al. 2020, in prep.).

However, some known deficits of common eddy parameterizations potentially lead to a false representation of the simulated ocean's role in climate change: The vertical ocean heat transport and therefore also the heat uptake from the atmosphere is expected to be poorly represented without resolved eddies (Griffies et al., 2015; von Storch et al., 2016; Wolfe et al., 2008). Furthermore, the ocean mean circulation in some highly climate relevant regions differs significantly between eddy-resolving and coarse-resolution models. These regions include the southern ocean (SO) that takes up huge amounts of carbon (Frölicher et al., 2015; Gnanadesikan et al., 2015; Ito et al., 2010) and heat (Griffies et al., 2015; Marshall and Speer, 2012); the northern hemisphere convection regions that form large parts of the global deep water (Brüggemann and Katsman, 2019; Georgiou et al., 2019; Spall, 2010); and of course the Atlantic meridional overturning circulation (AMOC) that is the largest contributor to the meridional oceanic heat transport (Groeskamp et al., 2017; Marshall et al., 2017b; Romanou et al., 2017). Based on this, it seems surprising that the comparisons between eddying and non-eddying climate models (Bryan et al., 2014; Winton et al., 2014) suggest that eddies are of minor importance for climate sensitivity. Winton et al. (2014) therefore propose that, by shaping the mean circulation, eddies might exert an indirect influence on the climate response that is not reflected within the measure of climate

sensitivity. In the next section, I review the most common ideas on how eddies can affect the circulation and I thereby highlight some gaps in our understanding that I try to fill with this dissertation.

1.1.3 *Circulation*

When the Deepwater Horizon blowout occured in the gulf of Mexico in April 2010, eddies were heavily involved in the advection of oil into the Florida current and ultimately into the North Atlantic ocean (Adcroft et al., 2010). But eddies not only transport *passive* tracers such as oil. They also advect salinity and heat and thus, via their influence on the density distribution, shape the geostrophic mean flow from which they were generated in the first place. It is this interaction between the eddy and the mean field which makes eddy research so interesting.

1.1.3.1 *Non-eddying climate models*

State-of-the-art climate models, such as the current generation of CMIP 6 models, mostly do not capture the ocean mesoscale and hence do not thoroughly represent ocean eddies[1]; these models require eddy parameterizations. Next, I revisit how such parameterizations work and thereby highlight the most important beliefs about the eddies' impact on the mean flow.

Two different eddy parameterizations are commonly used in coarse-resolution ocean models and each of the two relates to one specific eddy effect: The *Redi* parameterization mimics eddy-induced mixing of tracers along density surfaces (Redi, 1982). Consequently, Redi has no effect on mean density and therefore no direct dynamical impact. Nevertheless, it may exert a huge impact on temperature or the distribution of biogeochemical tracers (Pradal and Gnanadesikan, 2014). On the other hand, the *Gent-McWilliams* (GM) parameterization has the potential to modify mean density significantly. It is based on the assumptions that (i) eddies reduce the available potential energy of the mean flow and that they (ii) do this via adiabatic rearrangement of water masses (Gent and Mcwilliams, 1990; Gent et al., 1995). Assumption (ii) relies on the notion of a mostly adiabatic ocean interior (Wüst and Defant, 1936): If in the steady state density budget $\nabla \cdot (\overline{\mathbf{u}}\overline{\rho}) + \nabla \cdot (\overline{\mathbf{u}'\rho'}) = Q$, with $\overline{\mathbf{u}}$ being the 3D mean flow and $\overline{\rho}$ being the mean density, the diabatic forcing Q is set to zero, the eddy flux of density, $\overline{\mathbf{u}'\rho'}$, must be directed *along* isopycnals in an integral sense (Eden et al., 2007b). This then implies that eddies cannot cause diabatic changes to the ocean density field. The adiabatic nature of ocean eddies was intensely discussed (Eden and Greatbatch,

1 This is true with the exception of those CMIP models participating in the High Resolution Model Intercomparison Project (HighResMIP) that prescribes 0.25° horizontal resolution. This is considered *eddy-permitting* (Haarsma et al., 2016).

2008; Eden et al., 2007b; Radko and Marshall, 2004), and challenged in particular for the eddy-rich western boundary currents (Aiki et al., 2016; Eden et al., 2007b; Zhai et al., 2010).

Assumption (i) was already mentioned earlier in this text, it roots in the theory of baroclinic instability developed for atmospheric flow (e.g., Charney, 1947; Eady, 1949). We will see in Section 1.2 that eddies systematically deviate from this assumption in the deep ocean. But before that, I provide some more context on how the parameterization works.

Adiabatic density rearrangements in GM are achieved via an additional advection velocity, the so-called *skew flux* (it arises from the anti-symmetric, skew elements of the diffusivity tensor; Griffies, 1998). For a zonally averaged flow, the skew flux $\mathbf{u}_{\text{eddy}}$ reads

$$\mathbf{u}_{\text{eddy}} = \begin{pmatrix} v_{\text{eddy}} \\ w_{\text{eddy}} \end{pmatrix} = \begin{pmatrix} -\partial(sK_{GM})/\partial z \\ \partial(sK_{GM})/\partial y \end{pmatrix},$$

where $s = -(\partial\overline{\rho}/\partial\overline{y})/(\partial\overline{\rho}/\partial z)$ is the isopycnal slope and K_{GM} the GM diffusivity (Gent and Mcwilliams, 1990). In the most simple case of baroclinic instability near a surface-intensified geostrophic flow, the parameterized skew flux has the form of an overturning that flattens isopycnals *everywhere* (e.g., Olbers et al., 2012). In Figure 1.2 a, I show a schematic of such a GM induced overturning near a surface intensified flow (such as the ACC) which is in geostrophic balance with a sloping density front; in the left part of the front, isopycnals are pushed downwards and in the right part, they are pushed upwards. The effect is a flattening of the density front via the parameterization which is equivalent to a horizontal diffusion of thickness (Gent et al., 1995). Without any resupply of energy, e.g. via wind-driven Ekman pumping, the isopycnals would become horizontal in Figure 1.2 a and thus, the flow would decay to zero after a while. However, if additional energy input is provided, the isopycnals reach a state in which energy input and energy drain through eddies balance each other and this way, GM can set the strength of the geostrophic flow. When introduced in the early 90s, the GM parametrization brought major improvements to ocean models because previous parameterizations did not account for the predominantly adiabatic nature of eddies (Danabasoglu and Mc Williams, 1995; Danabasoglu et al., 1994; Gent, 2011).

1.1.3.2 *Difficulties with the parameterization*

Like all simple representations of complex processes GM has drawbacks. I think that the most important ones can be classified into two groups that I call *region* and *response*.

(i) GM does not distinguish between local and non-local eddy effects and thus cannot represent eddies correctly in certain *regions*. Being based

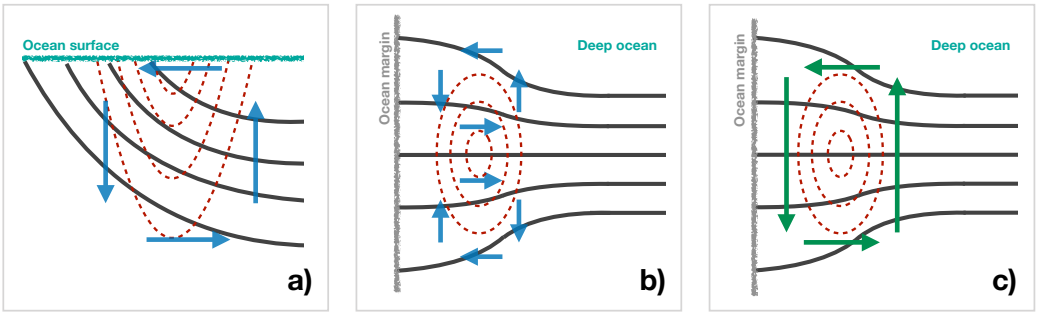

Figure 1.2: Schematic of eddy overturning at different types of flow. The GM-induced flow is shown in blue and the flow induced by realistic eddies in green. Black lines are isopycnals, red lines are mean flow contours for (a) a surface-intensified zonal flow (such as the ACC) and (b-c) a deep flow near a lateral boundary. In case of the deep flow, the parameterized eddies flatten isopycnals *everywhere* (b, two overturning cells in blue), whereas resolved eddies flatten isopycnals in the upper part of the flow but steepen them in the lower part (c, one overturning cell in green).

on baroclinic instability, the parameterization has an effect only where the theory predicts instabilities to occur. In the real ocean, however, eddies generated in one location can be advected to another location. This is most obvious when comparing global maps of eddy kinetic energy (EKE) predicted from baroclinic instability theory on the one hand, and observed or simulated in eddy-resolving ocean models on the other hand. While the predicted EKE is very much centered around the strongest currents, the observed/modeled EKE has a larger horizontal spread (Chen et al., 2014; Vollmer and Eden, 2013). The consequences are severe, because where baroclinic eddies are generated, their *local* effect agrees with the parameterized effect (releasing available potential energy). In contrast, when eddies are carried away from their generation region, several studies find that *non-locally*, eddies have the contrary effect and feed available potential energy to the mean flow (Eden et al., 2007a; Jayne and Marotzke, 2002; Vollmer and Eden, 2013; Waterman and Jayne, 2011, 2012). Analogous to the horizontal dimension, eddies are not confined to the depth level where the baroclinic instability is located but can have a large vertical extent (e.g., Sun et al., 2017). And as for the horizontally non-local eddy effects, we cannot be sure that the vertically non-local eddy effect agrees with what the GM parameterization expects locally. Rather, we will see in Section 1.2 that in certain *regions* such as in the deep western Atlantic, eddies systematically contradict our expectations of releasing available potential energy.

(ii) Furthermore, GM is not able to *respond* correctly to perturbations of the ocean mean state and thus may function in one particular setting but fail in another. Two prominent examples where this leads to a false response behavior of the ocean mean state itself lie in the southern

ocean (SO): The Antarctic circumpolar current (ACC) as well as the SO meridional overturning are strongly controlled by the inclination of the SO isopycnals (Marshall and Speer, 2012; Vallis, 2017); for the anticipated intensification of the SO westerlies (due to climate change, Gillett and Fyfe, 2013; Marshall, 2003; Thompson and Solomon, 2002), coarse-resolution ocean models with the standard GM parameterization predict a strong steepening of these isopycnals. In contrast, in eddy-resolving models, stronger winds mainly intensify the eddy field, which then compensates for some of the isopycnal steepening. This leads to a reduced wind sensitivity of the SO meridional overturning (Abernathey et al., 2011; Hallberg and Gnanadesikan, 2006; Henning and Vallis, 2005) and the ACC (Hallberg and Gnanadesikan, 2001; Marshall et al., 2017a; Munday et al., 2013). In Section 1.3, I show that eddies are also heavily involved in the response of the northern hemisphere (NH) overturning to wind forcing changes. And like in the mentioned examples, GM cannot correctly parameterize the eddy part of the response. This, however, is not due to the incorrect representation of eddy density fluxes but due to the missing representation of eddy momentum fluxes. The relation of the two types of fluxes and their impact on the mean flow is subject of the next sections.

1.1.3.3 *Another view on eddy fluxes*

So far, we have looked at how eddies affect density and noticed that they flatten isopycnals in regions where they are generated; less tilted isopycnals mean that less potential energy is available and via the thermal wind relation, this implies a weaker mean flow. But how can this impact of eddies on the *flow* be formalized? Greatbatch and Lamb (GL, 1990) were the first to show that adding a GM-like skew flux to the advection velocity in the density budget is equivalent to including an additional vertical mixing of horizontal momentum in the momentum equation. The effect of eddies (in the GM and the GL formulation) thus can be viewed as a smoothing of horizontal momentum in the vertical or a barotropization of the flow (Treguier et al., 2017).

That both formulations are indeed equivalent can be easily shown for the case of zonally averaged zonal flow via the transformed Eulerian mean (TEM) version of the momentum equation (Andrews and McIntyre, 1976, 1978; Vallis, 2017):

$$\frac{\partial \overline{u}}{\partial t} = f_0 \overline{v}^* + \frac{\partial}{\partial z}\left(\frac{f_0}{N^2}\overline{v'b'}\right) - \frac{\partial}{\partial y}\overline{v'u'}, \tag{1.1}$$

where f_0 is the reference Coriolis frequency and N^2 the buoyancy frequency. Please note that for convenience we use buoyancy $b = -g\rho/\rho_0$ instead of density here in contrast to the remainder of the manuscript.

In TEM, $\overline{v}^*$ is the residual flow, consisting of the Eulerian flow plus the eddy-induced flow,

$$\overline{v}^* = \overline{v} - \frac{\partial}{\partial z}\left(\frac{1}{N^2}\overline{v'b'}\right).$$

In GM, the latter is parameterized as the above mentioned skew flux (see also Figure 1.2 a for an example of such a skew flux) via the downgradient formulation $\overline{v'b'} = -K_{GM}\partial\overline{b}/\partial y$. Implementing this into the TEM momentum budget in Equation 1.1 and using the thermal wind relation $\partial\overline{b}/\partial y = -f_0\partial\overline{u}/\partial z$, the term containing the meridional eddy density flux in Equation 1.1 transforms to a vertical stress;

$$\frac{\partial\overline{u}}{\partial t} = f_0\overline{v}^* + \frac{\partial}{\partial z}\left(K^*\frac{\partial\overline{u}}{\partial z}\right) - \frac{\partial}{\partial y}\overline{v'u'}. \tag{1.2}$$

The vertical viscosity, $K^* = K_{GM}f_0^2/N^2$, is related to the original GM thickness diffusivity and in eddying ocean regions, it is expected to be much higher than the molecular viscosity (Greatbatch and Lamb, 1990). Although developed in the same year as GM, by that time the GL formulation was not implemented in ocean models on a large scale. However, it finds application in analytical models, e.g. of the ACC (e.g., Marshall et al., 2017a).

1.1.3.4 *Eddy momentum fluxes*

There is one term left in the TEM momentum budget (Equation 1.1) that was not yet mentioned, the Reynolds stress convergence $-\partial(\overline{v'u'})/\partial y$. It is known to drive recirculation gyres (Holland and Rhines, 1980; Lozier, 1997; Rhines and Holland, 1979) or jet extension flows (Aoki et al., 2016; Waterman and Hoskins, 2013; Waterman and Jayne, 2011, 2012). Yet, for many aspects of ocean circulation, Reynolds stresses (or eddy momentum fluxes) are expected to be negligible as compared to the above described eddy density fluxes (Eden, 2010; Hogg, 1983). We already said that the density flux can be interpreted as a vertical flux of zonal momentum (in the example of Equation 1.1). In contrast, the role of the momentum flux is to redistribute zonal momentum laterally[2], as can be seen from the meridional derivative in the last term of Equation 1.1.

Spall (1994) provides one out of few examples where eddy momentum fluxes are important at depth. In his idealized model of a deep boundary current, eddy momentum fluxes (and their counterpart in the vorticity equation) are an important control for the strength of the deep mean current and its recirculation. In Section 1.3, I present an example in which

2 Both fluxes can be written as *Eliassen Palm flux vector* (Andrews and McIntyre, 1976), $\mathbf{F} = (-\overline{u'v'}, f_0\overline{v'b'}/N^2)$. Then, Equation 1.1 becomes $\partial\overline{u}/\partial t = f_0\overline{v}^* + \nabla_x \cdot \mathbf{F}$, with $\nabla_x = (\partial/\partial y, \partial/\partial z)$. Momentum fluxes are on the horizontal, density fluxes on the vertical axis of the vector.

eddy momentum fluxes play an important role near the DWBC. They shape the response to changes in the surface wind stress.

As the last part of this introductory section, I now briefly review what is known about *deep eddies*.

1.1.4 *Deep eddies*

Most of the existing research on deep eddies is confined to certain geographical settings such as the Arctic ocean (Aagaard et al., 2008; Carpenter and Timmermans, 2012), the South China sea (Chen et al., 2015; Zhang et al., 2014) or the Mediterranean outflow (Bashmachnikov et al., 2009; Richardson et al., 1989, 2000). All of the above mentioned deal with eddies that are generated due to a particular combination of local topography and hydrography. For example, Carpenter and Timmermans (2012) describe how a certain type of anticyclonic eddy forms again and again near a deep overflow in the Canada basin. In those studies, the main interest lies rather in eddies as carriers of tracers and less on their dynamical impact on the flow.

In contrast, only few publications investigate deep eddies from a statistical, more general perspective that is independent of particular geographical settings. This is surprising because the deep ocean exhibits strong mean currents, some of which are meridionally oriented and therefore quite susceptible to baroclinic instability (Pedlosky, 2013; Smith, 2007). One such deep meridional current is the DWBC in the Atlantic, and several observational (Fischer et al., 2015; Lee et al., 1996; Schott et al., 2005; Stöber et al., 2008; Whitworth et al., 1991) as well as modeling studies (Dengler et al., 2004; Handmann et al., 2018) have mentioned eddy activity in its vicinity. Those eddies are subject to the next section, where I summarize the results of my first paper.

1.2 EDDY FLUXES NEAR THE DEEP WESTERN BOUNDARY CURRENT

One fundamental difference between a surface-intensified geostrophic flow, such as the ACC (sketched in Figure 1.2 a), and a flow that has its maximum velocity in the middle of the water column (a *deep* flow) is that the latter requires a sign change in the vertical flow shear at its core (the level of maximum flow). In Figure 1.2 b, red dashed lines sketch the contours of the DWBC in the northern hemisphere together with the density profile (black lines) that satisfies the thermal wind balance $\rho_0 \partial\overline{\rho}/\partial x = -f_0 g \partial\overline{v}/\partial z$ (please note that the flow is a mostly meridional flow that is directed southwards, it is located in the northern hemisphere so that $f_0 > 0$). *Below* the DWBC core, the density gradient points to the right (in the positive zonal direction, $\partial\overline{\rho}/\partial x > 0$) and the negative

meridional velocity increases ($\partial\overline{v}/\partial z < 0$). *Above* the core, the zonal density gradient and the vertical shear reverse sign.

Earlier in the manuscript, I wrote that observations (e.g., Whitworth et al., 1991) and models (e.g., Dengler et al., 2004) suggest eddy activity near the DWBC. The eddy-resolving STORM configuration (0.1° horizontal resolution in the region of interest at at low- and mid latitudes, von Storch et al., 2012) of the Max-Planck-Institute ocean model (MPI-OM) provides further evidence for a vigorous deep eddy field in the western Atlantic. And 3D snapshots of the deep flow (Figure 2.2) qualitatively support what the secondary EKE maximum at 13° N already suggested (Figure 1.1): Surface and deep eddies belong to two distinct eddy fields that are vertically separated by a level of lower EKE.

But how do these deep eddies interact with the deep density field near the DWBC, given the fact that the density structure of a deep flow differs from that of a surface-intensified flow? According to the assumption made within the GM framework, the *parameterized* skew flux (blue arrows in Figure 1.2) now has to consist of two distinct cells in order to flatten isopycnals everywhere in the water column. In this context, looking at *resolved* eddies in the STORM model, I ask the following two questions for the first paper (Lüschow et al., 2019):

1. What is the effect of the deep eddies on the DWBC mean density?
2. What are the implications for the DWBC mean flow?

In order to answer those questions I look at five individual DWBC segments from 25° N to 20° S, and analyze in the time averaged density budget, $\overline{\mathbf{u}} \cdot \nabla\overline{\rho} = -\nabla \cdot \overline{\mathbf{u}'\rho'} + Q$, the imprint of eddy density fluxes, $\overline{\mathbf{u}'\rho'}$, on the mean density $\overline{\rho}$. Averaging all quantities of interest along these segments of roughly 200 km length in the along-stream direction enhances the signal to noise ratio and eliminates spurious rotational eddy fluxes (Eden et al., 2007a; Griesel et al., 2014; Jochum and Malanotte-Rizzoli, 2004); at the same time, it allows me to distinguish between different parts of the DWBC.

1.2.1 *Two eddy density flux regimes in the vertical*

Instead of flattening isopycnals at all depth levels (as indicated by the blue arrows in Figure 1.2 b for the GM parameterization), resolved eddies flatten isopycnals *above* the DWBC core but steepen them *below*. Green arrows in Figure 1.2 c sketch the skew flux of the resolved eddies, it consists not of two cells as anticipated by GM but of only one cell that spans the whole vertical extent of the DWBC.

We need to leave the picture of the simplified density profiles sketched in Figure 1.2 in order to understand why the resolved eddies behave differently from the parametrized ones. In the ocean, evenly distributed isopycnals in density space are not evenly distributed in depth space.

Instead, the horizontal and vertical density shear (stratification) strongly increase when going up in the water column. What does this mean for the generation of eddies? We said earlier that in particular a strong horizontal density shear facilitates baroclinic instability; the likelihood of a flow to become baroclinically unstable and hence to generate eddies can be measured by the *Eady growth rate* (Olbers et al., 2012); and in case of the DWBC, the Eady growth rate has a maximum above the DWBC core (not shown) and therefore it is likely that those deep eddies are primarily generated above the DWBC core. My conclusion is that the steepening below the core is a side effect of eddies that are generated above the core, which is in agreement with earlier studies that distinguish between local and non-local eddy effects (e.g., Waterman and Jayne, 2012). As explained in Section 1.1.3, non-local effects cannot be captured by a GM-like parameterization.

1.2.2 *Mean overturning normal to the DWBC*

Diabatic contributions Q in the density budget turn out to be rather small near the DWBC and hence the main balance is between the density advection by the mean flow and the eddy density flux divergence (Lüschow et al., 2019). The Eulerian mean flow that balances the eddy effect is mainly in the plane normal to the DWBC and it has the form of a *pseudo-zonal* overturning circulation (it is normal to the DWBC which is not always strictly meridionally oriented). In the northern hemisphere, the overturning is oriented clockwise with upwelling close to the shore and downwelling further offshore. In the southern hemisphere, it switches orientation in agreement with the sign change in the Coriolis parameter. Signatures of this mean overturning are visible in the upwelling in 1900 m depth (Figure 1.3 middle). The zoom-in on the mid-latitude northern Atlantic shows the mentioned dipole structure with upwelling close to the shore and downwelling further offshore along the DWBC path. The bottom panel in Figure 1.3 shows the eddy-driven part of that upwelling that can be obtained from the mean density budget[3]. It explains most of the total upwelling. For comparison, I show the upwelling in the non-eddying GR15 model (1.5° horizonzal resolution, Figure 1.3 top). It contains no upwelling dipoles, providing further evidence for the importance of eddy density fluxes for the vertical flow in the western Atlantic.

The global map of deep upwelling shows that similar overturning circulations might also exist in other regions of the world ocean that exhibit deep boundary currents. In particular the North Pacific contains a strong upwelling dipole that apparently is mainly eddy-driven (Figure 1.3 middle and bottom). Like in the Atlantic, those eddies are perhaps

3 $\overline{w} = -\nabla \cdot \overline{\mathbf{u}'\rho'}/\overline{\rho}_z - \mathbf{u}_H \cdot \nabla_H \overline{\rho}/\overline{\rho}_z = w_{\text{Eddy}} + w_{\text{Horizontal}}$

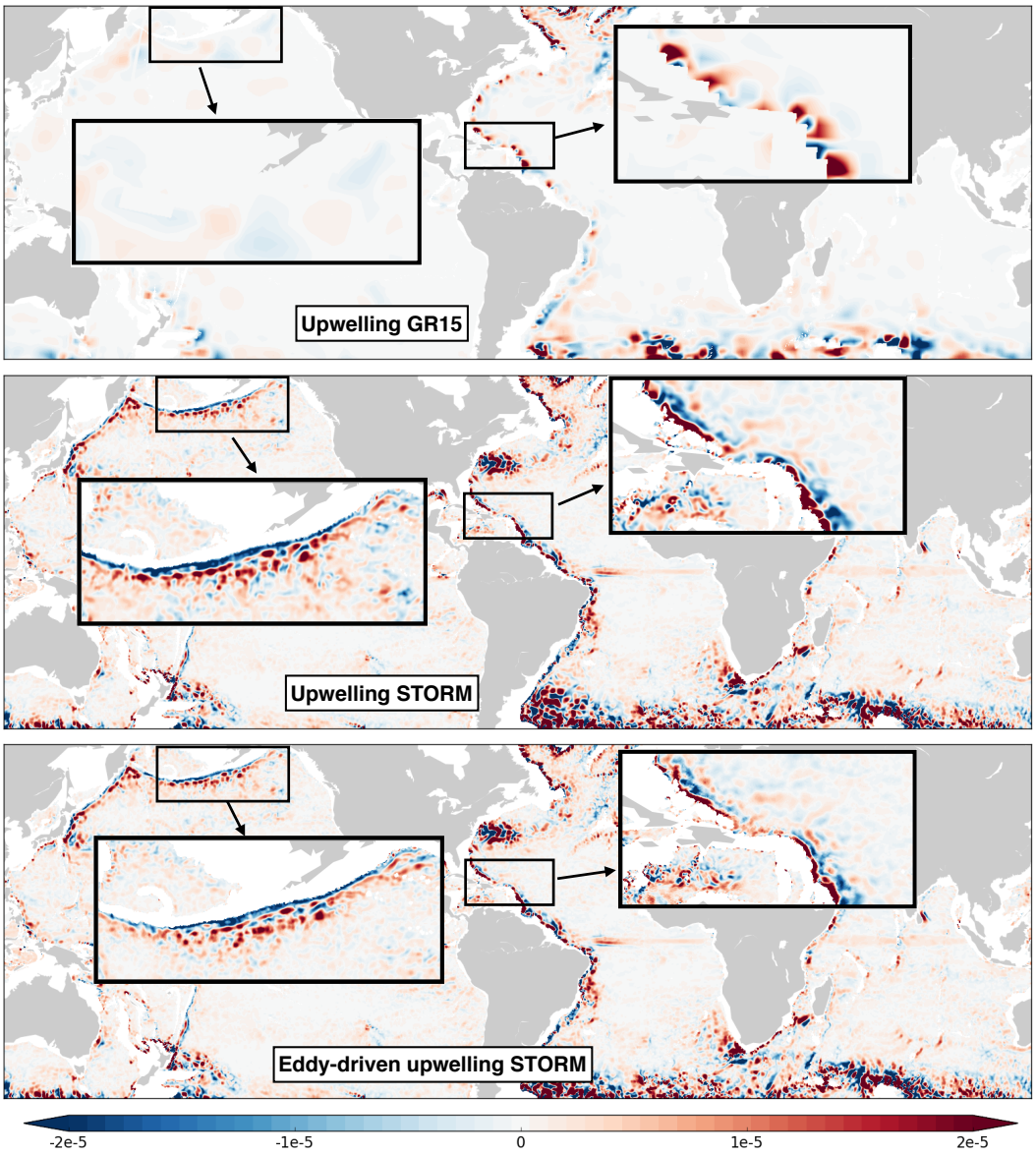

Figure 1.3: Upwelling at 1900 m depth in the non-eddying, coarse-resolution model GR15 (top), in the eddy-resolving STORM model (middle) and the part of the upwelling in STORM that is eddy-driven, $-\nabla \cdot \overline{\mathbf{u}'\rho'}/\rho_z$ (bottom). In the middle panel, the dipole structure in the right zoom-in shows the mean overturning normal to the DWBC with upwelling (positive) close to the shore and downwelling (negative) further offshore.The dipole is, at least partly, eddy-driven, as can be seen from the bottom panel. A similar structure can be found in the northern Pacific. The non-eddying model does not show any dipole and it has generally much weaker upwelling (top).

generated by the existing Pacific deep boundary currents (Hallock and Teague, 1996; Hautala, 2018; Kawabe and Fujio, 2010).

1.2.3 *Deepening of the DWBC via eddy density fluxes*

Perhaps even more interesting than the eddy-induced pseudo-zonal overturning is the impact of eddies on the DWBC flow itself. As mentioned above, in the TEM framework eddy density fluxes can be interpreted as a tendency term in the momentum equation. Similar to Equation 1.1, one can relate the mostly meridionally oriented DWBC flow to the mostly zonally oriented across-stream eddy density flux[4]. Evaluating this eddy density contribution to the momentum budget for the different segments of the DWBC, one finds that indeed, eddies tend to slow down the flow above the core and accelerate it below (not shown). Thereby, I provide the momentum view on what I show via the available potential energy in Lüschow et al. (2019): Eddies release energy from the mean above, and feed energy to the mean below the core. This leads to a net deepening of the DWBC through eddies and possibly explains why non-eddying models are reported to have a too shallow DWBC (Baehr et al., 2004).

What I presented in this section (and in Lüschow et al. (2019)) is an example of an eddy effect that cannot be captured by common parameterizations because it occurs in a *region* in which eddies are not generated, it is an example of a non-local eddy effect. I said earlier that parameterized eddies can also lie at odds with their realistic counterpart because the setting in which the parameterization operates changes. In the next section, I present simulations in which the ocean surface wind forcing was changed. We will see that a model in which eddies are resolved shows a different *response* to setting changes than a model in which eddies are parameterized.

1.3 THE RESPONSE BEHAVIOR OF AN EDDYING DEEP WESTERN BOUNDARY CURRENT

The DWBC has two roles in the meridional overturning circulation: On the one hand, it transports North Atlantic deep water (NADW) from the northern hemisphere convection regions towards the South and thereby constitutes the deep limb of the upper overturning cell. We usually refer to this upper cell when saying AMOC. On the other hand, the DWBC carries Antarctic bottom water (AABW) southwards that is initially formed in the southern ocean (SO), before it flows northwards in the abyss and successively gets upwelled into the DWBC (Herrford et al., 2017; Lumpkin and Speer, 2007). Thus, in its second role, the DWBC constitutes the upper limb of the bottom overturning cell which we usually refer

4 $\partial\overline{v}/\partial t = -f\overline{u}^* - \partial(f_0\overline{\mathbf{u}'\rho'}/N^2)/\partial z - \partial(\overline{v'u'})/\partial x$

to as AABW cell. However, the first role receives disproportionately more attention among researchers than the second one, perhaps due to the great importance of the upper overturning cell for our climate (e.g., Lynch-Stieglitz, 2017; Marshall et al., 2015).

In particular, the consequences of a future intensification of the SO westerlies with climate change (e.g., Gillett and Fyfe, 2013; Thompson and Solomon, 2002) are mostly under investigation with a focus on the upper overturning cell only. Yet, disregarding the bottom cell and consequently the second role of the DWBC results in a common misbelief: The DWBC (which is then seen only as carrier of NADW) must intensify if the upper overturning cell strengthens due to the elevated wind stress (e.g., Toggweiler and Samuels, 1995). In the second paper (Lüschow et al., 2020, in prep.), I analyze sensitivity experiments with the eddying STORM model in which a wind stress doubling leads to an intensification of the upper overturning cell and at the same time to a slow down of the DWBC. Regarding the transport balance of the two cells, this scenario becomes possible if the upper cell strengthening is accompanied by a lower cell weakening whose magnitude is larger than that of the upper cell strengthening. I am not aware of experiments that observe a similar DWBC response behavior. The key difference between my experiments and previous ones that look at the deep overturning sensitivity to wind forcing changes (Brix and Gerdes, 2003; Rahmstorf and England, 1997) is that the model used here *resolves* eddies. Thus, my research questions are:

1. Is the observed DWBC slow down that occurs as a response to the wind stress doubling related to mesoscale eddies?
2. And if yes, what are the implications for our understanding of the overturning response in the real (eddying) ocean?

To answer these questions I run an uncoupled twin experiment with the non-eddying GR15 and the eddying STORM configuration of the same ocean model, MPI-OM. The control run applies the standard NCEP forcing and in the sensitivity run the wind stress was doubled globally. Response differences between the eddying and the non-eddying configuration are likely to arise from resolution differences and hence are potentially related to mesoscale eddies. However, due to the resolution difference, the two configurations were in different basic states before applying the wind stress doubling. Disentangling response differences that are due to different basic states from those that are due to different resolutions is not trivial. However, in the following I provide arguments why the DWBC slow down can indeed be related to eddies.

1.3.1 *Eddies and the DWBC slow down*

Spall (1994) was the first to apply the ideas of Rhines and Holland (1979) and Holland and Rhines (1980) about eddy-driven recirculations to a deep boundary current. In his three layer model of the Brazil basin, he finds that the flow speed of the northward propagating AABW as well as the direction of its recirculation depend on whether the flow is stable or unstable (eddying). His explanation is based on eddy vorticity fluxes, which transport vorticity laterally out of the boundary current and thereby control the flow speed and the recirculation. Although his model is very much idealized and deals with the northward flowing AABW instead of the southward directed DWBC, the very concept of deep eddies fluxing vorticity laterally out of a mean current can be transferred to our case: The above described DWBC slow down is balanced by eddy fluxes of relative vorticity in the DWBC vorticity budget[5],

$$\beta \Delta \overline{v} \approx \Delta \frac{\partial^2}{\partial x^2} \overline{u'v'}, \tag{1.3}$$

where the Δ - symbol expresses a *response*; it refers to a difference between a quantity in the simulation with doubled wind stress and the control simulation. Thus, $\Delta\overline{v} > 0$ is the slow down of the southward directed (negative) DWBC[6]. The term on the right-hand-side is the response in the eddy flux of relative vorticity[7], it is likewise positive which indicates the reduction of negative vorticity, here. β denotes the meridional gradient of the Coriolis parameter. The given relation between DWBC slow down and eddy vorticity fluxes holds for the along-stream averaged DWBC between 20° N and 5° N which is a large fraction of the coherent part of the DWBC in the northern hemisphere mid-latitudes (Buckley and Marshall, 2016). As per the definition of a flux, the eddy vorticity flux can only redistribute vorticity, in this case laterally out of the boundary current. In the west of the current, this vorticity can be dissipated by boundary friction. What happens to the vorticity that is fluxed to the east towards the interior ocean is an interesting question for future research.

The balance in Equation 1.3 is an empirical statement and therefore, by itself, does not contain information about a causal relationship between the DWBC slow down and eddy fluxes. By analyzing the response chronology, the origin of the additional EKE near the DWBC and by comparison against an experiment in which the wind stress was not doubled

5 I use the along-stream averaged, quasi-geostrophic version of the vorticity equation (Olbers et al., 2012).

6 Please note that (u, v) is not exactly the zonal and meridional flow but in this case is the flow in the across-stream direction x, and along-stream direction y.

7 The cross-stream eddy flux of relative vorticity, $\overline{u'\zeta'}$, simplifies to $-\partial(\overline{u'v'})/\partial x$ when averaging in the along-stream direction (Vallis, 2017). In the along-stream averaged vorticity budget, only the across-stream convergence of the vorticity flux, $\partial^2(\overline{u'v'})/\partial x^2$, remains.

globally but only over the SO, I provide arguments that the response in the eddy field (right-hand-side of Equation 1.3) was triggered by an interaction between the DWBC and the overlying northward surface flow. This suggests that the DWBC slow down could indeed be *caused by* the eddy vorticity fluxes. However, further investigation is necessary to corroborate this speculation. Nevertheless, I can conclude from the diagnosed balance between DWBC slow down and eddy vorticity fluxes that without resolved eddies, the slow down would be unbalanced or balanced differently and hence cannot occur in this fashion. Thereby, I provide strong evidence that the response differences between the eddying STORM and the non-eddying GR15 are indeed related to resolution.

1.3.2 *Implications for the overturning response to forcing changes*

Evidence gained from various paleo proxies and climate simulations suggests a link between the AMOC and the AABW overturning cell (Broecker, 1998; Martin et al., 2015; Stocker, 1998). This link was named *ocean seesaw*, indicating that a weakening of the lower cell can lead to a strengthening of the upper cell and vice versa (Seidov et al., 2001). Patara and Böning (2014) even speculate that the retreat of the AABW cell induced by SO warming may cause an AMOC increase that might compensate for some of the anticipated AMOC weakening during the 21st century (Weaver et al., 2012).

The question is, how can the relation between the DWBC slow down and eddy vorticity fluxes (Section 1.3.1) contribute to our understanding of the ocean seesaw? A comparison to previous sensitivity experiments that analyze the ocean seesaw is not straightforward; in particular, the strengthening of the upper overturning cell in my experiments can either be due to the direct impact of the SO wind stress doubling (i.e. the Drake passage effect, Toggweiler and Samuels, 1995) or due to a seesaw-like effect, i.e. via a weakening of the bottom overturning cell. In contrast, earlier studies perturb the bottom overturning cell directly and then investigate the response of the upper cell[8] (Brix and Gerdes, 2003; Martin et al., 2015; Patara and Böning, 2014). However, earlier seesaw experiments that use non-eddying resolution and my experiment with the non-eddying GR15 configuration have in common that the responses in the upper and bottom overturning cells are of similar magnitude. Similar response magnitudes imply that the DWBC transport stays relatively constant. Therefore, I argue that the DWBC slow down, which I show depends on the presence of eddies, enables larger response differences between the upper and the bottom cell. In other words, resolving eddies

8 This might be worth trying in the STORM configuration because it could help to disentangle the impact of wind stress doubling and bottom cell weakening on the upper cell.

in a model, which is then probably closer to the real ocean, *decouples* the two overturning cells and thereby loosens the ocean seesaw.

1.4 CONCLUSION AND OUTLOOK

The initial motivation for this dissertation came from the observation that eddy kinetic energy is significantly elevated not only near the strong surface currents but also near the deep mean currents (von Storch et al., 2012). It turned out that the interaction of those *deep eddies* with the deep mean circulation had not yet been investigated systematically. The eddy-resolving STORM configuration of the Max Planck Institute ocean model is a powerful tool to begin this enterprise.

In the first part of the project (Section 1.2), I show that deep eddies have *vertically non-local* effects that conflict with the assumption of eddies releasing available potential energy. More specifically, eddies systematically steepen isopycnals below the core of the DWBC and thereby feed potential energy to the mean. I argue that the isopycnal steepening at large depth is a side effect of eddies that were generated further up in the water column. Similar non-local effects were already observed in the horizontal, but not yet in the vertical dimension. Two consequences arise: (i) A mean overturning circulation in the plane normal to the DWBC balances the anomalous effect of the eddies. It is clockwise oriented in the northern hemisphere (when looking northwards) with upwelling close to the shore and downwelling further offshore; it changes its orientation in the southern hemisphere. A global map of the deep vertical flow shows similar upwelling dipoles in many other regions of the world, some of which contain deep boundary currents. Hence, it seems beneficial to transfer this analysis to other deep currents. Furthermore, the eddy-induced mean overturning cells potentially play a role for the ventilation of the deep ocean. (ii) Down-gradient eddy fluxes above the core and up-gradient fluxes below the core cause a net *deepening* of the flow. The latter kind of eddy effect is not captured by the widely used GM parameterization so that the deepening effect is missing in models that depend on the parameterization. Therefore, the deepening by resolved eddies provides a potential explanation for reports of a too shallow DWBC in coarse-resolution ocean models (e.g., Baehr et al., 2004). If future eddy parameterizations want to handle this issue they need to identify the location (depth level) of eddy generation and accordingly, produce a non-local effect where eddies are not generated but still expected to have an influence.

In a second step (Section 1.3), I analyze the overturning response to an increase in the surface wind stress and thereby provide a novel perspective on why eddies are crucial for the reaction of the meridional

overturning to forcing changes. It is well known that the ACC or the SO meridional overturning respond quite differently to forcing changes in eddying and non-eddying ocean models (Bishop et al., 2016; Gent, 2016; Munday et al., 2013). However, I show that the response of the Atlantic DWBC, which closes the upper and bottom overturning cell in the southward direction, is of opposite sign if eddies are resolved instead of parameterized. This contrast in the response can be attributed to the action of eddy vorticity fluxes in the DWBC vorticity budget of the eddying simulation. Because the non-eddying simulation does not contain those eddy fluxes, it is not capable of producing the same reaction. What does this mean for the response of the real ocean to the anticipated strengthening of the SO westerlies (Gillett and Fyfe, 2013)? My findings suggest that the previously hypothesized link between the upper and bottom overturning cell (ocean seesaw, Broecker, 1998) might be weaker than expected because the DWBC does not couple both cells but instead is able to act rather independently. Further investigation of the ocean seesaw in eddying setups is required to make this statement more robust. For example, future research should analyze the overturning response to perturbations in the buoyancy field in the spirit of Patara and Böning (2014). A further line of inquiry could be the analysis of the interaction between surface northward flow, DWBC southward flow and AABW northward flow in a simplified setting such as the quasi-geostrophic layer model from Le Bras et al. (2018) or Jayne et al. (1996).

This dissertation builds on knowledge that was gained during the last decades by studying surface eddies, and applies it to those occurring in the deep ocean. Thereby, two exciting new facets of eddy dynamics were revealed. I am convinced that current generation eddy-resolving ocean models enable us to discover further unknown eddy phenomena at depth. However, future effort has to keep in mind that discoveries from models need to be explored in the real ocean. While writing this, I hope that some of the findings presented here can be confirmed by observations in the future.

2

DIAGNOSING THE INFLUENCE OF MESOSCALE EDDY FLUXES ON THE DEEP WESTERN BOUNDARY CURRENT IN THE 1/10° STORM/NCEP SIMULATION

THIS PAPER HAS BEEN PUBLISHED AS:

Lüschow, Veit, Jin-Song von Storch, and Jochem Marotzke. "Diagnosing the Influence of Mesoscale Eddy Fluxes on the Deep Western Boundary Current in the 1/10° STORM/NCEP Simulation." *Journal of Physical Oceanography* 49.3 (2019): 751-764.

AUTHOR CONTRIBUTIONS

VL and JSvS outlined the research questions. VL performed the research and drafted the manuscript with input from JSvS and JM. All authors contributed ideas to the interpretation of the results.

Diagnosing the Influence of Mesoscale Eddy Fluxes on the Deep Western Boundary Current in the 1/10° STORM / NCEP Simulation

Veit Lüschow, Jin-Song von Storch and Jochem Marotzke

Max Planck Institute for Meteorology, Bundesstr. 53, 20146 Hamburg, Germany

ABSTRACT

Using a 0.1-degree ocean model, this paper establishes a consistent picture of the interaction of mesoscale eddy density fluxes with the geostrophic deep western boundary current (DWBC) in the Atlantic between 26°N and 20°S. Above the DWBC core (the level of maximum southward flow, ~ 2000 m depth), the eddies flatten isopycnals and hence decrease the potential energy of the mean flow, which agrees with their interpretation and parametrization in the Gent-McWilliams framework. Below the core, even though the eddy fluxes have a weaker magnitude, they systematically steepen isopycnals and thus feed potential energy to the mean flow, which contradicts common expectations. These two vertically separated eddy regimes are found through an analysis of the eddy density flux divergence in stream-following coordinates. In addition, pathways of potential energy in terms of the Lorenz energy cycle reveal this regime shift. The two-fold eddy effect on density is balanced by an overturning in the plane normal to the DWBC. Its direction is clockwise (with upwelling close to the shore and downwelling further offshore) north of the equator. In agreement with the sign change in the Coriolis parameter, the overturning changes direction to anti-clockwise south of the equator. Within the domain covered in this study, except in a narrow band around the equator, this scenario is robust along the DWBC.

2.1 INTRODUCTION

Mesoscale eddies can contribute about 2/3 to the overall kinetic energy budget of the oceans (von Storch et al., 2012). In recent years, the increasing availability of eddy-resolving global ocean simulations (**vonStorch2016**; e.g., Griffies et al., 2015) as well as high resolution altimetry (e.g., Chelton et al., 2007) have substantially enhanced our knowledge of how eddies affect the large-scale ocean circulation. However, research on eddies has predominantly focused on those occurring near the surface,

while deep eddies and their interaction with deep ocean currents has received little attention. Here, we address one such current, namely the deep western boundary current (DWBC) in the Atlantic, and describe its interplay with mesoscale eddy fluxes.

The DWBC is expected to constitute the deep limb of the Atlantic meridional overturning circulation (AMOC, Fine, 1995). Yet, recent observational studies question the continuous nature of the DWBC, in particular near the Grand Banks at 42°N, and stress the importance of interior pathways for north Atlantic deep water (NADW) towards the south (Bower et al., 2009; Fischer and Schott, 2002). However, most authors agree that south of the Bahamas, the DWBC is a more or less coherent current and the primary conduit for NADW (Buckley and Marshall, 2016; Garzoli et al., 2015; Rhein et al., 2015). Hence, we focus our attention on the DWBC segment between the Bahamas (26°N) and the Trinidad seamount chain (20°S) where the DWBC is expected to become less coherent (Garzoli et al., 2015). Numerous observational records exist in this DWBC segment, and several of them report strong eddy activity (Dengler et al., 2004; Garzoli et al., 2015; Lee et al., 1996; Schott et al., 2005). According to the prevailing interpretation of eddy-mean flow interaction, eddies originate from baroclinic instabilities and act to release potential energy from the mean flow which is supported by the large-scale buoyancy or wind forcing (Charney, 1947; Gill et al., 1974). The Gent-McWilliams (GM) parametrization of mesoscale eddies, widely used in coarse-resolution ocean models, likewise follows this notion of eddies and flattens isopycnals via an additional eddy-induced advection (Gent et al., 1995). However, several authors report huge spatial variations as well as sign changes in the so called thickness-diffusivity κ that sets the magnitude of the additional advection (e.g., Eden et al., 2007a; Jayne and Marotzke, 2002). Sign changes in κ imply that eddies partly behave contrary to expectations by feeding potential energy to the mean flow. In this study, we address this confusion and clarify the effect of mesoscale eddy fluxes on the mean density distribution near the DWBC. To the best of our knowledge, this issue has not been investigated in the existing literature. We use the STORM / NCEP simulation, performed with the Max Planck-Institute Ocean Model (MPI-OM) at 0.1° horizontal resolution; because we expect the 0.1° model to resolve the major part of the eddy field, the GM-parametrization is switched off.

We begin this paper by assessing the ability of the STORM model to represent the observed DWBC (Section 2.2). In the same section, we provide a brief phenomenology of the simulated eddy-field near the DWBC, which is less known from observations. The results (Section 2.3) is organized in three segments: In the first segment (2.32.3.1), we analyze in detail the effect of the eddy density flux on the mean density. The second segment (2.32.3.2) takes a different perspective on the same issue and investigates pathways of potential energy near the DWBC. We dedicate

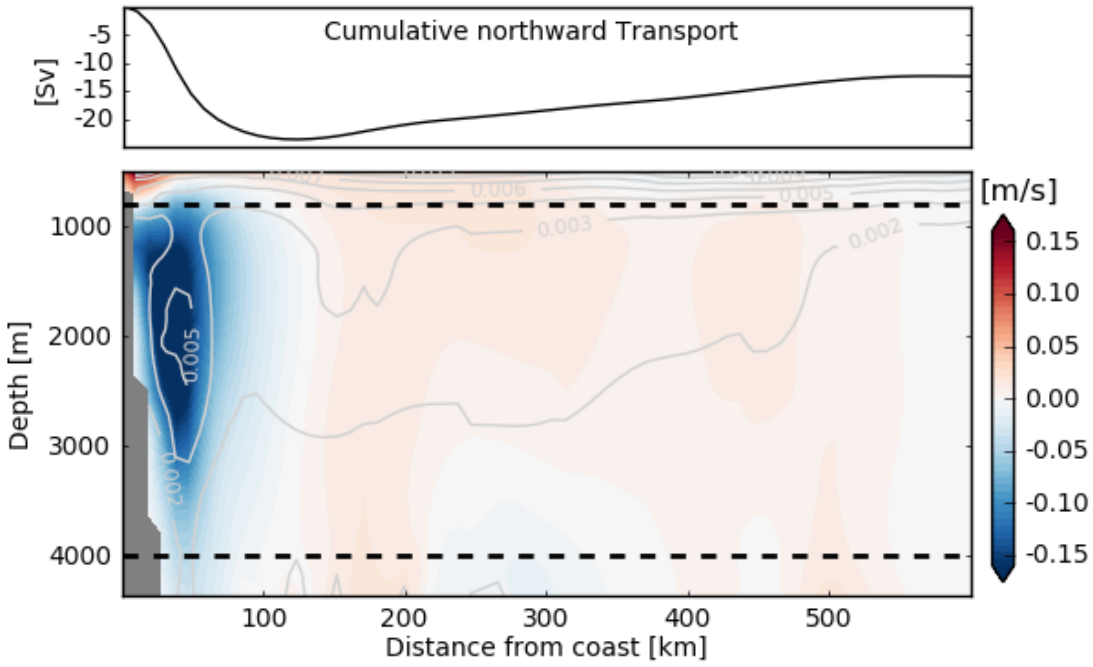

Figure 2.1: (Top): STORM cumulative meridional transport of NADW between 800 m and 4000 m depth. The transport is computed from the western boundary eastwards. (Bottom): Meridional section along 26.5°N. Meridional flow in colors (positive, red northwards). Grey contour lines show eddy kinetic energy (in m^2s^{-2}, EKE), the dashed lines define the layer of NADW, i.e. the area of DWBC transport relevant for the cumulative transport (top).

the third segment (2.32.3.3) to a mean circulation in the plane normal to the DWBC that balances the effect of eddy density fluxes on mean density. Section 2.4 provides our conclusions.

2.2 AN EDDYING DWBC IN THE STORM SIMULATION

We use the global ocean model MPI-OM, forced with NCEP-NCAR reanalysis-1 data (Kalnay et al., 1996) in the STORM configuration. It has a horizontal resolution of 0.1° near the equator. The model has 80 depth levels, with the layer thickness increasing from about 50 m to 150 m over the DWBC depth range, allowing for a reasonable representation of the vertical structure of the DWBC. The simulation was run from 1948-2010; here, we use the last 10 years of model output. Further details on the model can be found in von Storch et al. (2012), Li and von Storch (2013) and **vonStorch2016** present additional results inferred from this STORM simulation.

The STORM model represents the observed DWBC reasonably well in its meridional velocity magnitude and its lateral and vertical extension.

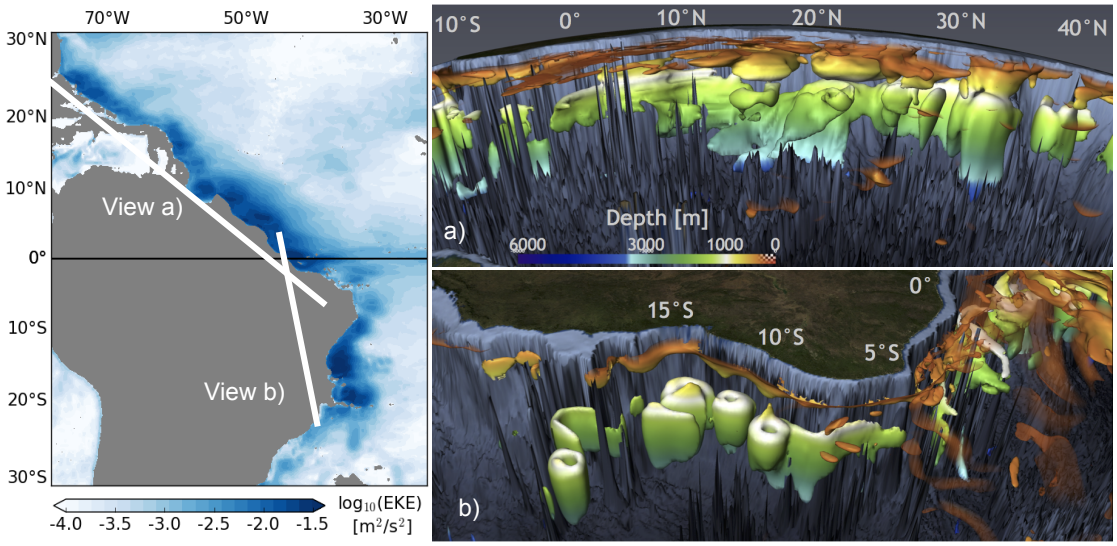

Figure 2.2: **Left:** Eddy kinetic energy (EKE) at 1941 m depth in logarithmic color scale (blue contours). **Right:** 3D snapshots of the 0.2 ms^{-1} velocity magnitude contour surface. The color indicates depth, with white at 1000 m, where the DWBC begins (the colorbar is nonlinear). The flow above 400 m is made transparent, because it would otherwise mask the DWBC. The angles of view of snapshot a) and b) are marked on the map in the left figure in white lines.

However, the net meridional transport in our model is too low by a factor of 2. We assess the realism of the DWBC in STORM by comparison against observations from 26.5°N, where the DWBC has been covered well by observations since the late 1980s. Estimates of its time-averaged southward transport range from 11 Sv (Meinen et al., 2006) to 40 Sv (Lee et al., 1996). This large spread originates from a large DWBC variability on different timescales (standard deviation of up to 20 Sv; Bryden et al., 2005a) as well as different observational setups. In our model, the effective southward DWBC transport at 26.5°N is 13 Sv. This transport consists of a narrow and strong boundary current of 120 km width that accounts for 23 Sv *southward* flow and an adjacent *northward* recirculation of 10 Sv that extends to about 550 km offshore (Figure 2.1(top)). Compared to recent observational studies by Meinen et al. (2013) and Johns et al. (2008) that use the RAPID array data (e.g., Cunningham et al., 2007; Kanzow et al., 2007), the net transport in our model seems to be too low, which we think is due to too strong northward recirculations. However, we find that the lateral and vertical extension of the flow, including the sign change in the meridional velocity at about 120 km offshore and the maximum velocity in the core (about 0.2 ms^{-1}, Figure 2.1), match observations (Bryden et al., 2005a; Lee et al., 1996). Although STORM does not resolve the two distinct vertically separated DWBC cores, consisting of upper and lower NADW (Meinen and Garzoli, 2014; Smeed et al., 2018), the DWBC core depth in

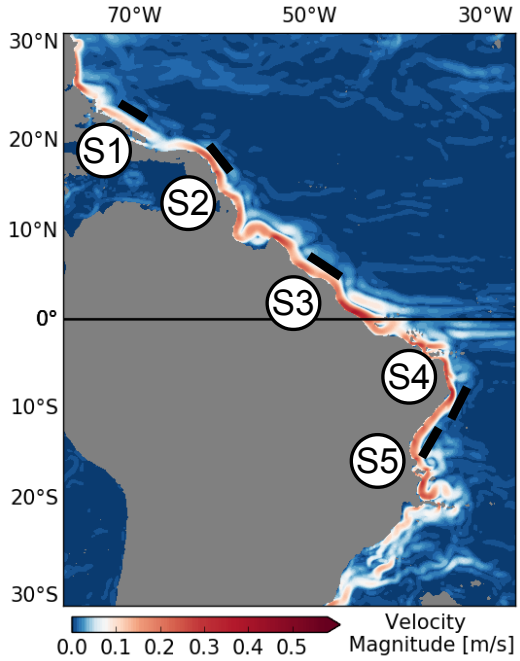

Figure 2.3: Mean-flow velocity magnitude $|\overline{\mathbf{u}}|$ at 1941 m depth (non-linear color scale). The black bars depict the 5 DWBC segments (S1-S5) that we analyze in this study.

our model (~2000 m) agrees with the mean depth of the two observed DWBC cores. This is in contrast to earlier modeling studies like Baehr et al. (2004) who find a too shallow DWBC in their 1/3° FLAME model with 45 depth levels. To clarify whether the improvement in simulating the DWBC is due to higher vertical or horizontal resolution, we conduct a second STORM simulation with 40 instead of 80 depth levels and the same horizontal resolution of 0.1°. The DWBC core depth in this simulation is still about correct (not shown), indicating that accurately resolving the mesoscale is key to modeling the DWBC core at the correct depth.

We find similarly good agreement between the DWBC in STORM and observations at other latitudes, such as at 18°S (Weatherly et al., 2000), between 5°S and 10°S (Schott et al., 2002) and at 25°N (Bryden et al., 2005b). Although the net transport in STORM seems to be considerably lower compared to observations, its 13 Sv southward transport account for 80 % of the southward transport which is necessary to balance the upper ocean northward transport at 26.5°N. We define the upper ocean northward transport as the zonally integrated transport above 800 m, which we find is 16.4 Sv at this latitude.

Several observational studies report eddy activity near the DWBC (Dengler et al., 2004; Garzoli et al., 2015; Lee et al., 1996; Schott et al., 2002; Schott et al., 2005); the distribution of eddy kinetic energy (EKE)

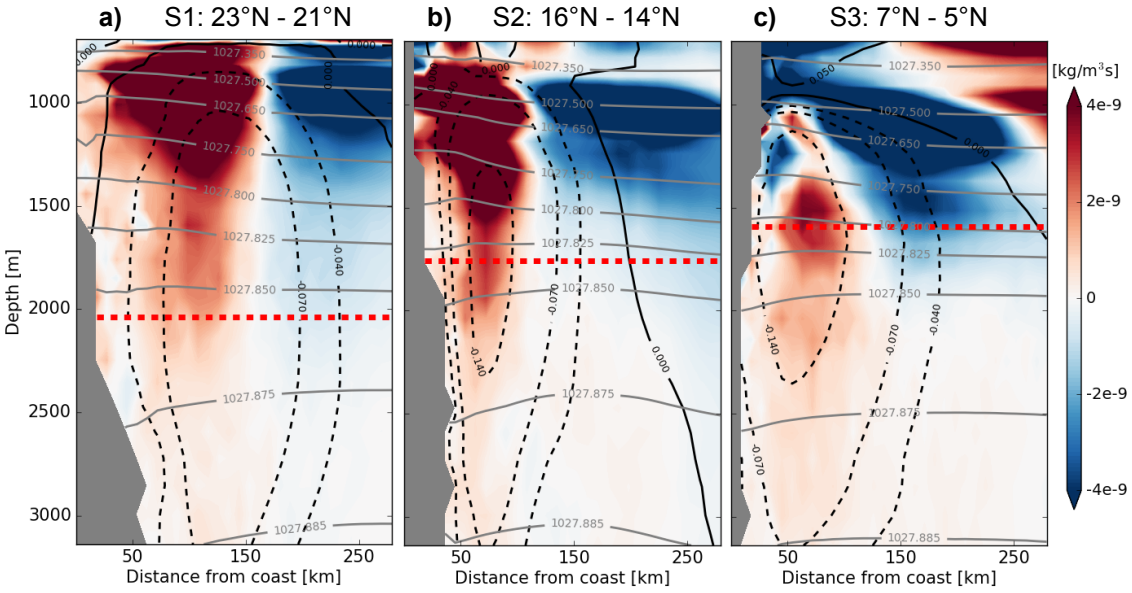

Figure 2.4: Pseudo-zonal sections of the along-stream average of the EDFD $\nabla \cdot (\overline{\mathbf{u}'\rho'})$ (colors), surface-referenced mean potential density $\overline{\sigma}_0$ (gray contour lines) and along-stream flow $\mathbf{u}_{||}$ (black contour lines, dashed southwards) between 23°N and 21°N (a, S1), 16°N and 14°N (b, S2) and 7°N and 5°N (c, S3). In this perspective, the DWBC flows out of the paper plane towards the reader. A positive (red) EDFD decreases and a negative (blue) EDFD increases density (note the minus sign in front of $\nabla \cdot (\overline{\mathbf{u}'\rho'})$ in Equation 2.1). The red dashed line marks the DWBC core depth, defined as the level at which the maximum southward velocity occurs.

in STORM likewise shows strong eddy activity near the DWBC (Figure 2.2(left) and Figure 2.1(bottom)). 3D snapshots of the flow field reveal strongly topographically controlled eddies, propagating alongshore southward. These eddies are nearly vertically coherent over the full depth range of the DWBC between 1000 m and 4000 m (Figure 2.2(right)). Furthermore, their intensity, measured by the EKE, varies little with depth (Figure 2.1(bottom)). An interesting feature of Figure 2.2(right) is that the DWBC eddies are mostly separated from the upper-ocean flow by a layer of no motion. In agreement with Dengler et al. (2004) and Schott et al., 2005, eddies south of 8°S are particularly strong (Figure 2.2b)). However, also further north, the model DWBC is accompanied by strong eddy features (Figure 2.2a)).

2.3 RESULTS

As expected for any large-scale ocean current and in accordance with DWBC observations (Kanzow et al., 2006) and other numerical simu-

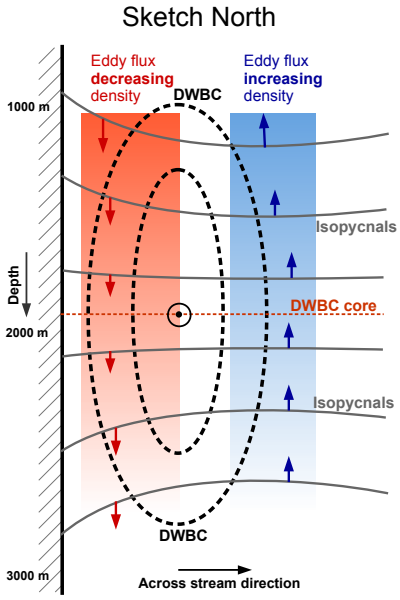

Figure 2.5: Sketch of Figure 2.4 that shows the EDFD (colors) and its relation to the isopycnals (gray contour lines) and along-stream velocity (black contour lines, dashed southwards). North of the equator, the EDFD *decreases density close to the shore* (red patches here and in Figure 2.4) and *increases density further offshore* (blue patches here and in Figure 2.4). A decrease of density causes a downward shift of the isopycnals (red arrows), whereas an increase causes an upward shift (blue arrows). Again, the red dashed line marks the DWBC core depth.

lations (Sijp et al., 2012), the DWBC in STORM is mainly geostrophic. Its deviation from geostrophy $\Delta = (|\mathbf{u} - \mathbf{u}_g|)/|\mathbf{u}_g|$, where $\mathbf{u}_g = (u_g, v_g)$ is the geostrophic velocity computed from the model pressure including a contribution from sea surface height, is everywhere lower than 10 % (not shown), except near the equator and in the westernmost grid cells, which are affected by boundary friction. The geostrophic nature of the flow implies that it is predominantly controlled by density via the thermal wind relation $\partial \mathbf{u}_H / \partial z = g/(f\rho_0)\mathbf{e_z} \times \rho$, where the subscript H denotes the horizontal component of the velocity field, f is the Coriolis parameter, g the gravitational acceleration, ρ_0 a reference density and $\mathbf{e_z}$ the vertical unit vector. This suggests that the effect of mesoscale eddies on the DWBC can best be understood by analyzing how the eddies affect density through eddy density fluxes. Nevertheless, the evolution of density and momentum is coupled, and hence, eddy momentum fluxes (Reynolds stresses) cannot be disregarded completely. We address eddy momentum fluxes at the end of the results section.

According to the prevailing interpretation of their effect on density, eddies release potential energy from the mean flow by flattening isopycnals through an eddy-induced advection (e.g., Gent et al., 1995). However,

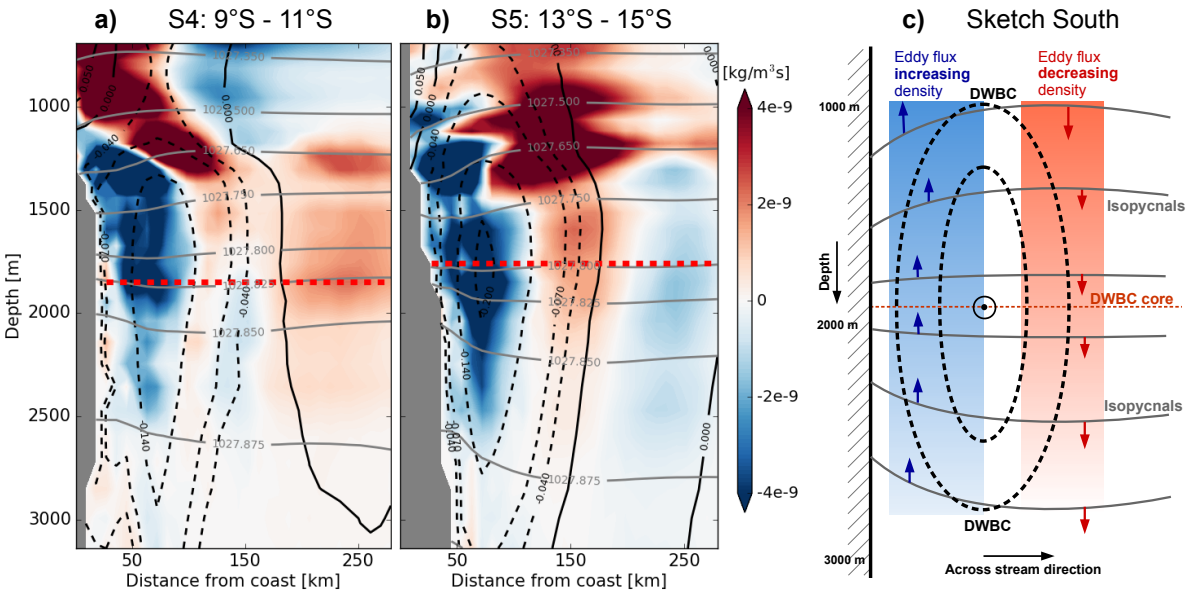

Figure 2.6: Along-stream average of EDFD $\nabla \cdot (\overline{\mathbf{u}'\rho'})$ (colors), surface-referenced mean potential density $\overline{\sigma}_0$ (gray contour lines) and along-stream flow $\mathbf{u}_{||}$ (black contour lines, dashed southwards) between 9°S and 11°S (a, S4), 13°S and 15°S (b, S5). (c) shows a sketch similar to Figure 2.5 but for the southern hemisphere. The red dashed line marks the DWBC core depth.

Jayne and Marotzke (2002) and Eden et al. (2007a) diagnose the thickness diffusivity κ, which sets the strength of this advection, in their models and report huge spatial variability and *sign changes* herein. This would imply that eddies partly steepen isopycnals. In the first results section, we clarify the effect of eddy density fluxes on the shape of the isopycnals near the DWBC. Subsequently, we consider the problem from an energy pathways perspective and investigate the conversion from mean to eddy potential energy. Then, we address the reaction of the mean flow to the eddies' effect.

2.3.1 *The effect of eddy density flux on mean density*

The evolution of mean potential density ρ can be described by the equation,

$$\frac{\partial \overline{\rho}}{\partial t} + \overline{\mathbf{u}} \cdot \nabla \overline{\rho} = -\nabla \cdot (\overline{\mathbf{u}'\rho'}) + Q, \tag{2.1}$$

where the total velocity $\mathbf{u} = \overline{\mathbf{u}} + \mathbf{u}'$ and potential density $\rho = \overline{\rho} + \rho'$ are each decomposed into a temporal mean (overbar) and a fluctuating (prime) component. In the remainder of this paper, density ρ always refers to potential density. $\overline{\mathbf{u}'\rho'}$ is the resolved eddy density flux, Q denotes unresolved and hence parametrized diabatic mixing and nonlinear effects

on density, such as cabbeling and thermobaricity. Furthermore, we expect $\partial\overline{\rho}/\partial t$ to be small, because $\overline{\rho}$ is a time-averaged quantity. In Section 2.3.3, we show that the main balance in Equation 2.1 is between the eddy density flux divergence (EDFD) and the mean advection of mean potential density $\overline{\mathbf{u}} \cdot \nabla\overline{\rho}$. Therefore, we expect the EDFD $\nabla \cdot (\overline{\mathbf{u}'\rho'})$ to be a major control for the shape of the mean isopycnals and hence for the geostrophic DWBC.

We diagnose the eddy density flux via $\overline{\mathbf{u}'\rho'} = \overline{\mathbf{u}\rho} - \overline{\mathbf{u}}\,\overline{\rho}$, where the overbar represents an average over the 10 years of data used in this study. Computed this way, $\overline{\mathbf{u}'\rho'}$ contains not only fluctuations on eddy time scales, but on all time scales from the numeric time step up to the averaging period of 10 years. However, **vonStorch2016** compared various eddy fluxes computed from monthly mean and from 30 year mean data and found that they do not differ significantly. Hence, we assume that $\overline{\mathbf{u}'\rho'}$ predominantly contains fluctuations due to eddies, i.e. eddy fluxes.

Previous studies dealing with the effect of eddies on density analyzed eddy diffusivities that were computed from the *raw* eddy flux $\overline{\mathbf{u}'\rho'}$ in the GM framework (Eden et al., 2007a; Jayne and Marotzke, 2002). Yet, the raw flux contains a dynamically irrelevant rotational component, which possibly masks the effective impact of the eddies on density to an unknown extent (Eden et al., 2007a; Fox-Kemper et al., 2003; Marshall and Shutts, 1981). In contrast to that, we analyze the divergence of the flux and thus automatically remove the rotational part and circumvent this ambiguity. The EDFD can be interpreted in combination with the inclination of the mean isopynals in order to assess if the eddies locally flatten or steepen isopycnals, i.e. if they release potential energy from or feed potential energy to the mean flow (Treguier, 1999).

The DWBC often does not flow strictly in the meridional direction but is locally aligned with the shoreline (see Figure 2.3). To obtain a unified picture of the DWBC dynamics, we conduct our analysis in stream-following coordinates, where one axis points in the along-stream direction ($x_{||}$) and one normal to it ($x_{\perp}$). The velocity field $\mathbf{u}$ is rotated accordingly, and its horizontal components will be referred to as along-stream velocity $u_{||}$ and across-stream velocity $u_{\perp}$. We average all quantities of interest along the along-stream axis within each of the 5 DWBC segments (S1 to S5) shown in Figure 2.3. Every segment spans about 2° in latitude, which corresponds to roughly 220 km. By averaging segment-wise, we can improve the signal-to-noise ratio of the data and at the same time preserve potential spatial heterogeneity of the eddy-mean-flow interaction in the along-stream direction of the DWBC.

Figure 2.4 shows pseudo-zonal sections of the three segments located in the northern hemisphere (S1-S3 in Figure 2.3). Pseudo-zonal means that the x-axis runs normal to the DWBC and the shoreline towards the open ocean. In all three segments S1-S3, above the DWBC core (~ 1800 m), the isopycnals (gray contour lines) are inclined upwards towards the

shore; below the core, they are inclined downwards towards the shore. The thermal wind balance provides an explanation for this change in the isopycnic inclination, because at the same depth, the vertical shear of velocity changes sign (southward flow increasing with depth above and decreasing below the core). We present a simplified picture of this scenario in Figure 2.5.

The EDFD $\nabla \cdot (\overline{\mathbf{u}'\rho'})$ (colors in Figure 2.4) peaks in the upper part of the DWBC between about 800 m and 1500 m depth. This is due to a local maximum in the density variance $\overline{\rho'^2}$ (not shown) and not due to stronger eddy activity. The latter is nearly constant with depth along the DWBC (see Figure 2.1(bottom) for the EKE at 26°N and also the vertically coherent eddies in Figure 2.2). The magnitude of the EDFD decreases with depth in all segments shown in Figure 2.4, yet its sign does not change with depth. Hence, eddies decrease density (positive EDFD) close to the shore, whereas they increase density (negative EDFD) further offshore throughout the whole water column. An increase in density pushes an isopycnal upwards; a decrease pushes it downwards. This suggests that eddies flatten the isopycnals above the DWBC core and steepen them below. We sketch this scenario in Figure 2.5, where the density increase and decrease are each visualized through upward and downward arrows, respectively.

In the two segments south of the equator (S4 and S5 in Figure 2.3), eddies mainly increase density (negative EDFD) close to the shore and decrease density (positive EDFD) further offshore (Figure 2.6a and Figure 2.6b). This is the opposite of what we observe in the northern segments. However, the inclination of the isopycnals is likewise reversed due to a sign change of the Coriolis parameter at the equator. Above the DWBC core, isopycnals are inclined downwards towards the shore and upwards below. Thus, the net effect of eddies on the isopycnic tilt is the same in the north and in the south: Eddies flatten isopycnals above the core and steepen them below. Again, we visualize the interplay between the geostrophic DWBC, the isopycnals and the EDFD in the southern hemisphere in Figure 2.6c.

2.3.2 *An energy pathways perspective on the DWBC-eddy interaction*

As already mentioned, mesoscale eddies are generally expected to extract potential energy from the mean flow and are commonly represented by a GM-parametrization, either with a spatially uniform or varying thickness diffusivity κ. The rationale behind this parametrization is reflected in the assumption that in the ocean, energy is introduced through ocean-atmosphere interactions on large scales before being transferred to smaller scales and finally dissipated. The *Lorenz energy cycle* provides a quantitative description for each of the four processes involved in this energy pathway (Lorenz, 1955). In the context of this study, the conversion

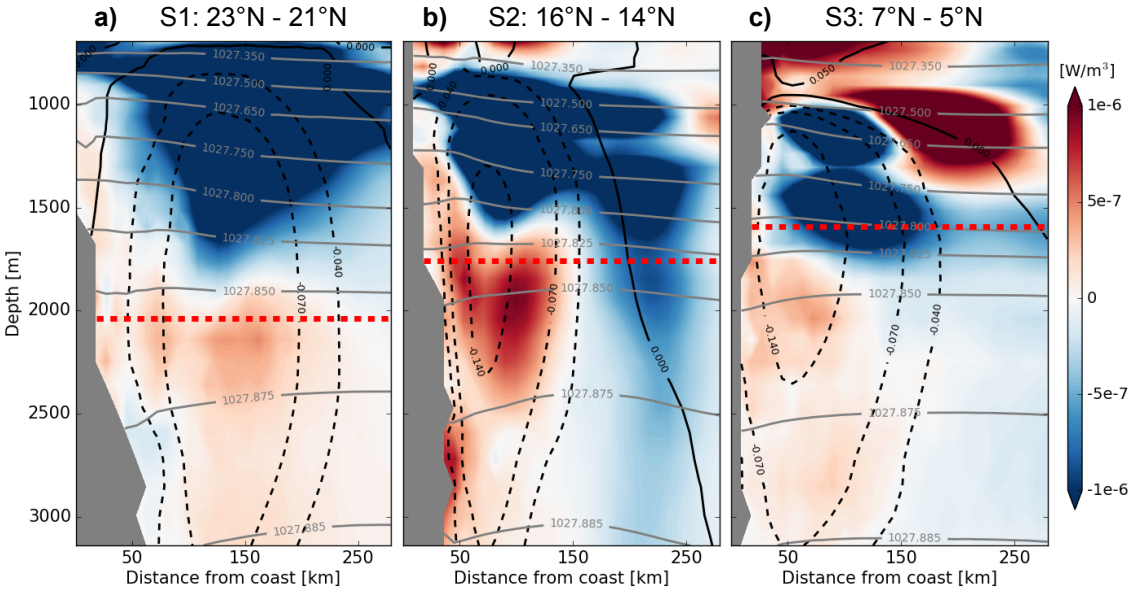

Figure 2.7: Along-stream average of the conversion from eddy potential energy P_e to mean potential energy P_m $\tilde{C}(P_e, P_m)$ (colors), surface-referenced mean potential density $\overline{\sigma}_0$ (gray contour lines) and along-stream flow $\mathbf{u}_{||}$ (black contour lines, dashed southwards) between 23°N and 21°N (a, S1), 16°N and 14°N (b, S2) and 7°N and 5°N (c, S3). A positive (red) $\tilde{C}(P_e, P_m)$ indicates a conversion $P_e \rightarrow P_m$. The red dashed line marks the DWBC core depth.

from mean potential energy P_m to eddy potential energy P_e is relevant. A GM-like parametrization transfers potential energy exclusively from P_m to P_e. In the following, we analyze the respective conversion term in each of the 5 segments S1-S5 (see Figure 2.3) along the DWBC in detail. For this purpose, we refer to the local conversion rate

$$c(P_e, P_m) = \frac{g}{n_0} \overline{\mathbf{u}'_H \rho'} \cdot \nabla_H \overline{\rho}, \tag{2.2}$$

which emerges from the quasi-geostrophic approximation of the available potential energy equation (von Storch et al., 2012). The subscript H denotes the horizontal components of the velocity $\mathbf{u}'$ and the differential operator ∇, n_0 is the vertical gradient of the mean potential density averaged over the area of the respective segment. The conversion term $c(P_e, P_m)$ from Equation 2.2 contains the horizontal components of the previously mentioned *raw* eddy flux $\overline{\mathbf{u}'\rho'}$ and thus a contribution from the dynamically irrelevant rotational part of $\overline{\mathbf{u}'\rho'}$. Marshall and Shutts (1981) identified the rotational contribution $(\overline{\mathbf{u}'_H \rho'})_R$ of $(\overline{\mathbf{u}'_H \rho'})$ in the eddy variance budget as the advection of eddy variance by the mean flow, $(\overline{\mathbf{u}'_H \rho'})_R \cdot \nabla_H \overline{\rho} = -\overline{\mathbf{u}}_H \cdot \nabla_H (\overline{\rho'^2}/2)$. When taking the along-stream average of the conversion $\tilde{C}(P_e, P_m) = 1/L \int_L c(P_e, P_m) dl$, where L denotes the along-stream segment length and assuming the along-stream homogeneity of the flow, only the across-stream component $-\overline{u}_\perp \partial/\partial x_\perp (\overline{\rho'^2}/2)$ of

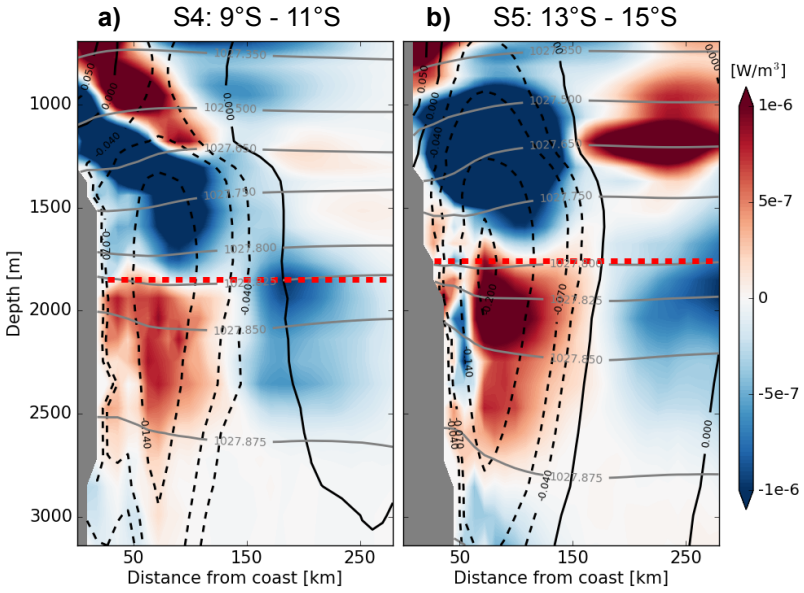

Figure 2.8: Along-stream average of the conversion from eddy potential energy P_e to mean potential energy P_m $\tilde{C}(P_e, P_m)$ (colors), surface-referenced mean potential density $\overline{\sigma}_0$ (gray contour lines) and along-stream flow $\mathbf{u}_{||}$ (black contour lines, dashed southwards) between 9°S and 11°S (a, S4), 13°S and 15°S (b, S5). The red dashed line marks the DWBC core depth.

$\overline{\mathbf{u}}_H \cdot \nabla_H(\overline{\rho'^2}/2)$ remains which should be small compared to the divergent part in the along-stream average. Griesel et al. (2014) use a similar along-stream averaging approach to minimize rotational eddy fluxes in estimates of isopycnal diffusivities. By the averaging procedure we expect $\tilde{C}(P_e, P_m)$ to contain predominantly the contribution from the divergent part of the eddy density flux $\overline{\mathbf{u}'\rho'}$. The fact that $\tilde{C}(P_e, P_m)$ agrees qualitatively well with the conversion from eddy potential energy to eddy kinetic energy $\tilde{C}(P_e, K_e) = 1/L \int_L g\overline{w'\rho'}$ (not shown) supports our assumption that $\tilde{C}(P_e, P_m)$ is a meaningful quantity (Eden et al., 2007a).

In agreement with the maximum of the EDFD between 800 m and 1500 m mentioned above, the overall magnitude of energy conversion likewise decreases with depth. Apart from that, we discern two distinct vertically separated regimes of potential energy conversion in the northern (Figure 2.7) as well as in the southern hemisphere (Figure 2.8): *Above* the DWBC core (~ 1800 m), eddies transfer potential energy mainly from the mean to the eddy compartment (negative $\tilde{C}(P_e, P_m)$ in Figure 2.7 and Figure 2.8). *Below* the core, eddies transfer potential energy mainly in the opposite direction from the eddy to the mean compartment (positive $\tilde{C}(P_e, P_m)$ in Figure 2.7 and Figure 2.8). Segments S3-S5 contain exceptions in form of smaller patches of positive conversion $\tilde{C}(P_e, P_m)$ ($P_e \rightarrow P_m$) above (S3-S5) and eastward (S3,S5) of the DWBC, that we do not discuss here. However, the two conversion regimes separated at the

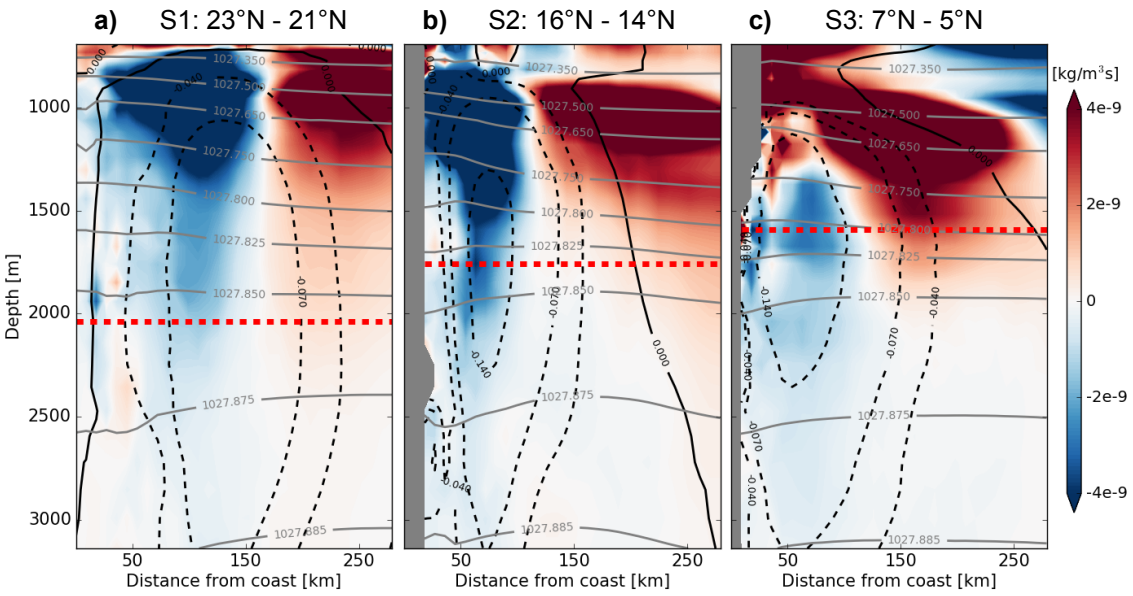

Figure 2.9: Advection of mean potential density by the mean flow $\overline{\mathbf{u}} \cdot \nabla\overline{\rho}$ (colors), surface-referenced mean potential density $\overline{\sigma}_0$ (gray contour lines) and along-stream flow $\mathbf{u}_{||}$ (black contour lines, dashed southwards) for the three segments north of the equator between 23°N and 21°N (a, S1), 16°N and 14°N (b, S2) and 7°N and 5°N (c, S3). The red dashed line marks the DWBC core depth.

DWBC core depth support the conclusion drawn from the analysis of the EDFD in the previous section: Mesoscale eddies have a two-fold effect on the mean density near the DWBC. Above the DWBC core, eddies release potential energy from the mean flow (they flatten isopycnals) and thus behave according to the GM interpretation. By contrast, below the DWBC core, they feed potential energy to the mean flow (they steepen isopycnals).

2.3.3 *Mean flow balancing the effect of eddies*

In our model, the budget of mean density, Equation 2.1, is mainly a balance between the mean advection of mean density and the EDFD, $\overline{\mathbf{u}} \cdot \nabla\overline{\rho} \approx -\nabla \cdot (\overline{\mathbf{u}'\rho'})$. The term $\overline{\mathbf{u}} \cdot \nabla\overline{\rho}$, shown in Figure 2.9 and Figure 2.10 for the segments S1-S5, closely resembles the EDFD shown in Figure 2.4 and Figure 2.6 (with opposite sign). The residual $\overline{\mathbf{u}} \cdot \nabla\overline{\rho} + \nabla \cdot (\overline{\mathbf{u}'\rho'})$ is about one order of magnitude smaller than the two individual terms (not shown). This indicates that in our model, diabatic mixing and non-linear effects on density such as cabbeling and thermobaricity (Q in Equation 2.1) are of minor importance near the DWBC compared to the EDFD and the density-advection by the mean flow $\overline{\mathbf{u}}$. After describing the effect of the eddy fluxes in the two previous sections, we now go one

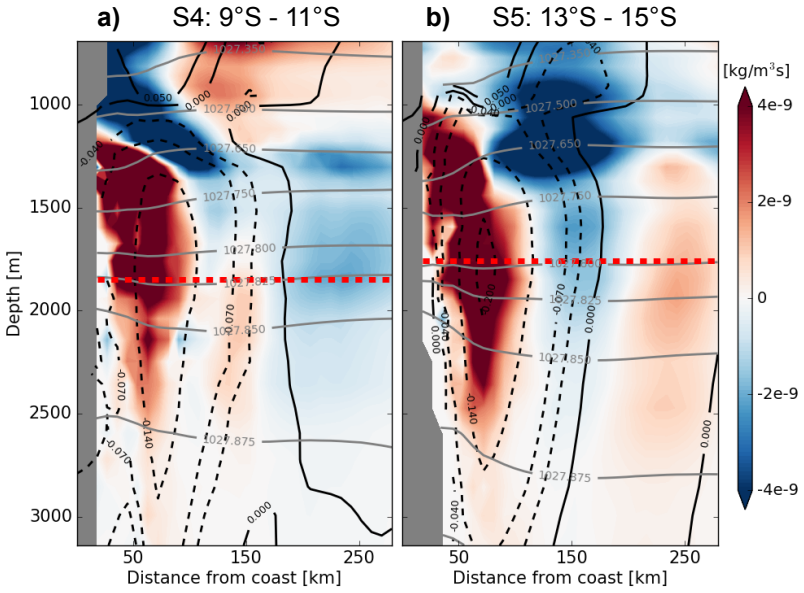

Figure 2.10: Advection of mean potential density by the mean flow $\overline{\mathbf{u}} \cdot \nabla \overline{\rho}$ (colors) (colors), surface-referenced mean potential density $\overline{\sigma}_0$ (gray contour lines) and along-stream flow $\mathbf{u}_{||}$ (black contour lines, dashed southwards) for the two segments south of the equator between 9°S and 11°S (a, S4), 13°S and 15°S (b, S5). The red dashed line marks the DWBC core depth.

step further and investigate the structure of the eddy-balancing mean flow $\overline{\mathbf{u}}$.

Within each of the DWBC segments S1-S5 shown in Figure 2.3, we assume the along-stream flow to be coherent, i.e. we assume the along-stream gradient of the along-stream velocity $\partial \overline{u}_{||}/\partial x_{||}$ to be small. Hence, the incompressibility condition, written in the along-stream / across-stream coordinate system, reduces to

$$\frac{\partial \overline{u}_\perp}{\partial x_\perp} + \frac{\partial \overline{w}}{\partial z} = 0. \tag{2.3}$$

Based on Equation 2.3, we introduce a *pseudo-zonal overturning streamfunction*

$$\tilde{\psi}(x_\perp, z) = \int_0^{x_\perp} \tilde{\overline{w}}(x_\perp, z)\, dx^*_\perp \tag{2.4}$$

which describes the time-mean flow in the plane normal to the DWBC. The tilde indicates a segment-wise along-stream average of the time-averaged vertical velocity $\overline{w}$; hence, the streamfunction ψ is also a segment-averaged quantity ($\tilde{\psi}$). It has the unit $m^2 s^{-1}$ and describes the pseudo-zonal overturning per 1 m of shoreline.

The three segments in the northern hemisphere S1-S3 shown in Figure 2.11 all show a dominant clockwise overturning cell in the plane

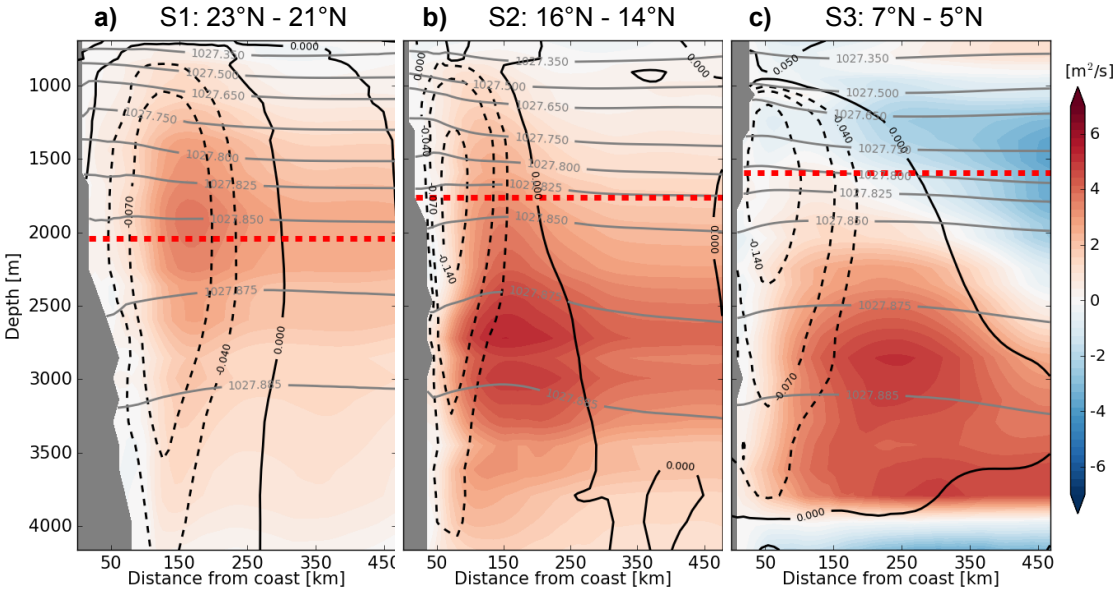

Figure 2.11: Pseudo-zonal overturning per 1 m of shoreline $\tilde{\Psi}$ (colors), surface-referenced mean potential density $\overline{\sigma}_0$ (gray contour lines) and along-stream flow $\mathbf{u}_{||}$ (black contour lines, dashed southwards) for the three segments north of the equator between 23°N and 21°N (a, S1), 16°N and 14°N (b, S2) and 7°N and 5°N (c, S3). Positive (red) $\tilde{\Psi}$ indicates clockwise overturning with upwelling close to the shore and downwelling further offshore. The red dashed line marks the DWBC core depth.

normal to the DWBC (positive $\tilde{\psi}$). The precise shape and depth of each of these cells is different. Whereas in S1 (Figure 2.11 a), the overturning cell is centered at the DWBC core depth (~2000 m), the cell center and the DWBC core depth diverge when approaching the equator. Compared to S1, the DWBC core moves upward in S2 (Figure 2.11 b) and S3 (Figure 2.11 c). At the same time, the overturning cell moves downward. Nevertheless, in all segments S1-S3, the upwelling close to the shore has an effect precisely opposite to that of the EDFD described above: Isopycnals are flattened below the DWBC core and steepened above. In accordance with the sign change in f and the related change in the isopycnic tilt, the pseudo-zonal overturning changes its direction in the southern hemisphere. Segments S4 and S5 each reveal a dominant anti-clockwise overturning (negative $\tilde{\psi}$ in Figure 2.12) normal to the DWBC, with downwelling close to the shore and upwelling further offshore. Similar to the northern hemisphere, the overturning cell depth and the DWBC core depth match at high latitudes in S5 (Figure 2.12 b), whereas the overturning cell lies deeper than the DWBC core close to the equator in S4 (Figure 2.12 a). However, the downwelling close to the shore flattens isopycnals below the DWBC core and steepens them above. The

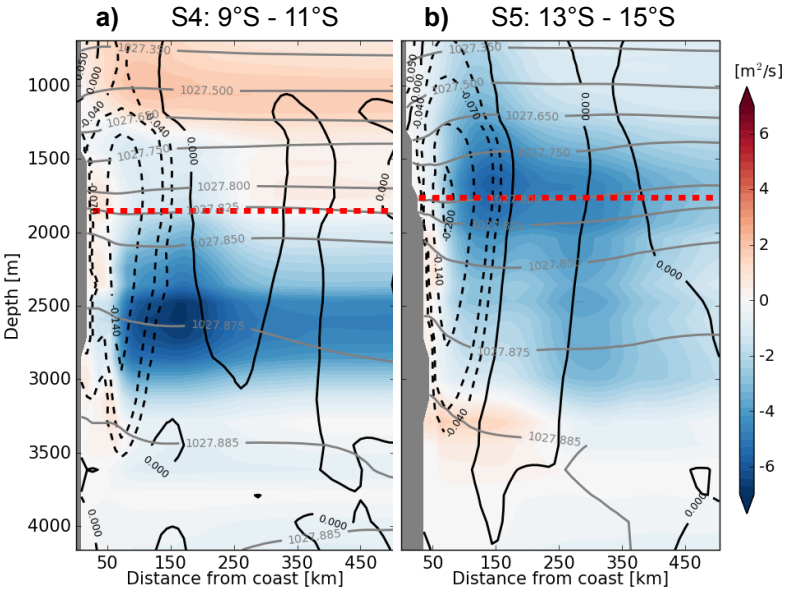

Figure 2.12: Pseudo-zonal overturning per 1 m of shoreline $\tilde{\Psi}$ (colors), surface-referenced mean potential density $\overline{\sigma}_0$ (gray contour lines) and along-stream flow $\mathbf{u}_{||}$ (black contour lines, dashed southwards) for the two segments south of the equator between 9°S and 11°S (a, S4), 13°S and 15°S (b, S5). Positive (red) $\tilde{\Psi}$ indicates clockwise overturning. The red dashed line marks the DWBC core depth.

interaction between the overturning and the EDFD is thus the same in both hemispheres, albeit anti-symmetric due to the sign-change in f.

Using an eddy-resolving version of the Los Alamos Parallel Ocean Program (POP) model, Li et al. (2016) find a similar overturning normal to the mean flow in distinct segments of the Antarctic circumpolar current (ACC) and relate that overturning to the horizontal convergence of eddy momentum fluxes. In the following, we assess the potential role of eddy momentum fluxes for the overturning normal to the DWBC. The quasi-geostrophic form of the along-stream-averaged along-stream momentum balance reads

$$\frac{\partial \overline{u}_{||}}{\partial t} - f\overline{u}_{\perp} = -\frac{\partial(\overline{u'_{\perp} u'_{||}})}{\partial x_{\perp}} + \mathcal{F}, \tag{2.5}$$

where $\mathcal{F}$ denotes frictional forces (Vallis, 2017). We assume the first term on the left-hand-side to be small because we look at time-averaged quantities. Via Equation 2.5, the eddy momentum flux convergence (EMFC) $-\partial\overline{u'_{\perp} u'_{||}}/\partial x_{\perp}$ is a potential driver of the mean across-stream flow $\overline{u}_{\perp}$ and hence for the mean overturning described above (Figure 2.11 and Figure 2.12). However, it becomes obvious from Figure 2.13, in which we show $-\partial\overline{u'_{\perp} u'_{||}}/\partial x_{\perp}$ for segment S5, that the EMFC cannot serve as an explanation for the overturning normal to the DWBC which is characterized by a $\overline{u}_{\perp}$ that changes sign in the vertical, with flow towards the shore

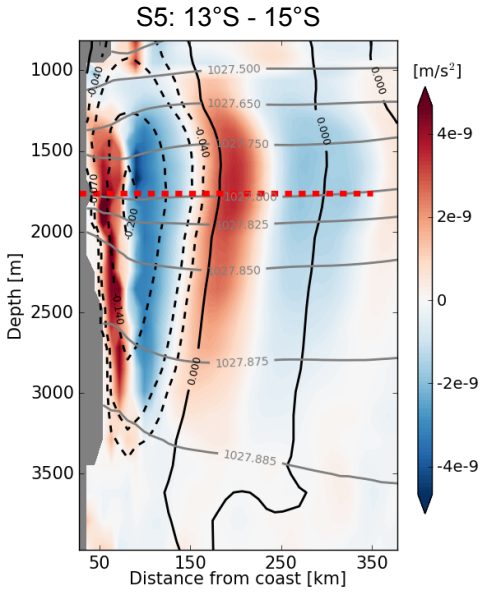

Figure 2.13: Across-stream EMFC $-\partial\overline{u'_\perp u'_\parallel}/\partial x_\perp$, surface-referenced mean potential density $\overline{\sigma}_0$ (gray contour lines) and along-stream flow $\mathbf{u}_\parallel$ (black contour lines, dashed southwards) for segment S5 from 13°S and 15°S. We compute the along-stream / across-stream momentum flux $\overline{u'_\perp u'_\parallel}$ from the model output via $\overline{u'_\perp u'_\parallel} = (1-2\sin^2\alpha)\overline{u'v'} + \sin\alpha\cos\alpha(\overline{u'^2} - \overline{v'^2})$, where u and v are the zonal and meridional velocity components and α is the angle between the zonal axis x and the along-stream axis $x_\parallel$. Negative (blue) indicates a deceleration of the southward DWBC through the EMFC. The red dashed line marks the DWBC core depth.

above the DWBC core and away from the shore below (see Figure 2.12 b). In case the overturning was related to $-\partial\overline{u'_\perp u'_\parallel}/\partial x_\perp$, this sign change would be reflected in the EMFC. On the contrary, Figure 2.13 does not show any significant sign change in the vertical that resembles the scale of the mean overturning visible in Figure 2.12 b. Instead, the EMFC seems to sharpen the DWBC flow by decelerating it at its edges (positive in Figure 2.13, note that the DWBC is directed southwards and hence $\overline{u}_\parallel$ negative) and accelerating it in its core (negative in Figure 2.13). The sharpening of mean currents through EMFC has been described before, predominantly for jet extension flows (e.g., Waterman and Hoskins, 2013). We can conclude, that the eddy momentum fluxes seem not to play a role for the overturning normal to the DWBC. Instead, the previous analysis suggests that frictional forces are key to the mean overturning. A detailed analysis hereof is beyond the scope of this study. We show the EMFC only for segment S5. However, the picture is very similar in all segments S1-S5. None of them suggests a connection between the EMFC and the overturning normal to the DWBC.

2.4 CONCLUSIONS

We provide a consistent picture of the effect that mesoscale eddies have on the mean density distribution near the deep western boundary current (DWBC) in the Atlantic and the related behavior of the mean flow in the plane normal to the DWBC between 26°N and 20°S. Eddies are crucial in shaping mean density, contributing to leading order to the mean density balance. However, the way they act on density near the DWBC is two-fold, revealing an interesting new eddy behavior: *Above* the DWBC core depth, eddies *flatten* isopycnals, whereas *below* the core, they *steepen* them, albeit much weaker. This implies that eddies decrease potential energy above the core (in agreement with a GM-like parametrization) and increase potential energy below the core (in contradiction to a GM-like parametrization). It has to be noted that the GM-like eddy effect above the core is considerably stronger then the isopycnal-steepening eddy effect below the core (Figure 2.4 and Figure 2.6).

Coarse resolution ocean models that apply a GM-like eddy parametrization, which exclusively flattens isopycnals, cannot capture the steepening of isopycnals below the DWBC core. Potentially, this leads to a misrepresentation of the true DWBC depth in coarse resolution ocean models (e.g., Baehr et al., 2004), because the steepening below the core can be interpreted as a downward extension of the DWBC through eddies. A detailed comparison of the DWBC depth in our eddy-resolving STORM simulation and a coarse resolution version of MPI-OM is planned.

We find evidence for the two-fold eddy scenario by analyzing the eddy density flux divergence (EDFD) as well as the pathways of potential energy, which gives us confidence that the described eddy effect is a robust property of the DWBC in our model.

Furthermore, we find that mean density near the DWBC is characterized by a balance between the EDFD and density advection by the mean flow. The eddy-balancing mean advection has the shape of a pseudo-zonal overturning circulation in the plane normal to the DWBC. In the northern hemisphere, we observe a clockwise overturning, with upwelling close to the shore and downwelling further offshore. Consistent with the sign change in the Coriolis parameter, the overturning changes its direction to anti-clockwise in the southern hemisphere. We could not find any link between the overturning normal to the DWBC and eddy momentum fluxes, that was recently established by Li et al. (2016) for an overturning normal to the ACC. Instead, we hypothesize that boundary friction plays a crucial role for the overturning normal to DWBC.

In our analysis, we focus on the Atlantic with its strong DWBC. However, other DWBCs, e.g. in the Pacific, might reveal a comparable two-fold eddy-behavior, because like the DWBC in the Atlantic, they should be characterized by a sign change in the lateral density gradient at the DWBC core depth.

Our analysis is based on geostrophy and therefore does not apply to a narrow band around the equator. However, outside this band, the two-fold effect of eddies on density as well as the related pseudo-zonal overturning are present *everywhere* along the DWBC from 26°N to 20°S. On the one hand, this scenario constitutes a systematic deviation from what is commonly expected from mesoscale eddies. On the other hand, the overturning normal to the DWBC, to the best of our knowledge, was not mentioned in the literature so far and deserves further exploration.

ACKNOWLEDGMENTS

We thank Michael Böttinger for providing the 3D-images of the DWBC shown in Figure 2.2. Furthermore, we thank Dian Putrasahan and three anonymous reviewers for carefully reading the manuscript and giving valuable comments hereon. Helmuth Haak supported us in all technical concerns. This work was supported by the Max Planck Society and the International Max Planck Research School on Earth System Modelling. We also thank the German consortium project STORM, especially the cluster of excellence CliSAP of the University Hamburg, for making the 0.1-degree simulation possible.

3

OVERTURNING RESPONSE TO A DOUBLING OF THE SURFACE WIND STRESS IN AN EDDYING AND A NON-EDDYING OCEAN

THIS PAPER IS IN PREPARATION FOR SUBMISSION AS:

Lüschow, Veit, Jin-Song von Storch, and Jochem Marotzke (2020). Overturning response to a surface wind stress doubling in an eddying and a non-eddying ocean, *in preparation*.

AUTHOR CONTRIBUTIONS

VL and JSvS designed the sensitivity experiments with input from JM. VL outlined the research questions and performed the research and drafted the manuscript with inputs from JSvS and JM. All authors contributed ideas to the interpretation of the results.

Overturning response to a doubling of the surface wind stress in an eddying and a non-eddying ocean

VEIT LÜSCHOW, JIN-SONG VON STORCH AND JOCHEM MAROTZKE

Max Planck Institute for Meteorology, Bundesstr. 53, 20146 Hamburg, Germany

ABSTRACT

We compare the overturning response to wind stress changes of an eddying and a non-eddying ocean and find differences in the deep overturning cell in the Atlantic with substantial implications for the deep western boundary current (DWBC). Numerous modeling studies have already demonstrated the importance of mesoscale eddies for the response of certain ocean features such as the southern ocean overturning. However, the role that eddies play for the deep overturning response is less clear. We ran an uncoupled twin experiment with the non-eddying GR15 and the eddying STORM configuration of the MPI ocean model, using the standard NCEP forcing and the NCEP forcing with 2x surface wind stress. The response in the Atlantic meridional overturning circulation is similar in the eddying STORM and the non-eddying GR15, showing an increase by about 4 Sv (~25%, 1 Sv = 10^6 $m^3 s^{-1}$). In contrast, the DWBC responds with a speedup in GR15 and a slowdown in STORM. We demonstrate that eddy vorticity fluxes are heavily involved in the DWBC slowdown in STORM and thereby we provide an explanation for the response difference between the eddying and non-eddying configuration. Our results emphasize the importance of mesoscale eddies in shaping the deep overturning response and furthermore suggest the existence of a so far unknown eddy-induced interaction between the upper and the bottom overturning cell in the Atlantic between 20° N and 5 ° N.

3.1 INTRODUCTION

Modifications to the Earth's surface wind field due to climate change has been observed (Marshall, 2003; Thompson and Solomon, 2002), and further changes are likely in the future (e.g., Bracegirdle et al., 2013; Farneti et al., 2015; Gillett and Fyfe, 2013). In particular for the southern ocean (SO) westerlies, which are anticipated to strengthen and shift southwards, we expect these changes to have considerable influence on the ocean mean state. The strength and shape of the Atlantic meridional

overturning circulation (AMOC), which is responsible for large parts of the global oceanic meridional heat transport, might be significantly affected by changes in the SO winds. A detailed understanding of the AMOC response to surface wind changes is required in the light of climate change.

Previous studies about the overturning's wind sensitivity mostly focused on the direct response of the upper overturning cell, which we usually refer to as AMOC cell. It was expected to strengthen linearly with increasing SO wind stress ('Drake passage effect', Toggweiler and Samuels, 1995, 1998) until Henning and Vallis (2005) and Hallberg and Gnanadesikan (2006) detected a reduction in the overturning wind sensitivity when switching from non-eddying to more realistic eddy-permitting ocean models (see Gent (2016) for a review on this process named 'eddy compensation'). Nevertheless, the vital role of the wind stress in controlling the SO pathway for dense water towards the surface and thus its role for the AMOC remains undisputed (Marshall and Speer, 2012).

Besides this *direct* link between wind stress and AMOC, the concept of the 'ocean seesaw' (Broecker, 1998) provides a possible second, *indirect* link. Patara and Böning (2014) recently demonstrated how a weakening of the bottom overturning cell induced by reduced Antarctic bottom water (AABW) formation may lead to a stronger upper AMOC cell. While the AABW reduction in their experiment was initiated by perturbations in the SO buoyancy, AABW formation can also be influenced by SO winds (e.g., Brix and Gerdes, 2003; Poulsen et al., 2018). Hence, the ocean seesaw opens up a second route for the SO wind stress to affect the AMOC strength.

In this manuscript, we present wind sensitivity experiments conducted with one non-eddying and one eddying configuration of the same realistic-geometry Max-Planck-Institute ocean model (MPI-OM). It turns out that the response to a wind stress doubling is a seesaw characterized by a strengthening of the upper (AMOC) cell and a weakening of the bottom (AABW) cell in both configurations. However, the bottom cell and the DWBC, which comprises both the lower limb of the AMOC cell and the upper limb of the bottom cell, respond differently in the two configurations. The difference points to the need for a more detailed inspection of the response of the deep circulation and the role of eddies there. As far as we know, this deep response has not yet been studied in eddy-resolving setups and so it will be investigated here.

Based on the described outcome of our sensitivity experiments, we formulate the following guiding research questions: (i) Can we relate the response differences in the DWBC to whether eddies are resolved or not? (ii) And if yes, what are the implications for our understanding of the ocean seesaw in the real (eddying) ocean? By answering these questions, we try to provide a new perspective on what role mesoscale eddies may play for the AMOC response to forcing changes: Besides dampening

the above discussed *direct* impact of SO wind stress on AMOC (eddy compensation), eddies might also control the response of the DWBC to forcing changes and in doing so exert an *indirect* control over the overturning response.

The design of our wind sensitivity experiment is not guided by the most likely future state of the wind field. We choose to double the wind stress in order to provoke a large signal in the ocean response. Our aim is rather to gain a conceptual understanding of the processes involved than to quantify the actual strength of the overturning response to changes in the surface winds. Due to the high computational costs of the STORM configuration, we could run the sensitivity experiments for only 31 years from 1980 to 2010, and thus we will focus on the decadal scale response. Nevertheless, we finds significant modifications of the ocean mean state within that period and thus consider our results meaningful. Other high-resolution sensitivity studies analyze simulations of comparable length (e.g., Bishop et al., 2016; Hogg et al., 2017; Poulsen et al., 2018).

The paper begins with a description of our experimental setup (Section 3.2), before illustrating the quasi-steady state overturning response. It shows a substantial DWBC slowdown in the eddying STORM configuration (Section 3.3). In Section 3.4, we show that a link exists between this DWBC slowdown and eddy vorticity fluxes (EVF). We then analyze in detail the evolution of the response signal and suggest a potential response mechanism that caused the DWBC slowdown. Section 3.6 contains a discussion and conclusions.

3.2 EXPERIMENT DESIGN

We use two different configurations of the global ocean model MPI-OM. One was developed within the German consortium project STORM with a tripolar grid at 0.1° horizontal resolution ('STORM'), which we assume to be *eddying*. The other is a standard MPI-OM version and utilizes a bipolar grid with an effective resolution of about 1.5° ('GR15'), which we assume to be *non-eddying*. Running three different scenarios with three different surface wind stresses in each model configuration (eddying and non-eddying) enables us to test if the ocean's response to changes in the surface wind stress depends on whether mesoscale eddies are resolved or not.

In the control scenario, we apply the standard NCEP-NCAR Reanalysis-1 forcing (Kalnay et al., 1996) and run it from 1948 to 2010. These runs will be referred to as S1X for the STORM and G1X for the GR15 configuration. Please note also the gray table in Figure 3.1 for the experiment labeling. In the first sensitivity scenario, we double the zonal and meridional wind stress by adding their monthly climatology to the original NCEP wind stress from the year 1980 onward (experiments referred to as S2X for STORM and G2X for GR15, Figure 3.1). In the second sensitivity scenario,

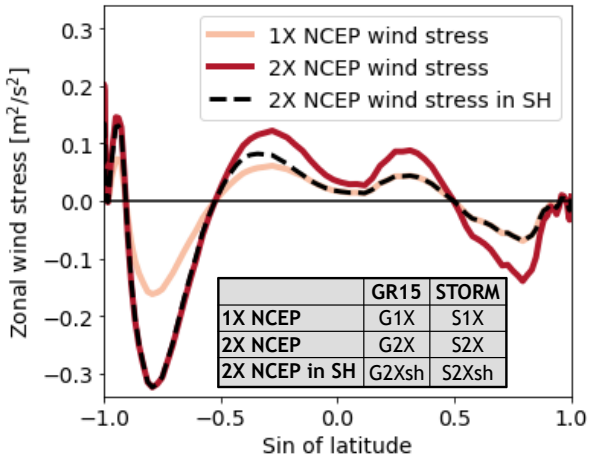

Figure 3.1: Three different zonal mean zonal wind stress fields that we use for this paper, averaged in the period between 1948 to 2016: Standard NCEP wind stress (1X NCEP, light red), globally doubled NCEP wind stress (2X NCEP, dark red) and NCEP wind stress doubled only in the southern hemisphere (2X NCEP in SH, dashed black). The gray table gives an overview over the experiments we ran (3 different wind stresses × 2 different model configurations = 6 experiments).

we double the wind stress only in the southern hemisphere by adding to the standard NCEP wind stress the monthly climatology multiplied by a sine function. This sine function is centered around the maximum negative wind stress at 48° S and declines to zero at the equator and at the south pole (S2Xsh for STORM and G2Xsh for GR15, Figure 3.1).

Thus, in total we analyze six different experiments, three of which resolve mesoscale eddies (S1X, S2X, S2Xsh) and three that do not (G1X, G2X, G2Xsh). Running one set of experiments with winds enhanced globally and one set with winds enhanced only in the southern hemisphere makes a distinction between local and remote wind effects possible. However, the long-term response in the mean AMOC and DWBC transport as well as their vertical response structure is quite similar in the experiments S2X and S2Xsh on the one hand as well as G2X and G2Xsh on the other hand. Therefore, in this manuscript we mainly focus on the two scenarios S2X and G2X with globally doubled wind stress.

The STORM configuration with its tripolar grid has two coordinate poles in the northern hemisphere (NH) over Asia and North America, ensuring an essentially uniform resolution. STORM's ability to represent large parts of the mesoscale eddy field was demonstrated for surface eddies (e.g., Li and von Storch, 2013; von Storch et al., 2012, 2016) and also for deep eddies (Lüschow et al., 2019). The GR15 configuration uses a bipolar grid with a resolution of about 180 km in our region of interest at low latitudes, rendering it mostly free of eddies. Consequently, the Gent-McWilliams (GM) eddy-parameterization (Gent et al., 1995) is

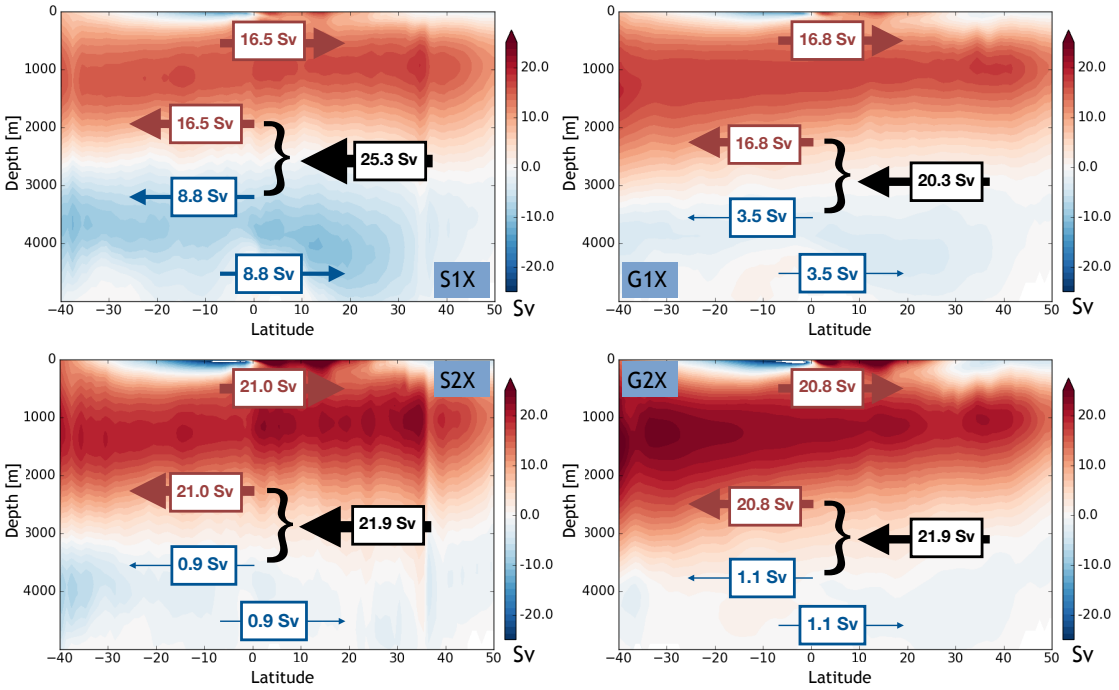

Figure 3.2: AMOC stream functions for the four experiments with standard NCEP wind stress, S1X (top-left) and G1X (top-right) and with doubled NCEP wind stress, S2X (bottom-left) and G2X (bottom-right). Stream functions are computed from data averaged between 2001 and 2010. Red numbers and arrows belong to the upper (AMOC) overturning cell. They are diagnosed at 1000 m depth and averaged between 5° N and 20 ° N. Blue numbers and arrows belong to the bottom (AABW) cell, diagnosed at 4000 m depth and likewise averaged between 5° N and 20 ° N. Black numbers and arrows show the total southward DWBC transport.

switched off in STORM while switched on in GR15. The strength of the parameterization in GR15 is controlled via the GM thickness diffusivity that is defined as a value scaled with the grid size in MPI-OM. In these experiments, we use the GR15 standard of 94 $m^2 s^{-1}$ per 100 km grid size which is a very low value compared to other models that use a value about 10 times larger (von Storch et al., 2016). Both models have 80 vertical levels that range from 10 m level thickness at the surface to about 250 m at the ocean bottom. Further model details as well as more results inferred from the STORM configuration of MPI-OM can be found in von Storch et al. (2012, 2016). Details on the GR15 configuration are available in Jungclaus et al. (2006, 2013).

3.3 STEADY STATE OVERTURNING RESPONSE TO THE WIND STRESS DOUBLING

The eddying STORM and the non-eddying GR15 configuration both show signatures of the ocean seesaw with a strengthening of the upper (AMOC) and a weakening of the bottom (AABW) overturning cell as response to the wind stress doubling. In this section, we portray the quasi-steady state of this response, where the AMOC and AABW transport stay relatively constant. The quasi-steady state response arises after about 15 to 20 years and lasts for at least the last ten years of the simulation from 2001 to 2010. Therefore, for the remainder of this and the next section, we use data that was time-averaged between 2001 and 2010; Figure 3.2 visualizes the overturning stream functions for this period. AMOC's steady state response is characterized by a 25 % increase in G2X and S2X. Both configurations also share a weakening of the AABW cell. Yet, we find significant differences in the extent of this weakening. In the following, we will see that this has consequences for the DWBC.

Doubling the wind stress leads to an increase in the northward surface transport of about 4.5 Sv in STORM and 4.0 Sv in GR15, respectively. Necessarily, the southward return flow of NADW has to increase, too. However, the relatively strong AABW cell in S1X (8.8 Sv) significantly weakens in S2X (0.9 Sv). This means that although the upper overturning cell strengthens when the wind stress is doubled, the DWBC transport, consisting of NADW from the upper and AABW from lower cell, *decreases* from S1X (25.3 Sv) to S2X (21.9 Sv). The bottom cell in G1X is already comparatively weak (3.5 Sv), and it further decreases in G2X (1.1 Sv). Nevertheless, this implies a net *increase* in the DWBC transport from G1X (20.3 Sv) to G2X (21.9 Sv). In addition to different response *signs* in S2X and G2X, the DWBC response magnitude differs by a factor of two (-3.4 Sv in S2X and +1.6 Sv in G2X). In terms of flow speed, the described transport changes translate to a DWBC *slowdown* in the eddying S2X (see Figure 3.3) and a *speedup* in the non-eddying G2X (not shown).

This response difference might be caused entirely by different basic states in STORM and GR15. In particular, the bottom overturning cell in S1X is more than twice as strong as in G1X (see Figure 3.2). In order to get a better understanding of what role the basic state plays for the response, we conduct two more runs with the non-eddying GR15 configuration which we call G1X* and G2X*. In the new runs, we increase the surface salinity nudging south of of 65° S by 1 psu. In agreement with Brix and Gerdes (2003), such a tuning leads to more AABW formation and hence a stronger bottom overturning cell without significantly affecting the upper cell; G1X* now shows 4.9 Sv bottom overturning, whereas G2X* has 1.5 Sv. The response magnitude of the bottom cell in G2X* (3.4 Sv) is of the same magnitude as in G2X (2.4 Sv), but significantly lower than in S2X (7.9 Sv). And analogous to G2X, the DWBC in G2X* speeds up

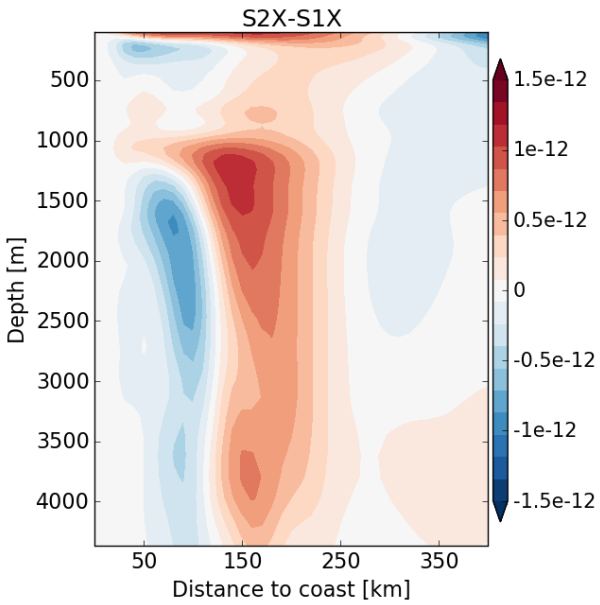

Figure 3.3: Depth/across-stream view of the DWBC: Difference S2X-S1X in the along-stream flow, multiplied by $\beta\sin\alpha$, $\beta\sin\alpha\Delta\overline{u}_{\|}$ (II in Equation 3.6), averaged along the DWBC between 20° N and 5° N. We also applied a Gaussian filter in the across-stream direction with a half-width of 10 km.

as compared to the control run G1X*. Despite the tuning, the bottom cell in G1X* is still significantly weaker than in S1X. Nonetheless, the similarity in the response of G2X and G2X* together with the fact that they both differ considerably from S2X suggests that the basic state is less important than the resolution. In the next section, we will provide further evidence for the resolution dependence of the response by showing that a link exists between the DWBC slowdown in the STORM configuration and mesoscale eddy fluxes.

3.4 EDDIES AND THE DWBC SLOW DOWN IN THE STEADY STATE REPONSE

Rhines and Holland (1979) and Holland and Rhines (1980) provide one of the first detailed descriptions of how mesoscale eddy fluxes can drive a mean flow. In their two-layer quasi-geostrophic model, eddy fluxes of potential vorticity $\overline{\mathbf{u}'q'}$ drive a mean flow $\overline{\mathbf{u}}$ via the time-averaged potential vorticity equation

$$\overline{\mathbf{u}} \cdot \nabla \overline{q} = -\nabla \cdot (\overline{\mathbf{u}'q'}), \tag{3.1}$$

where primed quantities denote fluctuations due to mesoscale eddies, overbars indicate mean fields and q is potential vorticity. Van Sebille et al. (2012) only recently used a 0.1° horizontal resolution primitive equation

ocean model to link the pathway of the eastward going branch of the DWBC near the southern tip of Africa to upper ocean eddies (the famous Aghulas rings), likewise via eddy fluxes of potential vorticity and now a 3D version of Equation 3.1.

Applying the quasi-geostrophic approximation and averaging in the along-stream direction, the eddy flux of potential vorticity, $\overline{\mathbf{u}'q'}$, can be written as a sum of two parts,

$$\langle\overline{\mathbf{u}'q'}\rangle = -\frac{\partial}{\partial x_\perp}\left\langle\overline{u'_\parallel u'_\perp}\right\rangle + \frac{\partial}{\partial z}\left\langle f\frac{\overline{u'_\perp \rho'}}{\partial\overline{\rho}/\partial z}\right\rangle, \tag{3.2}$$

(e.g., Olbers et al., 2012) with $x_\parallel$ being the along-stream and $x_\perp$ the across-stream direction, angle brackets $\langle\cdot\rangle$ denote an along-stream average and ρ is density. In the literature, the first term on the right-hand-side (rhs) of Equation 3.2 refers to the eddy vorticity flux (EVF) and the second term to the eddy thickness flux (ETF, e.g., Vallis, 2017), comprising the across-stream eddy density flux $\overline{u'_\perp \rho'}$. In both of the above examples, eddies are primarily generated in the upper ocean (the upper layer, respectively) and drive, via the ETF component a mean flow $\overline{\mathbf{u}}$ across isolines of $\overline{q}$ in the layer underneath. In both studies, the EVF component is less important (Holland and Rhines, 1980; Van Sebille et al., 2012). However, Spall (1994) speculates that the EVF potentially also plays a significant role near the DWBC.

3.4.1 *Eddy vorticity fluxes and DWBC slow down*

In this section, we show that the DWBC slow down in the eddying STORM configuration is closely linked to EVF. Our starting point is the Reynolds-averaged, quasi-geostrophic version of the vorticity equation

$$\frac{D_H}{Dt}(\overline{\zeta} + \beta y) = f\frac{\partial\overline{w}}{\partial z} - \nabla_H \cdot \overline{\mathbf{u}'\zeta'} \tag{3.3}$$

(e.g., Olbers et al., 2012), where $\zeta = \partial v/\partial x - \partial u/\partial y$ is the z-component of the relative vorticity and $\beta = \partial f/\partial y$ is the meridional gradient of the Coriolis parameter f. We describe the vertical velocity by w. Please note that the material derivative $D_H/Dt = \partial/\partial t + \overline{u}\,\partial/\partial x + \overline{v}\,\partial/\partial y$ contains only the horizontal advection by the mean flow.

Furthermore, we transform Equation 3.3 into an along/across-stream coordinate system in which one horizontal axis points into the negative along-stream direction $x_\parallel$ ($x_\parallel$ is directed approximately northwards) and the other in the across-stream direction $x_\perp$ ($x_\perp$ is directed approximately westwards towards the shore). Averaging along the DWBC (in $x_\parallel$-direction) from 20° N to 5° N, we are left with

$$\langle\overline{\mathbf{u}}_H \cdot \nabla_H\overline{\zeta}\rangle + \langle\beta\overline{u}_\parallel \sin\alpha\rangle + \langle\beta\overline{u}_\perp\cos\alpha\rangle = \left\langle f\frac{\partial\overline{w}}{\partial z}\right\rangle + \frac{\partial^2}{\partial x_\perp^2}\left\langle\overline{u'_\parallel u'_\perp}\right\rangle. \tag{3.4}$$

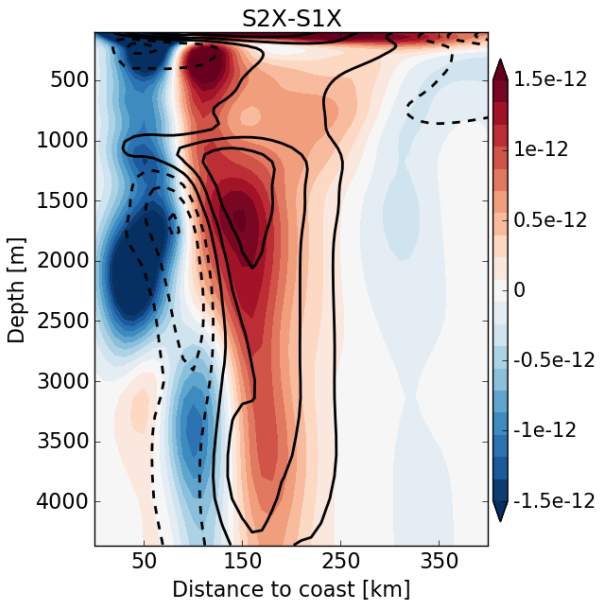

Figure 3.4: Depth/across-stream view of the DWBC: Colors show the difference S2X-S1X in the convergence of the EVF, $\partial^2/\partial x_\perp^2 \Delta[\overline{u'_\parallel u'_\perp}]$ (IV in Equation 3.6). Black contour lines show the difference S2X-S1X in the along-stream flow, $\beta \sin\alpha \Delta\overline{u}_\parallel$ (II in Equation 3.6). Solid lines denote positive, dashed lines negative values, the contour interval is 1.5×10^{-12}. All quantities are averaged along the DWBC between 20° N and 5° N, and we applied a Gaussian filter in the across-stream direction with a half-width of 10 km. Please note that $\beta \sin\alpha \Delta\overline{u}_\parallel$ can also be found in Figure 3.3 in colors.

The convergence of the EVF (last term on the rhs of Equation 3.3) simplifies when taking the along-stream average (e.g., Olbers et al., 2012). Furthermore, the DWBC is directed approximately southwards, the angle α between the zonal (x-) axis and the negative DWBC is close to 90°, so that $|\sin\alpha| > |\cos\alpha|$. Given the fact that by definition, the along-stream flow $\overline{u}_\parallel$ is stronger than the across-stream flow $\overline{u}_\perp$, we assume the third term on the left-hand-side (lhs) of Equation 3.4 to be much smaller than the second one. In other words, the across-stream advection of planetary vorticity is negligible compared to the along-stream advection. This yields

$$\left\langle \overline{\mathbf{u}}_H \cdot \nabla_H \overline{\zeta} \right\rangle + \left\langle \beta \overline{u}_\parallel \sin\alpha \right\rangle = \left\langle f \frac{\partial \overline{w}}{\partial z} \right\rangle + \frac{\partial^2}{\partial x_\perp^2} \left\langle \overline{u'_\parallel u'_\perp} \right\rangle . \tag{3.5}$$

Because we are interested in what causes the DWBC slow down, i.e. the difference in the along-stream flow $\overline{u}_\parallel$ between S1X and S2X, we formulate Equation 3.5 for both and form their difference S2X-S1X:

$$\underbrace{\Delta \left[\overline{\mathbf{u}}_H \cdot \nabla_H \overline{\zeta} \right]}_{\text{I}} + \underbrace{\beta \sin\alpha \, \Delta \overline{u}_\parallel}_{\text{II}} = \underbrace{f \frac{\partial \Delta \overline{w}}{\partial z}}_{\text{III}} + \underbrace{\frac{\partial^2}{\partial x_\perp^2} \Delta \left[\overline{u'_\parallel u'_\perp} \right]}_{\text{IV}} . \tag{3.6}$$

The symbol Δ denotes the difference of a quantity between S1X and S2X, $\Delta[\cdot] = (\cdot)_{S2X} - (\cdot)_{S1X}$. Please note that we omitted the angle brackets $\langle\cdot\rangle$ from the along-stream averaging. The resulting relation provides a possible link between the convergence of the EVF (IV in Equation 3.6) and the flow in $x_{\parallel}$-direction (II in Equation 3.6). For this link to be meaningful, the remaining terms I and III need to be small either because the respective terms are small in both S1X and S2X, or because they are similar in S1X and S2X and therefore their difference is negligible.

We show term II from Equation 3.6 in Figure 3.3. The narrow weak negative (blue) anomaly close to the shore indicates a region in which the DWBC in S2X is stronger than in S1X (the DWBC is going southwards and hence shows up as negative $\overline{u}_{\parallel}$). However, more dominant is a larger region further offshore, where Figure 3.3 shows a strong patch of positive (red) $\Delta\overline{u}_{\parallel}$. This is the DWBC slowdown that causes the reduced DWBC transport discussed in Section 3.3. Because we plot an average between 20° N and 5° N, we expect the DWBC slowdown in Figure 3.3 to be representative for most of the coherent part of the DWBC in the NH which is said to range from south of the Bahamas (25° N) to the equator (e.g., Buckley and Marshall, 2016; Rhein et al., 2015).

The colored shadings in Figure 3.4 depict the difference in the convergence of the EVF (IV from Equation 3.6). For comparison, the difference in the advection of planetary vorticity (i.e. the DWBC slowdown, II in Equation 3.6, see Figure 3.3) is shown in black contour lines. We observe quite good agreement between the two terms in their spatial distribution as well as in their magnitude: The weak negative flow-anomaly (dashed black contours between about 50 and 110 km from the coast in Figure 3.4) as well as the dominant positive flow anomaly (solid black contours between about 150 and 220 km from the coast in Figure 3.4) coincide with negative (blue) and positive (red) values in term IV from Equation 3.6, i.e. with the convergence of the EVF.

The magnitude of the vortex stretching term $f\partial\Delta\overline{w}/\partial z$ (III in Equation 3.6), shown in Figure 3.5, is significantly smaller than the respective EVF-term IV, shown in Figure 3.4. Likewise, the difference in the mean advection of relative vorticity $\Delta[\overline{\mathbf{u}}_H \cdot \nabla_H\overline{\zeta}]$ (I from Equation 3.6) is of smaller magnitude than the EVF-term (compare Figure 3.6 and Figure 3.4).

The analysis of the terms I-IV from Equation 3.6 suggests that the dominant balance is between the advection of planetary vorticity (II) and the convergence of the EVF (IV, see Figure 3.4)

$$\beta \sin\alpha \, \Delta\overline{u}_{\parallel} \approx \frac{\partial^2}{\partial x_{\perp}^2} \Delta\left[\overline{u'_{\parallel} u'_{\perp}}\right]. \tag{3.7}$$

Because β and $\sin\alpha$ are independent of the wind stress, we conclude that the DWBC slow down visible in the time-averaged response ($\Delta\overline{u}_{\parallel} > 0$ in Figure 3.3) is primarily balanced by EVF. This EVF is not present in the

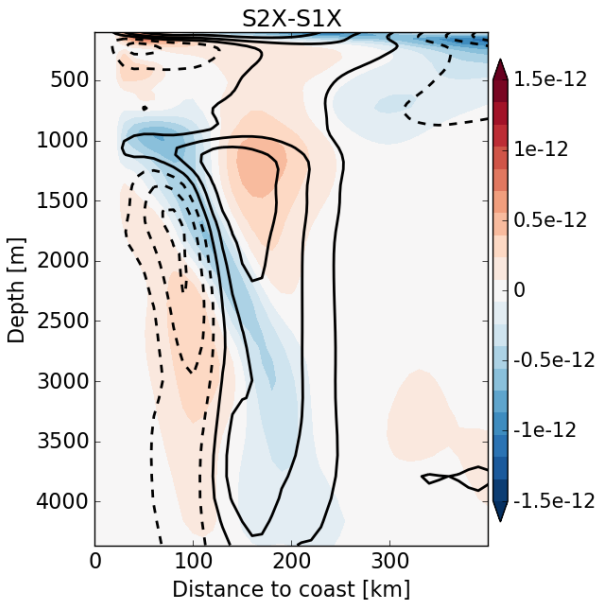

Figure 3.5: Depth/across-stream view of the DWBC: Colors show the difference S2X-S1X in the vortex stretching, $f\partial\Delta\overline{w}/\partial z$ (III in Equation 3.6). Black contour lines show the the difference S2X-S1X in the along-stream flow, $\beta\sin\alpha\Delta\overline{u}_{\|}$ (II in Equation 3.6). Solid lines denote positive, dashed lines negative values, contour interval is 1.5×10^{-12}. All quantities are averaged along the DWBC between 20° N and 5° N, and we applied a Gaussian filter in the across-stream direction with a half-width of 10 km. Please note that $\beta\sin\alpha\Delta\overline{u}_{\|}$ can also be found in Figure 3.3 in colors.

coarse resolution configuration GR15 and is also not captured by the GM parameterization for mesoscale eddies.

In this manuscript, we look only at the *difference* between the vorticity budget in S1X and S2X, in which the planetary vorticity advection term (II in Equation 3.6) is largely balanced by the EVF term (IV in Equation 3.6, see Figure 3.4). However, the EVF also contributes significantly to the individual vorticity budgets for S1X and S2X, helping to balance the advection of planetary vorticity by the mostly southward directed DWBC (we show each term from the vorticity budget in the order in which they appear in Equation 3.5 for S1X and for S2X in the Appendix). This is a remarkable finding because in the classic Stommel and Aarons model of the abyssal circulation (Stommel and Arons, 1959), planetary vorticity advection is balanced by the vortex stretching resulting from uniform upwelling in the interior ($f\partial w_0/\partial z \approx \beta v$). In the western boundary region (i.e. in the DWBC), mainly boundary friction (e.g., Olbers et al., 2012) or the mean advection of relative vorticity (e.g., Edwards and Pedlosky, 1998; Johnson et al., 2019) have been discussed as candidates to balance the planetary vorticity advection, while the EVF is mentioned less.

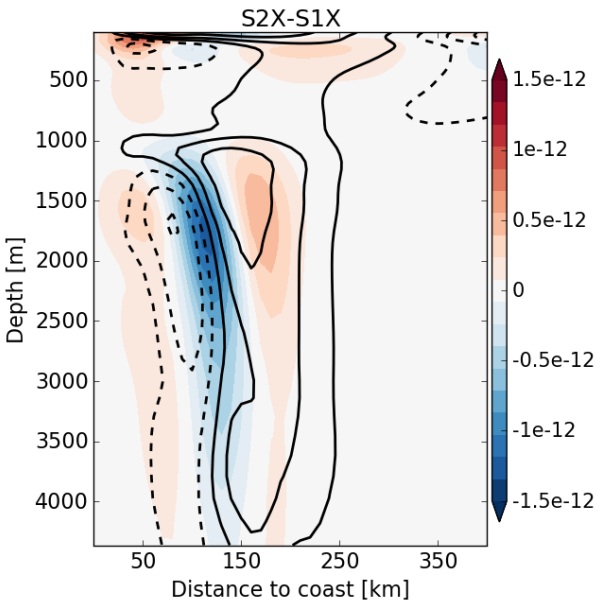

Figure 3.6: Depth/across-stream view of the DWBC: Colors show the difference S2X-S1X in the mean advection of relative vorticity, $\Delta[\overline{\mathbf{u}}_H \cdot \nabla_H \overline{\zeta}]$ (I in Equation 3.6). Black contour lines show the the difference S2X-S1X in the along-stream flow, $\beta \sin\alpha \Delta\overline{u}_{\parallel}$ (II in Equation 3.6). Solid lines denote positive, dashed lines negative values, contour interval is 1.5×10^{-12}. All quantities are averaged along the DWBC between 20° N and 5° N, and we applied a Gaussian filter in the across-stream direction with a half-width of 10 km. Please note that $\beta \sin\alpha \Delta\overline{u}_{\parallel}$ can also be found in Fig. Figure 3.3 in colors.

3.4.2 *Eddy thickness fluxes*

We have shown that the DWBC slow down ($\Delta\overline{u}_{\parallel} > 0$), occurring as a response to a doubling of the surface wind stress, is directly related to the convergence of the EVF. But what about the eddy thickness flux (second term on rhs of Equation 3.2), whose magnitude is usually assumed to be larger than that of the vorticity flux (Hogg, 1983; Holland and Rhines, 1980; Van Sebille et al., 2012)?

Eliminating $\overline{w}$ between Equation 3.5 and the time averaged density budget, which we assume to be reasonably approximated by $\overline{\mathbf{u}} \cdot \nabla\overline{\rho} \approx -\nabla \cdot \overline{\mathbf{u}'\rho'}$ near the DWBC (Lüschow et al., 2019), yields the along-stream averaged potential vorticity equation

$$\left\langle \overline{\mathbf{u}}_H \cdot \nabla_H \left(\overline{\zeta} + f\frac{\partial\overline{\rho}}{\partial z} \right) \right\rangle + \left\langle \beta\overline{u}_{\parallel} \sin\alpha \right\rangle = -\frac{\partial}{\partial z}\left\langle f\frac{\nabla \cdot \overline{\mathbf{u}'\rho'}}{\partial\overline{\rho}/\partial z} \right\rangle + \frac{\partial}{\partial x_{\perp}}\left(\frac{\partial}{\partial x_{\perp}} \left\langle \overline{u'_{\parallel} u'_{\perp}} \right\rangle \right). \quad (3.8)$$

It allows a direct comparison of the ETF component (first term on the rhs) and the EVF component (second term on the rhs). In other words,

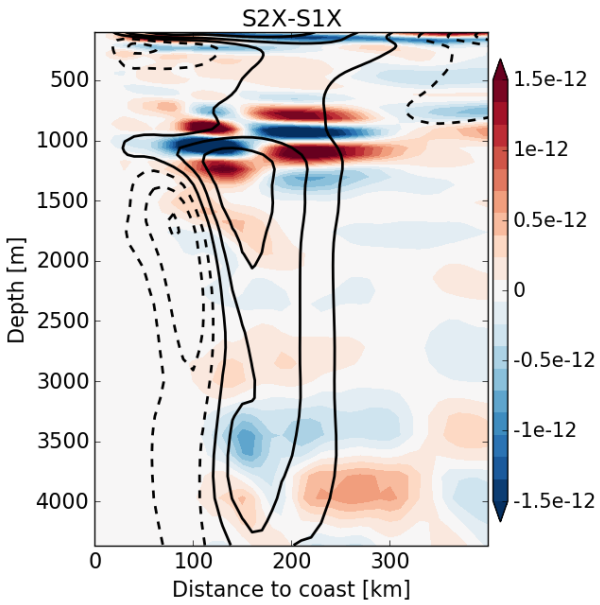

Figure 3.7: Depth/across-stream view of the DWBC: Colors show the difference S2X-S1X in the divergence of the ETF, $\partial/\partial z \Delta[f\,\nabla\cdot\overline{\mathbf{u}'_\perp\rho'}/\partial\overline{\rho}/\partial z]$. Black contour lines show the the difference S2X-S1X in the along-stream flow, $\beta\sin\alpha\Delta\overline{u}_{\|}$ (II in Equation 3.6). Solid lines denote positive, dashed lines negative values, contour interval is 1.5×10^{-12}. All quantities are averaged along the DWBC between 20° N and 5° N, and we applied a Gaussian filter in the across-stream direction with a half-width of 10 km. Please note that $\beta\sin\alpha\Delta\overline{u}_{\|}$ can also be found in Fig. Figure 3.3 in colors.

Equation 3.8 enables us to compare the influence of eddy vorticity versus eddy density fluxes on the DWBC mean flow. The difference S2X-S1X of the ETF term in Equation 3.8, $\partial/\partial z\Delta[f\,\nabla\cdot\overline{\mathbf{u}'_\perp\rho'}/\partial\overline{\rho}/\partial z]$, is shown in Figure 3.7. Its magnitude is significantly smaller than the respective EVF term (shown in Figure 3.4) and its spatial distribution does not resemble the flow difference $\Delta\overline{u}_{\|}>0$ (black contour lines in Figure 3.7). We conclude that eddy fluxes of thickness are less relevant for the DWBC slow down in S2X. This seems reasonable when regarding the ratio of EVF and ETF in Equation 3.2,

$$R=\frac{\frac{V'^2}{\delta x_\perp}}{\frac{V'\rho' f}{\rho}}=\frac{V'}{\rho'}\frac{\rho}{\delta x_\perp f} \tag{3.9}$$

It increases with depth for strong, deep eddies because the eddy swirl speed V' stays more or less constant with depth while variations in density ρ' decrease with depth like the surrounding stratification does. Thus, the relative importance of eddy vorticity fluxes can be expected to increase for vertically coherent eddies such as those in the DWBC (Lüschow et al., 2019).

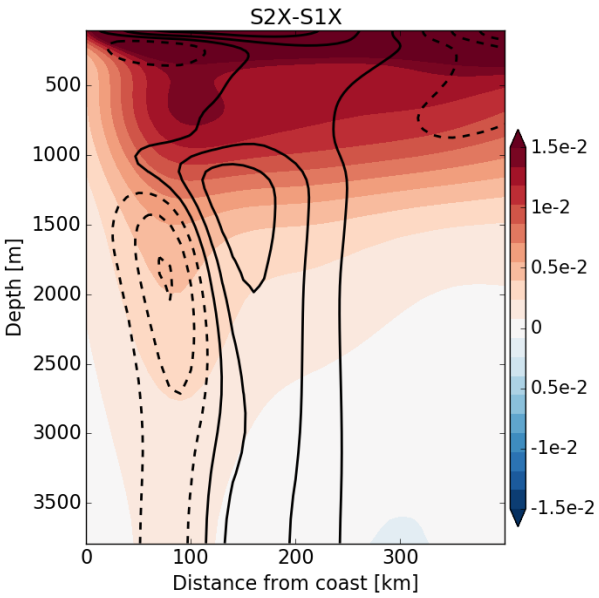

Figure 3.8: Depth/across-stream view of the DWBC: Colors show the difference S2X-S1X in eddy kinetic energy (EKE). Black contour lines show the difference S2X-S1X in the along-stream flow, $\beta \sin\alpha \Delta\overline{u}_{\|}$ (term II in Equation 3.6). Solid lines denote positive, dashed lines negative values, the contour interval is 1.5×10^{-12}. All quantities are averaged along the DWBC between 20° N and 5° N, and we applied a Gaussian filter in the across-stream direction with a half-width of 10 km.

3.4.3 *Causes for the DWBC slow down*

The relation between DWBC slow down and EVF (Figure 3.4) in the time-averaged vorticity budget is an empirical statement about a balance. By itself, it does not contain an answer to the question if the eddy fluxes play an active or passive role for the slow down. With *passive*, we mean that eddies only react to the elsewhere caused DWBC slow down by providing the vorticity input that is necessary to compensate for the change in planetary vorticity advection. With *active* on the other hand, we refer to a scenario in which a change in the eddy field actively slows down the DWBC via eddy fluxes. In case the eddies play an active role, the question arises what causes the change in the eddy field and thereby triggers the DWBC slow down. This subsection as well as the following section contain arguments why we think that eddies might indeed play a rather active role for the DWBC slow down and that the change in the eddy field is triggered by a response in the northward flow that lies above the DWBC.

The response of the EVF is not confined to the depth range of the DWBC between 1000 m and 4000 m but instead extends over the whole water column (Figure 3.4). Furthermore, the response in EKE shows a strong increase not only in the upper ocean but also near the DWBC (see

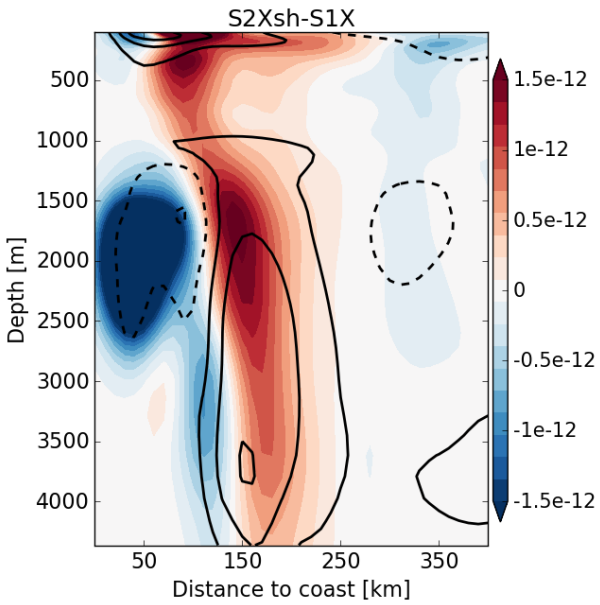

Figure 3.9: Same plot as in Figure 3.4, but now for scenario S2Xsh. Colors show the difference S2Xsh-S1X in the convergence of the EVF, $\partial^2/\partial x_\perp^2 \Delta[\overline{u'_\parallel u'_\perp}]$ (analogue to term IV in Equation 3.6 for scenario S2Xsh instead of S2X). Black contour lines show the difference S2Xsh-S1X in the along-stream flow, $\beta \sin\alpha \Delta\overline{u}_\parallel$ (analogue to term II in Equation 3.6). Solid lines denote positive, dashed lines negative values, the contour interval is 1.5×10^{-12}. All quantities are averaged along the DWBC between 20° N and 5° N, and we applied a Gaussian filter in the across-stream direction with a half-width of 10 km.

Figure 3.8). In a DWBC that slows down, the generation of mesoscale eddies likewise declines. Hence, that EKE near the DWBC rises implies that the additional EKE originates not in the DWBC but is generated nonlocally, most likely in the upper ocean northward flow. Taken together, the responses of EKE and EVF suggest that changes of the DWBC eddy field originate not in the DWBC depth range but are caused *above* the DWBC where the northward flow lies.

At this point, use the second sensitivity experiment, S2Xsh, in which we double the wind stress only over the SO. This experiment allows a distinction between remote and local effects of the wind stress doubling. The DWBC slow down in S2Xsh resembles that of S2X in its spatial structure and magnitude (see the black contour lines in Figure 3.9 that is an S2Xsh analogue to Figure 3.4). And also the response in the EVF term (IV from (3.6)) is quite similar in S2X and S2Xsh (compare colored contours in Figure 3.9 and Figure 3.4). Hence, the NH response in the eddy field near the DWBC, in particular in the EVF visible in Figure 3.4 and Figure 3.9, cannot be due to changes in the local NH wind forcing. Instead, it must be caused by the wind stress doubling over the SO.

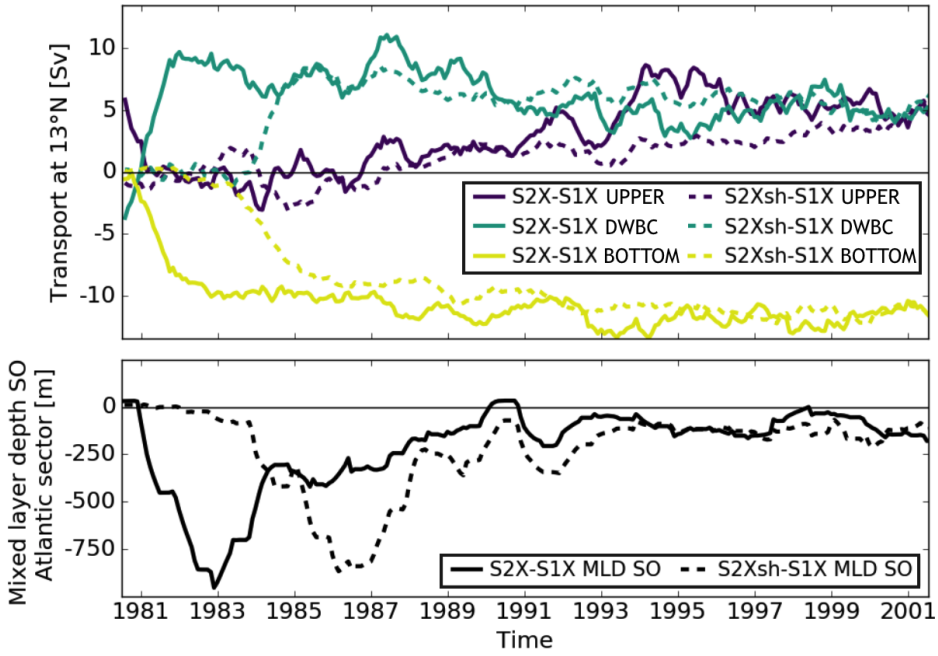

Figure 3.10: 12 months running mean response at 13° N of: (Top panel): Total meridional transport between the surface and 1000 m depth ('UPPER', purple), between 1000 m and 4000 m ('DWBC', turquoise) and between 4000m and 6000 m depth ('BOTTOM', yellow); (lower panel): AABW formation indexed by the mixed layer depth in the Atlantic sector in the SO, 50° W –17° W, 66° S –73° S ('MLD SO', black). All solid lines refer to the response of the scenario with globally doubled wind stress, S2X-S1X. All dashed lines refer to the response of the scenario with the wind stress doubled only over the SO, S2Xsh-S1X. The wind stress doubling in S2X and S2Xsh was executed in the year 1980.

However, changes in the NH eddy field need to be triggered by changes in the local NH mean flow. In the next section, we show that one potential candidate for such a mean flow change is the increase in surface flow that occurs before the DWBC transport declines.

3.5 EVOLUTION OF THE RESPONSE IN THE STORM RUNS S2X AND S2XSH

The top panel of Figure 3.10 shows the response time series for the meridional transport at 13° N. This latitude is one example within the domain studied; however, the qualitative behavior is similar everywhere between 5° N and 20° N. Following Shakespeare and Hogg (2012), we split the transport into three layers: upper ocean (northward) transport between 0 m and 1000 m depth (Figure 3.10); DWBC (southward) transport between 1000 m and 4000 m depth; bottom (northward) transport between 4000 m and the ocean bottom.

The quasi-steady state response of S2X was already discussed via the time-averaged overturning streamfunctions (Figure 3.2); it emerges in its final form around 1995: The decrease in DWBC (Figure 3.10) is linked to the strong decrease in BOTTOM and partly counteracted by a milder increase in UPPER. But how does the wind induced signal propagate from the surface where the wind stress is doubled towards the deep ocean where the bottom overturning cell declines?

The most obvious propagation route would be via the SO, where the wind stress potentially affects the rate of AABW formation that feeds the bottom overturning (e.g., Brix and Gerdes, 2003; Poulsen et al., 2018; Rahmstorf and England, 1997; Shakespeare and Hogg, 2012). However, previous studies expect the cross-equatorial propagation of AABW signals from the SO towards the NH to take at least a decade (e.g., Masuda et al., 2010; Zanowski and Hallberg, 2017). In contrast, the S2X response at 13° N occurs after only 2 years in 1982. This suggests that the response mechanism is rather local in the NH. A potential trigger for this local response is the upper ocean northward transport, (UPPER, solid purple in Figure 3.10): It shows a strong increase within a short time period right before BOTTOM (solid yellow) and DWBC (solid turquoise) begin to decay. This increase in the northward mean flow right above the DWBC might be responsible for the EKE increase near the DWBC (Figure 3.8) and the response in the EVF (Figure 3.4).

Again, it is informative to compare the responses of S2Xsh (dashed lines in Figure 3.10) and S2X (solid lines). Their quasi-steady state overturning response is nearly identical, implying that on decadal timescale, the response is controlled by the SO wind stress. However, all time series in Figure 3.10 show that the response in S2Xsh is delayed by about 4 years as compared to S2X. Like in S2X, we note in S2Xsh a short increase in UPPER (dashed purple line) right before BOTTOM and DWBC decline. If the above-mentioned interaction between the surface northward flow (UPPER) and the DWBC exists, it provides a potential explanation for the response delay in S2Xsh. Because while in S2X, the initial peak in UPPER is caused by the NH wind stress doubling, UPPER at 13° N in S2Xsh can increase only due to the remote effect of the SO wind stress doubling, i.e. via the Drake passage effect. This however happens on interannual to decadal timescales (e.g., Klinger and Cruz, 2009) and thus serves as an explanation for the 4 years response delay of S2Xsh.

One further peace of evidence comes from the time series of AABW formation shown in the lower panel of Figure 3.10 (indexed by the mixed layer depth in the Atlantic sector of the SO). Apparently, the amount of AABW formation decreases *after* the DWBC and BOTTOM cell transport at 13° N decline. Such an order of events is in contrast to previous studies that report perturbations in the AABW formation to precede changes in the bottom overturning cell (e.g., Patara and Böning, 2014; Purkey and Johnson, 2012).

Hence, the response time series in Figure 3.10 provides three hints for the existence of a local NH response mechanism that slows down the DWBC via eddy fluxes and thereby weakens the bottom overturning cell: (i) a decline of the bottom overturning cell rooted in a reduction of AABW formation, as was used as an explanation in previous studies, can be ruled out. The bottom overturning declines *before* the AABW formation goes down. Furthermore, two years response time in S2X is not enough time for a signal induced in the SO to travel to 13° N; (ii) in both S2X and S2Xsh, the rapid decline in the southward DWBC transport is preceded by a strengthening of the overlying northward transport; (iii) an interaction between the surface flow and the DWBC could explain the remarkable response delay in S2Xsh; while the northward flow strengthens more or less immediately in S2X due to the local impact of the wind stress doubling, it takes a couple of years longer in S2Xsh because here it happens via the Drake passage effect in the SO.

3.6 DISCUSSION AND CONCLUSION

In this manuscript, we compare a set of wind sensitivity experiments in one eddying ('STORM', 0.1° resolution) and one non-eddying ('GR15', 1.5° resolution) configuration of the same realistic geometry ocean model MPI-OM. This final section begins with the discussion of the analysis of the steady state response (Section 3.6.1). After that, we discuss ideas on what we can learn from the temporal evolution of the response (Section 3.6.2), before drawing conclusions (Section 3.6.3).

3.6.1 *Quasi-steady state response*

All sensitivity runs reach a new quasi-steady state within about 15 years after the wind stress doubling. We analyze this quasi-steady state response by looking at time-averaged data from 2001 to 2010, which gives us robust statistics of the effect of mesoscale eddy fluxes.

In both configurations, the response is in principal agreement with the ocean seesaw concept; the upper (AMOC) cell strengthens whereas the bottom (AABW) cell weakens. Yet, while the two configuration's response magnitude in the upper cell is similar (roughly 4 Sv increase), they strongly disagree regarding the magnitude of the bottom cell response (8 Sv decrease in STORM and 2 Sv decrease in GR15). This leads to opposing responses in the DWBC, which speeds up in GR15 and slows down in STORM (see Figure 3.2). GR15 and STORM have different basic states regarding the bottom overturning cell, which may have an influence on their response behavior. However, we provide strong evidence that the response differences are rather rooted in the fact that STORM explicitly resolves mesoscale eddies whereas GR15 does not. By analyzing along-

stream averages between 20° N and 5° N, we show that eddy fluxes of relative vorticity essentially balance the DWBC slow down in the time-averaged vorticity budget of STORM (Section 3.4). Based on this analysis, we cannot robustly say that mesoscale eddy fluxes actively slow down the DWBC. But we can conclude from the diagnosed balance between the slow down and the EVF (Figure 3.4 and Figure 3.9) that without explicit representation of eddies (as in GR15), the observed slow down would be balanced differently and hence, cannot occur in GR15. Therefore, our vorticity budget analysis has implications for the ocean seesaw.

In the non-eddying GR15 experiments, both cells change by roughly the same magnitude and this agrees with expectations inferred from previous non-eddying setups (e.g., Patara and Böning, 2014). The DWBC slow down in STORM, which we argue is dependent on resolved eddy fluxes, allows for larger differences in the response magnitude between upper and bottom cell. We interpret this as a *decoupling* of the two overturning cells and hence conclude that the seesaw effect might be weaker in the real (eddying) ocean than was observed in non-eddying ocean models.

Furthermore, if the wind stress is doubled only over the SO (S2Xsh / G2Xsh), the response magnitude and spatial structure are the same as with globally doubled wind stress (S2X / G2X). For the response of STORM, this implies that the diagnosed balance between DWBC slow down and EVF is almost the same in S2Xsh and S2X (compare Figure 3.4 and Figure 3.9). Hence, the steady state response in the eddy field and the related DWBC slow down are set by the SO wind stress and remain unaffected by the local, NH wind stress perturbation. This is in agreement with earlier sensitivity experiments which find the bottom cell response to be controlled by SO processes (Brix and Gerdes, 2003; Patara and Böning, 2014; Swingedouw et al., 2009). However, the temporal evolution of the response shows that the *response mechanism* must be different in our case.

3.6.2 *Temporal evolution of the response in STORM*

In previous experiments, a perturbation applied to the SO causes a change in the AABW formation which *then* propagates northwards as response signal. In contrast the overturning cell in STORM abruptly declines in the NH (yellow in Figure 3.10) *before* the AABW formation ceases (black in Figure 3.10). Hence, the bottom cell weakening cannot be caused by the reduction of AABW formation. Also the very fast bottom cell response in the NH within 2 years in S2X and 6 years in S2Xsh, respectively, conflicts with the notion of a remote (SO induced) trigger for the bottom cell response (Section 3.5).

Instead, we hypothesize that a local NH interaction with the upper ocean northward flow via mesoscale eddy fluxes causes the DWBC to slow down and in turn the bottom overturning cell to weaken. The

trigger for this interaction would be the short strengthening of the surface northward flow (purple in Figure 3.10) right before the DWBC declines (turquoise in Figure 3.10). This strengthening would then lead to an increase in the upper ocean eddy activity and in doing so, would also fuel the deep eddy field (cf. the response in the EKE in Figure 3.8). Based on this, we speculate that also the response in the EVF which extends the whole water column (Figure 3.4 and Figure 3.9) is caused by the strengthening of the upper ocean flow.

The hypothesis of an interaction between upper ocean northward and DWBC flow furthermore provides a potential explanation for the 4 years response delay in scenario S2Xsh: In S2X, doubling the NH wind stress almost immediately strengthens the upper ocean Ekman transport. In contrast, the intensification of the upper ocean flow in S2Xsh occurs on the interannual to decadal timescale of the Drake passage effect (e.g., Klinger and Cruz, 2009). Hence, the trigger for the response in the DWBC eddy field is delayed in S2Xsh and consequently, the DWBC slow down is delayed, too. Although the long-term response seems to be controlled by the SO wind stress, our proposed local response mechanism enables the NH hemisphere conditions to affect the (short-term,interannual) response behavior in the deep overturning.

3.6.3 *Conclusions*

We show that mesoscale eddies are necessary to balance the DWBC slow down in the quasi-steady state response. Thereby, we explain why the slow down can be observed in the eddying STORM but not in the non-eddying GR15 configuration. For the interplay between the upper and bottom overturning cells, this explanation implies that the tight link between the two cells (ocean seesaw) might be an artifact of non-eddying ocean models. Only with resolved eddies, it might be possible to capture the DWBC slow down observed in STORM and hence to allow for the two cells to develop more independently.

The response chronology in which the bottom overturning cell in the NH declines before the AABW formation goes down suggests that a so far unknown response mechanism is at work in the eddying STORM configuration. We hypothesize that the intensification of the upper ocean northward flow triggers the DWBC slow down via eddy fluxes and thereby also cause the bottom cell to weaken. However, more evidence in this point is required. E.g., the interaction of upper, DWBC and bottom flow should be investigated in an idealized layer model such as the one from Jayne et al. (1996) that was recently used by Le Bras et al. (2018) for a similar purpose.

With this manuscript, we shed new light on the vorticity dynamics near the DWBC. To the best of our knowledge, eddy vorticity fluxes were not yet mentioned in the context of the DWBC response to forcing

changes. We furthermore think that the described eddy-based response mechanism deserves further attention and that it might be helpful in interpreting the real ocean's overturning response behavior.

ACKNOWLEDGMENTS

We thank Alexa Griesel for valuable discussions on the manuscript and Helmuth Haak who supported us in all technical concerns. This work was supported by the Max Planck Society and the International Max Planck Research School on Earth System Modelling. We also thank the German consortium project STORM, especially the cluster of excellence CliSAP of the University Hamburg, for making the 0.1-degree simulation possible.

APPENDIX TO CHAPTER 3

In the main text, we show only the differences S2X-S1X of the individual terms in the vorticity budget because we were interested in the DWBC slow down $\Delta\overline{u}_{\parallel} = \overline{u}_{\parallel,S2X} - \overline{u}_{\parallel,S1X}$. The individual terms from Equation 3.5 can be found in Figure 3.11 for S1X and in Figure 3.12 for S2X in the order in which they appear in Equation 3.5.

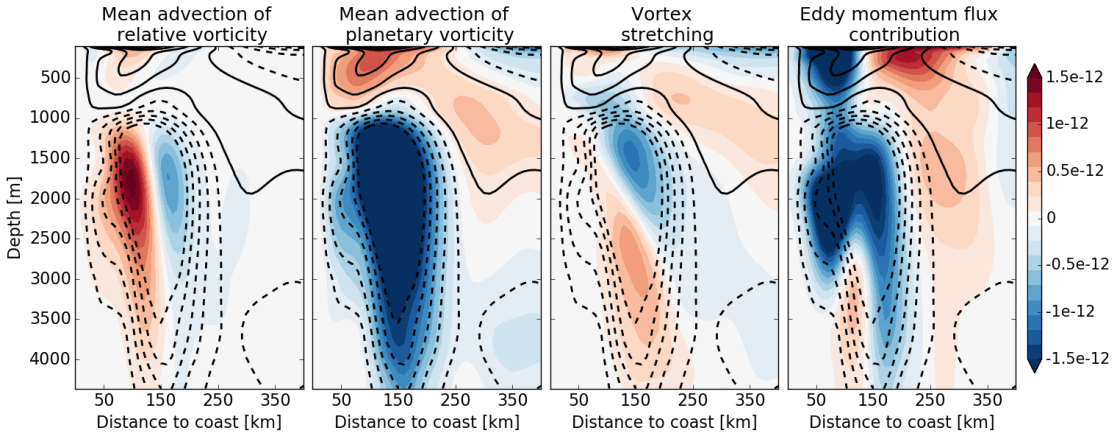

Figure 3.11: Individual contributions to the DWBC vorticity equation for scenario S1X, averaged between 20° N and 5° N in the order in which they appear in Equation 3.5.

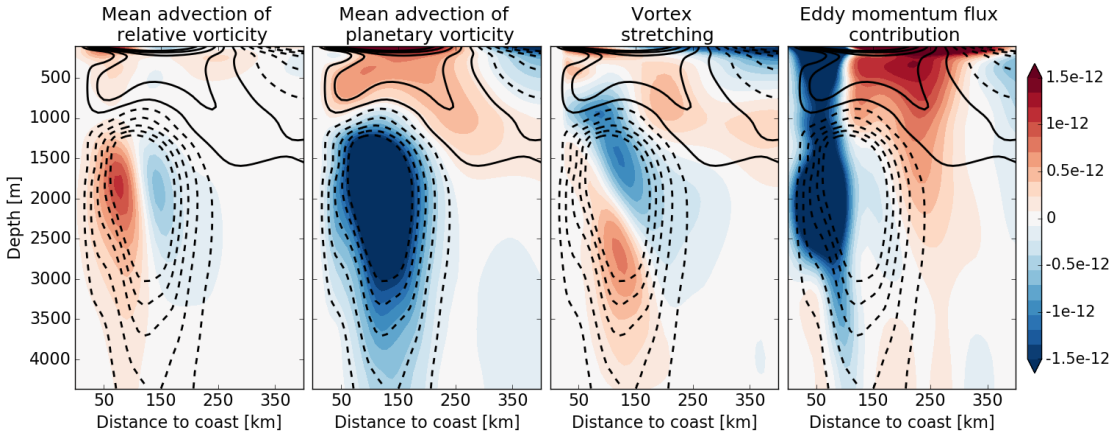

Figure 3.12: Individual contributions to the DWBC vorticity equation for scenario S2X, averaged between 20° N and 5° N in the order in which they appear in Equation 3.5.

BIBLIOGRAPHY

Aagaard, Knut, Roger Andersen, James Swift, and James Johnson (2008). "A large eddy in the central Arctic Ocean." In: *Geophysical Research Letters* 35, pp. 1–6.

Abernathey, Ryan, John Marshall, and David Ferreira (2011). "The Dependence of Southern Ocean Meridional Overturning on Wind Stress." In: *Journal of Physical Oceanography* 41, pp. 2261–2278.

Adcroft, Alistair, Robert Hallberg, John P. Dunne, Bonita L. Samuels, J. A. Galt, Christopher H. Barker, and Debra Payton (2010). "Simulations of underwater plumes of dissolved oil in the Gulf of Mexico." In: *Geophysical Research Letters*.

Aiki, Hidenori, Xiaoming Zhai, and Richard J Greatbatch (2016). "Energetics of the Global Ocean : the Role of Mesoscale Eddies." In: *Indo-Pacific Climate Variability and Predictability*, pp. 109–134.

Andrews, D. G. and M. E. McIntyre (1976). "Planetary Waves in Horizontal and Vertical Shear: the Generalized Eliassen-Palm Relation and the Mean Zonal Acceleration." In: *Journal of the Atmospheric Sciences* 33, pp. 2031–2048.

– (1978). "Generalized Eliassen-Palm and Charney-Drazin Theorems for Waves oin Axismmetric Mean Flows in Compressible Atmospheres." In: *Journal of the Atmospheric Sciences* 35, pp. 175–185.

Aoki, Kunihiro, Atsushi Kubokawa, Ryo Furue, and Hideharu Sasaki (2016). "Influence of Eddy Momentum Fluxes on the Mean Flow of the Kuroshio Extension in a $1/10^\circ$ Ocean General Circulation Model." In: *Journal of Physical Oceanography* 46, pp. 2769–2784.

Baehr, Johanna, Joël Hirschi, Jens-Olaf Beismann, and Jochem Marotzke (2004). "North Atlantic : A model-based array design study." In: *Journal of Marine Research* 62, pp. 283–312.

Bashmachnikov, I., F. Machín, A. Mendonça, and A. Martins (2009). "In situ and remote sensing signature of meddies east of the mid-Atlantic ridge." In: *Journal of Geophysical Research: Oceans* 114, pp. 1–16.

Bishop, Stuart P., Peter R. Gent, Frank O. Bryan, Andrew F. Thompson, Matthew C. Long, and Ryan Abernathey (2016). "Southern Ocean Overturning Compensation in an Eddy-Resolving Climate Simulation." In: *Journal of Physical Oceanography* 46, pp. 1575–1592.

Bower, Amy S., M. Susan Lozier, Stefan F. Gary, and Claus W. Böning (2009). "Interior pathways of the North Atlantic meridional overturning circulation." In: *Nature* 459, pp. 243–247.

Bracegirdle, Thomas J., Emily Shuckburgh, Jean Baptiste Sallee, Zhaomin Wang, Andrew J.S. Meijers, Nicolas Bruneau, Tony Phillips, and Laura J. Wilcox (2013). "Assessment of surface winds over the atlantic, indian,

and pacific ocean sectors of the southern ocean in CMPI5 models: Historical bias, forcing response, and state dependence." In: *Journal of Geophysical Research Atmospheres* 118, pp. 547–562.

Brix, H. and R. Gerdes (2003). "North Atlantic Deep Water and Antarctic Bottom Water: Their interaction and influence on the variability of the global ocean circulation." In: *Journal of Geophysical Research C: Oceans* 108, pp. 4–1.

Broecker, W S (1998). "Paleocean circulation during the last deglaciation: A bipolar seesaw?" In: *Paleoceanography* 13, pp. 119–21.

Brüggemann, Nils and Caroline A. Katsman (2019). "Dynamics of downwelling in an eddying marginal sea: contrasting the Eulerian and the isopycnal perspective." In: *Journal of Physical Oceanography*, pp. 3017–3035.

Bryan, Frank O., Peter R. Gent, and Robert Tomas (2014). "Can southern ocean eddy effects be parameterized in climate models?" In: *Journal of Climate* 27, pp. 411–425.

Bryden, H.L., W.E. Johns, and P.M. Saunders (2005a). "Deep western boundary current east of Abaco: mean structure and transport." In: *Journal of Marine Research* 63, pp. 35–57.

Bryden, Harry L., Hannah R. Longworth, and Stuart A. Cunningham (2005b). "Slowing of the Atlantic meridional overturning circulation at 25° N." In: *Nature* 438, pp. 655–657.

Buckley, Martha W and John Marshall (2016). "Observations, inferences, and mechanisms of the Atlantic Meridiona Overturning Circulation: A review." In: *Reviews of Geophysics* 54.1, pp. 5–63.

Carpenter, J. R. and M. L. Timmermans (2012). "Deep mesoscale eddies in the Canada Basin, Arctic Ocean." In: *Geophysical Research Letters* 39, pp. 1–6.

Charney, J. G. (1947). "The Dynamics of Long Waves in a Baroclinic Westerly Current." In: *Journal of Meteorology* 4, pp. 136–162.

– (1971). "Geostrophic Turbulence." In: *Journal of the Atmospheric Sciences* 28, pp. 1087–1095.

Chelton, Dudley B., Michael G. Schlax, Roger M. Samelson, and Roland A. de Szoeke (2007). "Global observations of large oceanic eddies." In: *Geophysical Research Letters* 34, pp. 1–5.

Chen, Gengxin, Dongxiao Wang, Changming Dong, Tingting Zu, Huijie Xue, Yeqiang Shu, Xiaoqing Chu, Yiquan Qi, and Hui Chen (2015). "Observed deep energetic eddies by seamount wake." In: *Scientific Reports* 5, pp. 1–10.

Chen, Ru, Glenn R. Flierl, and Carl Wunsch (2014). "A Description of Local and Nonlocal Eddy–Mean Flow Interaction in a Global Eddy-Permitting State Estimate." In: *Journal of Physical Oceanography* 44, pp. 2336–2352.

Chouksey, Manita, Carsten Eden, and Nils Brüggemann (2018). "Internal gravity wave emission in different dynamical regimes." In: *Journal of Physical Oceanography* 48, pp. 1709–1730.

Church, John A., Neil J. White, Catia M. Domingues, Didier P. Monselesan, and Elaine R. Miles (2013). "Sea-level and ocean heat-content change." In: *Ocean Circulation and Climate: A 21st Century Perspective*. 2nd ed. Vol. 103. Elsevier Ltd. Chap. Chapter 27, pp. 697–725.

Cunningham, Stuart a et al. (2007). "Temporal Variability of the Atlantic Meridional Overturning Circulation at 26.5°N." In: *science* 317, pp. 935–938.

Danabasoglu, Gokhan and James C. Mc Williams (1995). "Sensitivity of the Global Ocean Circulation to Parameterizations of Mesoscale Tracer Transports." In: *Journal of Climate* 8, pp. 2967–2987.

Danabasoglu, Gokhan, James C. Mcwilliams, and Peter R. Gent (1994). "The Role of Mesoscale Tracer Transports in the Global Ocean Circulation." In: *Science, New Series* 264, pp. 1123–1126.

Dengler, M., F. A. Schott, C. Eden, P. Brandt, J. Fischer, and R. J. Zantopp (2004). "Break-up of the Atlantic deep western boundary current into eddies at 8° S." In: *Nature* 432, pp. 1018–1020.

Eady, E. T. (1949). "Long Waves and Cyclone Waves." In: *Tellus* 1, pp. 33–52.

Eden, Carsten (2010). "Parameterising meso-scale eddy momentum fluxes based on potential vorticity mixing and a gauge term." In: *Ocean Modelling* 32, pp. 58–71.

Eden, Carsten and Richard J. Greatbatch (2008). "Diapycnal mixing by meso-scale eddies." In: *Ocean Modelling* 23, pp. 113–120.

Eden, Carsten, Richard J. Greatbatch, and Jürgen Willebrand (2007a). "A Diagnosis of Thickness Fluxes in an Eddy-Resolving Model." In: *Journal of Physical Oceanography* 37, pp. 727–742.

Eden, Carsten, Richard J. Greatbatch, and Dirk Olbers (2007b). "Interpreting Eddy Fluxes." In: *Journal of Physical Oceanography* 37, pp. 1282–1296.

Edwards, Christopher a. and Joseph Pedlosky (1998). "Dynamics of Nonlinear Cross-Equatorial Flow. Part I: Potential Vorticity Transformation." In: *Journal of Physical Oceanography* 28, pp. 2382–2406.

Farneti, Riccardo et al. (2015). "An assessment of Antarctic Circumpolar Current and Southern Ocean meridional overturning circulation during 1958-2007 in a suite of interannual CORE-II simulations." In: *Ocean Modelling* 93, pp. 84–120.

Ferrari, Raffaele (2014). "Oceanography: What goes down must come up." In: *Nature* 513, pp. 179–180.

Fine, Rana A (1995). "Tracers , time scales , and the thermohaline circulation: The lower limb in the North Atlantic Ocean." In: *Reviews of Geophysics* 33(S2), pp. 1353–1365.

Fischer, J. et al. (2015). "Intra-seasonal variability of the DWBC in the western subpolar North Atlantic." In: *Progress in Oceanography* 132, pp. 233–249.

Fischer, Jürgen and Friedrich A. Schott (2002). "Labrador Sea Water Tracked by Profiling Floats — From the Boundary Current into the Open North Atlantic." In: *Journal of Physical Oceanography* 32(2), pp. 573–584.

Fox-Kemper, Baylor, Raffaele Ferrari, and Joseph Pedlosky (2003). "On the Indeterminacy of Rotational and Divergent Eddy Fluxes." In: *Journal of Physical Oceanography* 33, pp. 478–483.

Frölicher, Thomas L., Jorge L. Sarmiento, David J. Paynter, John P. Dunne, John P. Krasting, and Michael Winton (2015). "Dominance of the Southern Ocean in anthropogenic carbon and heat uptake in CMIP5 models." In: *Journal of Climate* 28, pp. 862–886.

Fu, L-L, Chelton D B, Pierre Yves Le Traon, and R. Morrow (2010). "Eddy dynamics from satellite altimetry." In: *Oceanography* 23, pp. 14–25.

Garzoli, Silvia L., Shenfu Dong, Rana Fine, Christopher S. Meinen, Renellys C. Perez, Claudia Schmid, Erik Van Sebille, and Qi Yao (2015). "The fate of the Deep Western Boundary Current in the South Atlantic." In: *Deep-Sea Research Part I: Oceanographic Research Papers* 103, pp. 125–136.

Gent, Peter R. (2011). "The Gent-McWilliams parameterization: 20/20 hindsight." In: *Ocean Modelling* 39, pp. 2–9.

– (2016). "Effects of Southern Hemisphere Wind Changes on the Meridional Overturning Circulation in Ocean Models." In: *Annual Review of Marine Science* 8, pp. 79–94.

Gent, Peter R. and James C. Mcwilliams (1990). "Isopycnal Mixing in Ocean Circulation Models." In: *Journal of Physical Oceanography* 20, pp. 150–155.

Gent, Peter R., Jürgen Willebrand, Trevor J. McDougall, and James C. McWilliams (1995). "Parameterizing Eddy-Induced Tracer Transports in Ocean Circulation Models." In: *Journal of Physical Oceanography* 25(4), pp. 463–474.

Georgiou, Sotiria, Carine G. van der Boog, Nils Brüggemann, Stefanie L. Ypma, Julie D. Pietrzak, and Caroline A. Katsman (2019). "On the interplay between downwelling, deep convection and mesoscale eddies in the Labrador Sea." In: *Ocean Modelling* 135, pp. 56–70.

Gill, A. E., J. S.A. Green, and A. J. Simmons (1974). "Energy partition in the large-scale ocean circulation and the production of mid-ocean eddies." In: *Deep-Sea Research and Oceanographic Abstracts* 21.

Gillett, N. P. and J. C. Fyfe (2013). "Annular mode changes in the CMIP5 simulations." In: *Geophysical Research Letters* 40, pp. 1189–1193.

Gnanadesikan, Anand, Marie Aude Pradal, and Ryan Abernathey (2015). "Isopycnal mixing by mesoscale eddies significantly impacts oceanic an-

thropogenic carbon uptake." In: *Geophysical Research Letters* 42, pp. 4249–4255.

Greatbatch, Richard J. and Kevin G. Lamb (1990). "On Parameterizing Vertical Mixing of Momentum in Non-eddy Resolving Ocean Models." In: *Journal of Physical Oceanography* 20, pp. 1634–1637.

Griesel, A., J. L. McClean, S. T. Gille, J. Sprintall, and C. Eden (2014). "Eulerian and Lagrangian Isopycnal Eddy Diffusivities in the Southern Ocean of an Eddying Model." In: *Journal of Physical Oceanography* 44, pp. 644–661.

Griffies, Stephen M. (1998). "The Gent-McWilliams Skew Flux." In: *Journal of Physical Oceanography* 28, pp. 831–841.

Griffies, Stephen M. et al. (2015). "Impacts on ocean heat from transient mesoscale eddies in a hierarchy of climate models." In: *Journal of Climate* 28, pp. 952–977.

Groeskamp, Sjoerd, Bernadette M. Sloyan, Jan D. Zika, and Trevor J. McDougall (2017). "Mixing Inferred from an Ocean Climatology and Surface Fluxes." In: *Journal of Physical Oceanography* 47, pp. 667–687.

Haarsma, Reindert J. et al. (2016). "High Resolution Model Intercomparison Project (HighResMIP v1.0) for CMIP6." In: *Geoscientific Model Development* 9, pp. 4185–4208.

Hallberg, Robert and Anand Gnanadesikan (2001). "An Exploration of the Role of Transient Eddies in Determining the Transport of a Zonally Reentrant Current." In: *Journal of Physical Oceanography* 31, pp. 3312–3330.

– (2006). "The Role of Eddies in Determining the Structure and Response of the Wind-Driven Southern Hemisphere Overturning: Results from the Modeling Eddies in the Southern Ocean (MESO) Project." In: *Journal of Physical Oceanography* 36, pp. 2232–2252.

Hallock, Zachariah R. and William J. Teague (1996). "Evidence for a north pacific deep western boundary current." In: *Journal of Geophysical Research C: Oceans* 101, pp. 6617–6624.

Handmann, Patricia, Jürgen Fischer, Martin Visbeck, Johannes Karstensen, Arne Biastoch, Claus Böning, and Lavinia Patara (2018). "The Deep Western Boundary Current in the Labrador Sea From Observations and a High-Resolution Model." In: *Journal of Geophysical Research: Oceans* 123, pp. 2829–2850.

Hautala, Susan L. (2018). "The abyssal and deep circulation of the Northeast Pacific Basin." In: *Progress in Oceanography* 160, pp. 68–82.

Henning, Cara C and Geoffrey K. Vallis (2005). "The Effects of Mesoscale Eddies on the Stratification and Transport of an Ocean with a Circumpolar Channel." In: *Journal of Physical Oceanography* 35, pp. 880–896.

Herrford, Josefine, Peter Brandt, and Walter Zenk (2017). "Property changes of deep and bottom waters in the Western Tropical Atlantic."

In: *Deep-Sea Research Part I: Oceanographic Research Papers* 124, pp. 103–125.

Hogg, Andrew Mc C., Paul Spence, Oleg A. Saenko, and Stephanie M. Downes (2017). "The Energetics of Southern Ocean Upwelling." In: *Journal of Physical Oceanography* 47, pp. 135–153.

Hogg, Nelson G. (1983). "A note on the deep circulation of the western North Atlantic: its nature and causes." In: *Deep Sea Research Part A, Oceanographic Research Papers* 30, pp. 945–961.

Holland, William R. and Peter B. Rhines (1980). "An example of Eddy-Induced Ocean Circulation." In: *Journal of Physical Oceanography* 10, pp. 1010–1031.

Ito, T., M. Woloszyn, and M. Mazloff (2010). "Anthropogenic carbon dioxide transport in the Southern Ocean driven by Ekman flow." In: *Nature* 463, pp. 80–83.

Jayne, Steven R. and Jochem Marotzke (2002). "The Oceanic Eddy Heat Transport." In: *Journal of Physical Oceanography* 32, pp. 3328–3345.

Jayne, Steven R., Nelson G. Hogg, and Paola Malanotte-Rizzoli (1996). "Recirculation Gyres Forced by a Beta-Plane Jet." In: *Journal of Physical Oceanography* 26, pp. 492–504.

Jochum, Markus and Paola Malanotte-Rizzoli (2004). "A new theory for the generation of the equatorial subsurface countercurrents." In: *Journal of Physical Oceanography* 34, pp. 755–771.

Johns, W.E., L.M. Beal, M.O. Baringer, J.R. Molina, S.a. Cunningham, T. Kanzow, and D. Rayner (2008). "Variability of shallow and deep western boundary currents off the Bahamas during 2004-05: results from the 26°N RAPID-MOC Array." In: *Journal of Physical Oceanography* 38, pp. 605–623.

Johnson, Helen L., Paola Cessi, David P. Marshall, Fabian Schloesser, and Michael A. Spall (2019). "Recent Contributions of Theory to Our Understanding of the Atlantic Meridional Overturning Circulation." In: *Journal of Geophysical Research: Oceans* 124, pp. 5376–5399.

Jungclaus, J. H., N. Fischer, H. Haak, K. Lohmann, J. Marotzke, D. Matei, U. Mikolajewicz, D. Notz, and J. S. Von Storch (2013). "Characteristics of the ocean simulations in the Max Planck Institute Ocean Model (MPIOM) the ocean component of the MPI-Earth system model." In: *Journal of Advances in Modeling Earth Systems* 5, pp. 422–446.

Jungclaus, Johann H., Noel Keenlyside, Michael Botzet, H. Haak, J. J. Luo, Mojib Latif, J. Marotzke, U. Mikolajewicz, and Erich Roeckner (2006). "Ocean circulation and tropical variability in the coupled model ECHAM5/MPI-OM." In: *Journal of Climate* 19, pp. 3952–3972.

Kalnay, E. et al. (1996). "The NCEP/NCAR 40-year reanalysis project." In: *Bulletin of the American Meteorological Society* 77, pp. 437–471.

Kanzow, Torsten, Uwe Send, Walter Zenk, Alan D. Chave, and Monika Rhein (2006). "Monitoring the integrated deep meridional flow in the tropical North Atlantic: Long-term performance of a geostrophic

array." In: *Deep-Sea Research Part I: Oceanographic Research Papers* 53, pp. 528–546.

Kanzow, Torsten et al. (2007). "Observed Flow Compensation Associated with the MOC at 26.5°N in the Atlantic." In: *Science, New Series* 317, pp. 938–941.

Kawabe, Masaki and Shinzou Fujio (2010). "Pacific ocean circulation based on observation." In: *Journal of Oceanography* 66, pp. 389–403.

Klinger, Barry A. and Carlos Cruz (2009). "Decadal response of global circulation to Southern Ocean Zonal wind stress perturbation." In: *Journal of Physical Oceanography* 39, pp. 1888–1904.

Le Bras, Isabela A, Steven R Jayne, and John M Toole (2018). "The Interaction of Recirculation Gyres and a Deep Boundary Current." In: *Journal of Physical Oceanography* 48, pp. 573–590.

Lee, Thomas N., William E. Johns, Rainer J. Zantopp, and Eve R. Fillenbaum (1996). "Moored Observations of Western Boundary Current Variability and Thermohaline Circulation at 26.5°N in the Subtropical North Atlantic." In: *Journal of Physical Oceanography* 26, pp. 962–983.

Li, Hongmei and Jin-Song von Storch (2013). "On the Fluctuating Buoyancy Fluxes Simulated in a OGCM." In: *Journal of Physical Oceanography* 43, pp. 1270–1287.

Li, Qian, Sukyoung Lee, and Alexa Griesel (2016). "Eddy Fluxes and Jet-Scale Overturning Circulations in the Indo-Western Pacific Southern Ocean." In: *Journal of Physical Oceanography* 46, pp. 2943–2959.

Lorenz, Edward N. (1955). "Available Potential Energy and the Maintenance of the General Circulation." In: *Tellus* 7, pp. 157–167.

Lozier, M. Susan (1997). "Evidence for large-scale eddy-driven gyres in the North Atlantic." In: *Science* 277, pp. 361–364.

Lumpkin, Rick and Kevin Speer (2007). "Global Ocean Meridional Overturning." In: *Journal of Physical Oceanography* 37, pp. 2550–2562.

Lüschow, Veit, Jin-Song Von Storch, and Jochem Marotzke (2019). "Diagnosing the Influence of Mesoscale Eddy Fluxes on the Deep Western Boundary Current in the 1/10° STORM / NCEP Simulation." In: *Journal of Physical Oceanography* 49, pp. 751–764.

Lüschow, Veit, Jin Song von Storch, and Jochem Marotzke (2020). "Overturning response to a surface wind stress doubling in an eddying and a non-eddying ocean." In: *in preparation*.

Lynch-Stieglitz, Jean (2017). "The Atlantic Meridional Overturning Circulation and Abrupt Climate Change." In: *Annual Review of Marine Science* 9, pp. 83–104.

Marshall, David P., Maarten H.P. Ambaum, James R. Maddison, David R. Munday, and Lenka Novak (2017a). "Eddy saturation and frictional control of the Antarctic Circumpolar Current." In: *Geophysical Research Letters* 44, pp. 286–292.

Marshall, Gareth J. (2003). "Trends in the Southern Annular Mode from observations and reanalyses." In: *Journal of Climate* 16, pp. 4134–4143.

Marshall, John and Glenn Shutts (1981). "A Note on Rotational and Divergent Eddy Fluxes." In: *Journal of Physical Oceanography* 11, pp. 1677–1680.

Marshall, John and Kevin Speer (2012). "Closure of the meridional overturning circulation through Southern Ocean upwelling." In: *Nature Geoscience* 5, pp. 171–180.

Marshall, John, Jeffery R. Scott, Kyle C. Armour, J. M. Campin, Maxwell Kelley, and Anastasia Romanou (2015). "The ocean's role in the transient response of climate to abrupt greenhouse gas forcing." In: *Climate Dynamics* 44, pp. 2287–2299.

Marshall, John, Jeffery R. Scott, Anastasia Romanou, Maxwell Kelley, and Anthony Leboissetier (2017b). "The dependence of the ocean's MOC on mesoscale eddy diffusivities: A model study." In: *Ocean Modelling* 111, pp. 1–8.

Martin, Torge, Wonsun Park, and Mojib Latif (2015). "Southern Ocean forcing of the North Atlantic at multi-centennial time scales in the Kiel Climate Model." In: *Deep-Sea Research Part II: Topical Studies in Oceanography* 114, pp. 39–48.

Masuda, S et al. (2010). "Simulated Rapid Warming of Abyssal." In: 329, pp. 319–322.

McWilliams, J C (2008). "The nature and consequence of oceanic eddies." In: *Eddy-Resolving Ocean Modeling* 1, p. 409.

McWilliams, James C. (2016). "Submesoscale currents in the ocean." In: *Proceedings of the Royal Society A: Mathematical, Physical and Engineering Sciences* 472.

– (2019). "A survey of submesoscale currents." In: *Geoscience Letters* 6, pp. 1–15.

Meinen, Christopher S. and Silvia L. Garzoli (2014). "Attribution of Deep Western Boundary Current variability at 26.5°N." In: *Deep-Sea Research Part I: Oceanographic Research Papers* 90, pp. 81–90.

Meinen, Christopher S., Molly O. Baringer, and Silvia L. Garzoli (2006). "Variability in deep Western boundary current transports: Preliminary results from 26.5°N in the Atlantic." In: *Geophysical Research Letters* 33, pp. 1–5.

Meinen, Christopher S., William E. Johns, Silvia L. Garzoli, Erik van Sebille, Darren Rayner, Torsten Kanzow, and Molly O. Baringer (2013). "Variability of the Deep Western Boundary Current at 26.5°N during 2004-2009." In: *Deep-Sea Research Part II: Topical Studies in Oceanography* 85, pp. 154–168.

Molemaker, M. Jeroen, James C. McWilliams, and Xavier Capet (2010). "Balanced and unbalanced routes to dissipation in an equilibrated Eady flow." In: *Journal of Fluid Mechanics* 654, pp. 35–63.

Morrow, Rosemary and Pierre Yves Le Traon (2012). "Recent advances in observing mesoscale ocean dynamics with satellite altimetry." In: *Advances in Space Research* 50, pp. 1062–1076.

Munday, David R., Helen L. Johnson, and David P. Marshall (2013). "Eddy Saturation of Equilibrated Circumpolar Currents." In: *Journal of Physical Oceanography* 43, pp. 507–532.

Munk, Walter and Carl Wunsch (1998). "Abyssal recipes II: energetics of tidal and wind mixing." In: *Deep-Sea Research Part I* 45, pp. 1977–2010.

Nikurashin, Maxim and Raffaele Ferrari (2013). "Overturning circulation driven by breaking internal waves in the deep ocean." In: *Geophysical Research Letters* 40, pp. 3133–3137.

Nikurashin, Maxim, Geoffrey K. Vallis, and Alistair Adcroft (2013). "Routes to energy dissipation for geostrophic flows in the Southern Ocean." In: *Nature Geoscience* 6, pp. 48–51.

Olbers, Dirk, Jürgen Willebrand, and Carsten Eden (2012). *Ocean Dynamics*. Springer Science and Business Media.

Otto, Alexander et al. (2013). "Energy budget constraints on climate response." In: *Nature Geoscience* 6, pp. 415–416.

Patara, Lavinia and Claus W. Böning (2014). "Abyssal ocean warming around Antarctica strengthens the Atlantic overturning circulation." In: *Geophysical Research Letters* 41, pp. 3972–3978.

Pedlosky, Joseph (2013). *Geophysical fluid dynamics*. Springer Science and Business Media.

Phillips, N. (1966). "Large-scale eddy motion in the western Atlantic." In: *Journal of Geophysical Research* 71, pp. 3883–3891.

Poulsen, Mads B., Markus Jochum, and Roman Nuterman (2018). "Parameterized and resolved Southern Ocean eddy compensation." In: *Ocean Modelling* 124, pp. 1–15.

Pradal, Marie Aude and Anand Gnanadesikan (2014). "How does the Redi parameter for mesoscale mixing impact global climate in an Earth System Model?" In: *Journal of Advances in Modeling Earth Systems* 6, pp. 586–601.

Purkey, Sarah G. and Gregory C. Johnson (2012). "Global contraction of Antarctic Bottom Water between the 1980s and 2000s." In: *Journal of Climate* 25, pp. 5830–5844.

Radko, Timour and John Marshall (2004). "Eddy-induced diapycnal fluxes and their role in the maintenance of the thermocline." In: *Journal of Physical Oceanography* 34, pp. 372–383.

Rahmstorf, Stefan and Matthew H. England (1997). "Influence of Southern Hemisphere winds on North Atlantic Deep Water flow." In: *Journal of Physical Oceanography* 27, pp. 2040–2054.

Redi, Martha H. (1982). "Oceanic isopycnal mixing by coordinate rotation." In: *Journal of Physical Oceanography* 12, pp. 1154–1158.

Rhein, Monika, Dagmar Kieke, and Reiner Steinfeldt (2015). "Advection of North Atlantic Deep Water from the Labrador Sea to the southern hemisphere." In: *Journal of Geophysical Research* 120, pp. 2471–2487.

Rhines, Peter B. and William R. Holland (1979). "A theoretical discussion of eddy-driven mean flows." In: *Dynamics of Atmospheres and Oceans* 3, pp. 289–325.

Richardson, P. L., J. F. Price, D. Walsh, L. Armi, and M. Schröder (1989). "Tracking Three Meddies with SOFAR Floats." In: *Journal of Physical Oceanography* 19, pp. 371–383.

Richardson, P. L., A. S. Bower, and W. Zenk (2000). "A census of Meddies tracked by floats." In: *Progress in Oceanography* 45, pp. 209–250.

Romanou, A., J. Marshall, M. Kelley, and J. Scott (2017). "Role of the ocean's AMOC in setting the uptake efficiency of transient tracers." In: *Geophysical Research Letters* 44, pp. 5590–5598.

Schott, Friedrich A., Peter Brandt, Meike Hamann, Jürgen Fischer, and Lothar Stramma (2002). "On the boundary flow off Brazil at 5-10°S and its connection to the interior tropical Atlantic." In: *Geophysical Research Letters* 29, pp. 21–1.

Schott, Friedrich a., Marcus Dengler, Rainer Zantopp, Lothar Stramma, Jürgen Fischer, and Peter Brandt (2005). "The Shallow and Deep Western Boundary Circulation of the South Atlantic at 5°–11°S." In: *Journal of Physical Oceanography* 35, pp. 2031–2053.

Scott, Robert B. and Faming Wang (2005). "Direct evidence of an oceanic inverse kinetic energy cascade from satellite altimetry." In: *Journal of Physical Oceanography* 35, pp. 1650–1666.

Scott, Robert B., Brian K. Arbic, Eric P. Chassignet, Andrew C. Coward, Mathew Maltrud, William J. Merryfield, Ashwanth Srinivasan, and Anson Varghese (2010). "Total kinetic energy in four global eddying ocean circulation models and over 5000 current meter records." In: *Ocean Modelling* 32, pp. 157–169.

Seidov, Dan, Bernd J. Haupt, Eric J. Barron, and Mark Maslin (2001). "Ocean Bi-polar seesaw and climate: Southern versus northern meltwater impacts." In: *Geophysical Monograph Series* 126, pp. 147–167.

Shakespeare, Callum J. and Andrew McC. Hogg (2012). "An Analytical Model of the Response of the Meridional Overturning Circulation to Changes in Wind and Buoyancy Forcing." In: *Journal of Physical Oceanography* 42, pp. 1270–1287.

Sijp, Willem P., Jonathan M. Gregory, Remi Tailleux, and Paul Spence (2012). "The Key Role of the Western Boundary in Linking the AMOC Strength to the North–South Pressure Gradient." In: *Journal of Physical Oceanography* 42, pp. 628–643.

Smeed, D. A. et al. (2018). "The North Atlantic Ocean is in a state of reduced overturning." In: *Geophysical Research Letters* 45, pp. 1527–1533.

Smith, K. Shafer (2007). "Eddy amplitudes in baroclinic turbulence driven by nonzonal mean flow: Shear dispersion of potential vorticity." In: *Journal of Physical Oceanography* 37, pp. 1037–1050.

Spall, Michael A (1994). "Wave-induced abyssal recirculations." In: *Journal of Marine Research* 52, pp. 1051–1080.

Spall, Michael A. (2010). "Dynamics of down welling in an eddy-resolving convective basin." In: *Journal of Physical Oceanography* 40, pp. 2341–2347.

Stöber, Uwe, Maren Walter, Christian Mertens, and Monika Rhein (2008). "Mixing estimates from hydrographic measurements in the Deep Western Boundary Current of the North Atlantic." In: *Deep-Sea Research Part I: Oceanographic Research Papers* 55, pp. 721–736.

Stocker, Thomas F. (1998). *The seesaw effect*.

Stommel, Henry and A.B. Arons (1959). "On the abyssal circulation of the world ocean - II. An idealized model of the circulation pattern and amplitude in oceanic basins." In: *Deep Sea Research (1953)* 6, pp. 217–233.

Sun, Wenjin, Changming Dong, Ruyun Wang, Yu Liu, and Kai Yu (2017). "Vertical structure anomalies of oceanic eddies in the Kuroshio Extension region." In: *Journal of Geophysical Research: Oceans* 121, pp. 5936–5951.

Swallow, J. C. (1971). "The Aries Current Measurements in the Western North Atlantic." In: *Philosophical Transactions of the Royal Society A: Mathematical, Physical and Engineering Sciences* 270, pp. 451–460.

Swingedouw, Didier, T. Fichefet, H. Goosse, and M. F. Loutre (2009). "Impact of transient freshwater releases in the Southern Ocean on the AMOC and climate." In: *Climate Dynamics* 33, pp. 365–381.

Thompson, David W J and Susan Solomon (2002). "Interpretation of Recent Southern Hemisphere Climate Change." In: *science* 296, pp. 895–900.

Toggweiler, J. R. and B. Samuels (1995). "Effect of drake passage on the global thermohaline circulation." In: *Deep-Sea Research Part I* 42, pp. 477–500.

– (1998). "On the Ocean's Large-Scale Circulation near the Limit of No Vertical Mixing." In: *Journal of Physical Oceanography* 28, pp. 1832–1852.

Treguier, Anne Marie, Eric P. Chassignet, Arnaud Le Boyer, and Nadia Pinardi (2017). "Modeling and forecasting the "weather of the ocean" at the mesoscale." In: *Journal of Marine Research* 75, pp. 301–329.

Treguier, a. M. (1999). "Evaluating eddy mixing coefficients from eddy-resolving ocean models: A case study." In: *Journal of Marine Research* 57, pp. 89–108.

Vallis, Geoffrey K (2017). *Atmospheric and oceanic fluid dynamics*. Cambridge University Press.

Van Sebille, Erik, William E. Johns, and Lisa M. Beal (2012). "Does the vorticity flux from Agulhas rings control the zonal pathway of NADW across the South Atlantic?" In: *Journal of Geophysical Research: Oceans* 117, pp. 1–12.

Vollmer, Lukas and Carsten Eden (2013). "A global map of meso-scale eddy diffusivities based on linear stability analysis." In: *Ocean Modelling* 72, pp. 198–209.

Von Storch, Jin-Song, Carsten Eden, Irina Fast, Helmuth Haak, Daniel Hernández-Deckers, Ernst Maier-Reimer, Jochem Marotzke, and Detlef Stammer (2012). "An Estimate of the Lorenz Energy Cycle for the World Ocean Based on the STORM/NCEP Simulation." In: *Journal of Physical Oceanography* 42, pp. 2185–2205.

Von Storch, Jin Song, Helmuth Haak, Eileen Hertwig, and Irina Fast (2016). "Vertical heat and salt fluxes due to resolved and parameterized meso-scale Eddies." In: *Ocean Modelling* 108, pp. 1–19.

Von Storch, Jin-Song, Gualtiero Badin, and Marcel Oliver (2019). "The Interior Energy Pathway: Inertia-Gravity Wave Emission by Oceanic Flows." In: *Energy Transfers in Atmosphere and Ocean*. Ed. by Carsten Eden and A. Iske. Springer-Verlag, pp. 53–85.

Waterman, Stephanie and Brian J. Hoskins (2013). "Eddy Shape, Orientation, Propagation, and Mean Flow Feedback in Western Boundary Current Jets." In: *Journal of Physical Oceanography* 43, pp. 1666–1690.

Waterman, Stephanie and Steven R. Jayne (2011). "Eddy-Mean Flow Interactions in the Along-Stream Development of a Western Boundary Current Jet: An Idealized Model Study." In: *Journal of Physical Oceanography* 41, pp. 682–707.

– (2012). "Eddy-Driven Recirculations from a Localized Transient Forcing." In: *Journal of Physical Oceanography* 42, pp. 430–447.

Weatherly, Georges, Yoo Yin Kim, and Evgeny A. Kontar (2000). "Eulerian Measurements of the North Atlantic Deep Water Deep Western Boundary Current at 18° S." In: *Journal of Physical Oceanography* 30, pp. 971–986.

Weaver, Andrew J. et al. (2012). "Stability of the Atlantic meridional overturning circulation: A model intercomparison." In: *Geophysical Research Letters* 39, pp. 1–8.

Whitworth, T., W. D. Nowlin, R. D. Pillsbury, M. I. Moore, and R. F. Weiss (1991). "Observations of the Antarctic Circumpolar Current and deep boundary current in the southwest Atlantic." In: *Journal of Geophysical Research* 96, p. 15105.

Winton, Michael, Whit G. Anderson, Thomas L. Delworth, Stephen M. Griffies, William J. Hurlin, and Anthony Rosati (2014). "Has coarse ocean resolution biased simulations of transient climate sensitivity'." In: *Geophysical Research Letters* 41, pp. 8522–8529.

Wolfe, C. L., P. Cessi, J. L. McClean, and M. E. Maltrud (2008). "Vertical heat transport in eddying ocean models." In: *Geophysical Research Letters* 35, pp. 1–5.

Wunsch, Carl and Raffaele Ferrari (2004). "Vertical Mixing, Energy, and the General Circulation of the Oceans." In: *Annual Review of Fluid Mechanics* 36, pp. 281–314.

Wüst, G and A Defant (1936). "Atlas zur Schichtung und Zirkulation des Atlantischen Ozeans. Schnitte und Karten von Temperatur, Salzgehalt

und Dichte." In: *Wissenschaftliche Ergebnisse der Deutschen Atlantischen Expedition Meteor* 6, 103 pp.

Zanowski, Hannah and Robert Hallberg (2017). "Weddell Polynya transport mechanisms in the Abyssal ocean." In: *Journal of Physical Oceanography* 47, pp. 2907–2925.

Zhai, Xiaoming, Helen L. Johnson, and David P. Marshall (2010). "Significant sink of ocean-eddy energy near western boundaries." In: *Nature Geoscience* 3, pp. 608–612.

Zhang, Zhixin, Fangli Qiao, and Jingsong Guo (2014). "Subsurface eddies in the southern South China Sea detected from in-situ observation in October 2011." In: *Deep-Sea Research Part I: Oceanographic Research Papers* 87, pp. 30–34.

ACKNOWLEDGMENTS

This dissertation is based on the incredible support I have received during the last three years in many different ways and from many different people. First of all, I want to express my deep gratitude to Jin-Song von Storch. You helped me immensely on my way to becoming a scientist: by providing guidance and inspiration about oceanography, but also by letting me work independently and by being available when I needed your help. From Jochem Marotzke, I learned many things about how to write and talk about science and thereby he shaped my thinking about it, thank you! I'm also overly grateful for a couple of very kind and sincere conversations about being a scientist with Johanna Baehr.

The MPI-M, and in particular the International Max Planck Research School, was a great place to do a PhD. Antje Weitz, Cornelia Kampmann and Michaela Born were immensely helpful in all non-scientific questions and in providing moral support, thank you very much! And Helmuth Haak, I'm grateful for your patience in helping with everything related to the MPI ocean model. Furthermore, I want to thank Kornelia Müller for her administrative support in many occasions as well as her loud laughs and film tips. The ocean department as a whole and in particular the ocean statistics group was an inspiring environment and taught me so many things about oceanography, I'm grateful that I had the opportunity to be here.

Of course, I'm deeply thankful for the friends I found at MPI. Christopher and Miriam welcomed me in the best way possible at MPI. Lukas, Bernhard and Alex, thank you for great lunch and coffee breaks and for the evenings we spent together. Alex and Christopher deserve an extra thanks for commenting on this manuscript! And there are so many more really nice, funny, inspiring and interesting people at this institute!

Last but not least, I'm deeply grateful for my parents and the rest of my family. Especially, Angelika and Frank, thanks so much that you enabled me to study and to learn. And Julia, thank you for being part of my life!

Versicherung an Eides statt

Declaration of Oath

Hiermit versichere ich an Eides statt, dass ich die vorliegende Dissertation mit dem Titel: "The Deep Western Boundary Current in an Eddying Ocean" selbstständig verfasst und keine anderen als die angegebenen Hilfsmittel – insbesondere keine im Quellenverzeichnis nicht benannten Internet-Quellen – benutzt habe. Alle Stellen, die wörtlich oder sinngemäß aus Veröffentlichung entnommen wurden, sind als solche kenntlich gemacht. Ich versichere weiterhin, dass ich die Dissertation oder Teile davon vorher weder im In- noch im Ausland in einem anderen Prüfungsverfahren eingereicht habe und die eingereichte schriftliche Fassung der auf dem elektronischen Speichermedium entspricht.

Hamburg, Februar 2020

Veit Magnus Lüschow

Hinweis / Reference

Die gesamten Veröffentlichungen in der Publikationsreihe des MPI-M
„Berichte zur Erdsystemforschung / Reports on Earth System Science“,
ISSN 1614-1199

sind über die Internetseiten des Max-Planck-Instituts für Meteorologie erhältlich:
http://www.mpimet.mpg.de/wissenschaft/publikationen.html

All the publications in the series of the MPI -M
„Berichte zur Erdsystemforschung / Reports on Earth System Science“,
ISSN 1614-1199

are available on the website of the Max Planck Institute for Meteorology:
http://www.mpimet.mpg.de/wissenschaft/publikationen.html